ENVIRONMENTAL EVOLUTION OF SUPERCELLS INTERACTING WITH THE APPALACHAIN MOUNTAINS

by

Sarah M. Purpura

A thesis submitted to the faculty of
The University of North Carolina at Charlotte
in partial fulfillment of the requirements
for the degree of Master of Science in
Earth Science

Charlotte

2021

Approved by:

_____
Dr. Casey Davenport

_____
Dr. Matthew Eastin

_____
Terry Shirley

ABSTRACT

SARAH M. PURPURA. Environmental Evolution of Supercells Interacting with the Appalachian Mountains (Under the direction of DR. CASEY DAVENPORT)

The Appalachian Mountains within the eastern United States have a considerable impact on day-to-day weather, including severe convection. However, the impact of the Appalachians on supercell thunderstorms is not well understood, posing a significant short-term forecast challenge across the region. While there have been some individual case studies conducted, there has yet to be a broad analysis of storm-scale modifications of supercells as they interact with complex terrain. To address this gap, this study examined 62 isolated supercells that occurred within the central and southern Appalachians between April and July from 2009 to 2019. Each supercell was broadly classified as either a "crosser" or "non-crosser" based on their ability to be maintained during their interaction with terrain; the majority of supercells (37) were not sustained downstream of the Appalachians. To identify the environmental controls resulting in crossing or non-crossing storms, near-storm model soundings (either the Rapid Update Cycle or the Rapid Refresh) were collected for each supercell at three points: (1) upstream of the mountains, (2) near the peak of the terrain, (3) and downstream of the terrain feature. These soundings were used to compute a number of different thermodynamic and kinematic parameters. Results indicate that the lowest 3 km of shear and storm-relative helicity (SRH) appear to best distinguish crossing and non-crossing supercells. Conversely, instability (CAPE and CIN) do not appear to be useful parameters in differentiating between crossers and non-crossers. Forecasters can use the lowest 3 km of SRH and shear, as well as the surface and mixed-layer equivalent potential temperature (θ_e) to aid in the short-term forecasting of isolated crossing supercells. Additionally, syntopic pattern recognition (e.g., the tilt of the upper-level

trough, location of the surface low pressure, and the boundary type) of these events may help forecasters identify if supercells will cross the Appalachian Mountains.

ACKNOWLEDGEMENTS

I would like to thank my advisor Dr. Casey Davenport and for their encouragement and support throughout this process. I also need to thank my committee, Dr. Matthew Eastin and Mr. Terry Shirley for their support and guidance throughout this research. This project would not have been possible without the funding assistance through the University of North Carolina at Charlotte, the Geography and Earth Science Department, and the National Oceanic and Atmospheric Administration's CSTAR program. This research was also made possible with the feedback and assistance of the Storm Prediction Center and the following National Weather Service Offices: Peachtree City, GA, Greenville-Spartanburg, SC, Jackson, KY, Charleston, WV, Blacksburg, VA, and Morristown, TN. I would also like to thank my fellow graduate students who helped me make this journey enjoyable. I especially would like to thank Katie McKeown for not only being a great research partner, but a great friend. This also would not have been possible without the support from my Valpo and Kappa Delta friends, as well as my roommate. Finally, I would like to thank my family, Sandy, Jim, Rachel, Leah, and Finn Purpura for their constant support as I would not have been able to do this without their help during a global pandemic.

DEDICATION

I would like to dedicate this to my family, my dog Finn, and my late dog Ryder, as you have all helped me to succeed in this endeavor.

TABLE OF CONTENTS:

LIST OF TABLES

LIST OF FIGURES

LIST OF ABBREVIATIONS

AIRS - Archive Information Request System

CAPE - Convective Available Potential Energy

CIN - Convective Inhibition

CM1 - Cloud Model 1

CWA - County Warning Area

DEM - Digital Elevation Model

DCAPE - Downdraft Convective Available Potential Energy

EF - Enhanced Fujita

EL - Equilibrium Level

KFFC - Locator name for the radar site in Peachtree City, GA

KFCX - Locator name for the radar site in Blacksburg, VA

GIS - Geographic Information Systems

KGSP - Locator name for the radar site in Greenville-Spartanburg, SC

hPa - Hectopascal

HRRR - High-Resolution Rapid Refresh

KJKL - Locator name for the radar site in Jackson, KY

LCL - Lifted Condensation Level

LFC - Level of Free Convection

MLCAPE - Mixed-layer Convective Available Potential Energy

MLCIN - Mixed-layer Convective Inhibition

KMRX Locator name for the radar site in Morristown, TN

MSLP - Mean Sea Level Pressure

MUCAPE - Most Unstable Convective Available Potential Energy

MLCAPE - Most Unstable Convective Inhibition

NCEI - National Centers of Environmental Information

NOAA - National Oceanic and Atmospheric Administration

NROT - Normalized Rotation

NWS - National Weather Service

RAP - Rapid Refresh region model

RH - Relative Humidity

RUC - Rapid Update Cycle regional model

KRLX - Locator name for the radar site in Charleston, WV

SBCAPE - Surface Based Convective Available Potential Energy

SBCIN - Surface Based Convective Inhibition

SCP - Supercell Composite Parameter

SPC - Storm Prediction Center

SRH - Storm Relative Helicity

STP - Significant Tornado Parameter

THREDDS - Thematic Real-time Environmental Distribution Data Services

UTC – Coordinated Universal Time

WFO - Weather Forecast Office

WRF - Weather Research Forecast model

θ_e- Equivalent Potential Temperature

CHAPTER 1: INTRODUCTION AND MOTIVATION

1.1 Introduction

Isolated supercells in the Appalachian Mountains are a fairly uncommon occurrence, yet can produce significant damage through a combination of severe straight-line winds, large hail, and tornadoes. There is limited knowledge of how supercells interact with complex terrain, which poses a significant challenge when it comes to short-term forecasting of their maintenance and subsequent impacts. One of the most notable examples of the struggle to forecast supercells in the Appalachian region is the 27-28 April 2011 outbreak, which produced several EF4 and EF5 tornadoes associated with long-lived supercells (Gaffin 2012; Lyza and Knupp 2014). Many of the outbreak supercells became more difficult to forecast as they moved from low-lying areas with excellent radar coverage, to areas of elevated complex terrain with poorer radar coverage.

Supercells in the Great Plains have been extensively studied (e.g., Lemon and Doswell 1979; Thompson and Edwards 2000; Bunkers et al. 2006); while structurally similar to supercells in the eastern United States, Great Plains supercells notably differ due to their relative lack of interaction with topography and are comparatively more straightforward to study than supercells in the eastern United States. Since there is limited observational data in the mountainous regions of the Appalachians, idealized models have been used to identify the characteristics of supercells as they interact with various complex terrain (Geerts et al. 2009; Markowski and Dotzek 2011; Lyza and Knupp 2014; Katona et al. 2016; Smith et al. 2016; Scheffknecht et al. 2017). These modeling studies are useful in identifying important sensitivities that supercells have when interacting with terrain (e.g., terrain-induced environmental variability, terrain height, etc).

Observational studies have elucidated how supercells are influenced by terrain, yet have been fairly limited to a few cases within specific subregions. Broad synoptic and climatological

scales impact supercell occurrence (Gaffin and Parker 2006; Stonefield and Hudgins 2006; Lane 2008), as well as details of the height and complexity of terrain the supercell is interacting with, including the local environment (Keighton et al. 2004; Bosart et al. 2006; Schneider 2009; Gaffin 2012; Prociv 2012; Tang et al. 2016). While these studies are helpful to understanding how the realistic terrain of the Appalachian Mountains plays a role in the supercell life cycle, they only reveal a snapshot of a few particular events and are reliant on limited radar and upper-air data.

To overcome the issue of insufficient storm-scale data, researchers have used hourly operational regional models such as the High-Resolution Rapid Refresh (HRRR), the Rapid Update Cycle (RUC), and the Rapid Refresh (RAP) (Thompson et al. 2003; Conigilio 2012; Reames 2017; Evans et al. 2018). This approach will also be utilized in this study to quantify variability in the inflow environment of supercells as they traverse the Appalachian Mountains. More broadly, this study seeks to bridge the gap between observational and idealized studies of supercells interacting with complex terrain in the Appalachian Mountains to enhance short-term forecasts and our understanding of how terrain interactions influence storm longevity and severe weather.

1.2 Motivation:

The Peachtree City, GA (KFFC), Greenville-Spartanburg, SC (KGSP), Jackson, KY (KJKL), Charleston, WV (KRLX), Blacksburg, VA (KFFC), and Morristown, TN (KMRX) National Weather Service (NWS) offices are responsible for forecasting and issuing timely and accurate severe weather warnings for the Southern Appalachian Mountains (Figs. 1.1-1.2). The Storm Prediction Center (SPC) is also responsible for issuing severe weather watches across the United States, including the Appalachian Mountains. This is a highly collaborative study, working alongside the NWS and SPC forecasters, which seeks to identify synoptic and

mesoscale parameters to better predict severe weather and supercells within this region. This project will supply additional knowledge of the effects the Appalachian Mountains have on isolated supercells by analyzing the inflow environments of these supercells at the initiation point (upstream), the point of the peak elevation (peak), and at the dissipation or linear point (downstream).

This study will analyze isolated supercells in the Appalachian Mountains to understand how these supercells are affected by complex terrain, with a focus on the relationship between the storm's inflow environment, underlying terrain, and subsequent storm evolution. The project aims to more accurately predict how isolated supercells will alter as they interact with the Appalachian Mountains. The goals of this research project include 1) determining the environmental conditions that favor crossing supercells, 2) identifying environmental factors that lead to supercell dissipation or intensification in relation to the mountains, and 3) evaluating how supercell environments vary as a result of interactions with complex terrain.

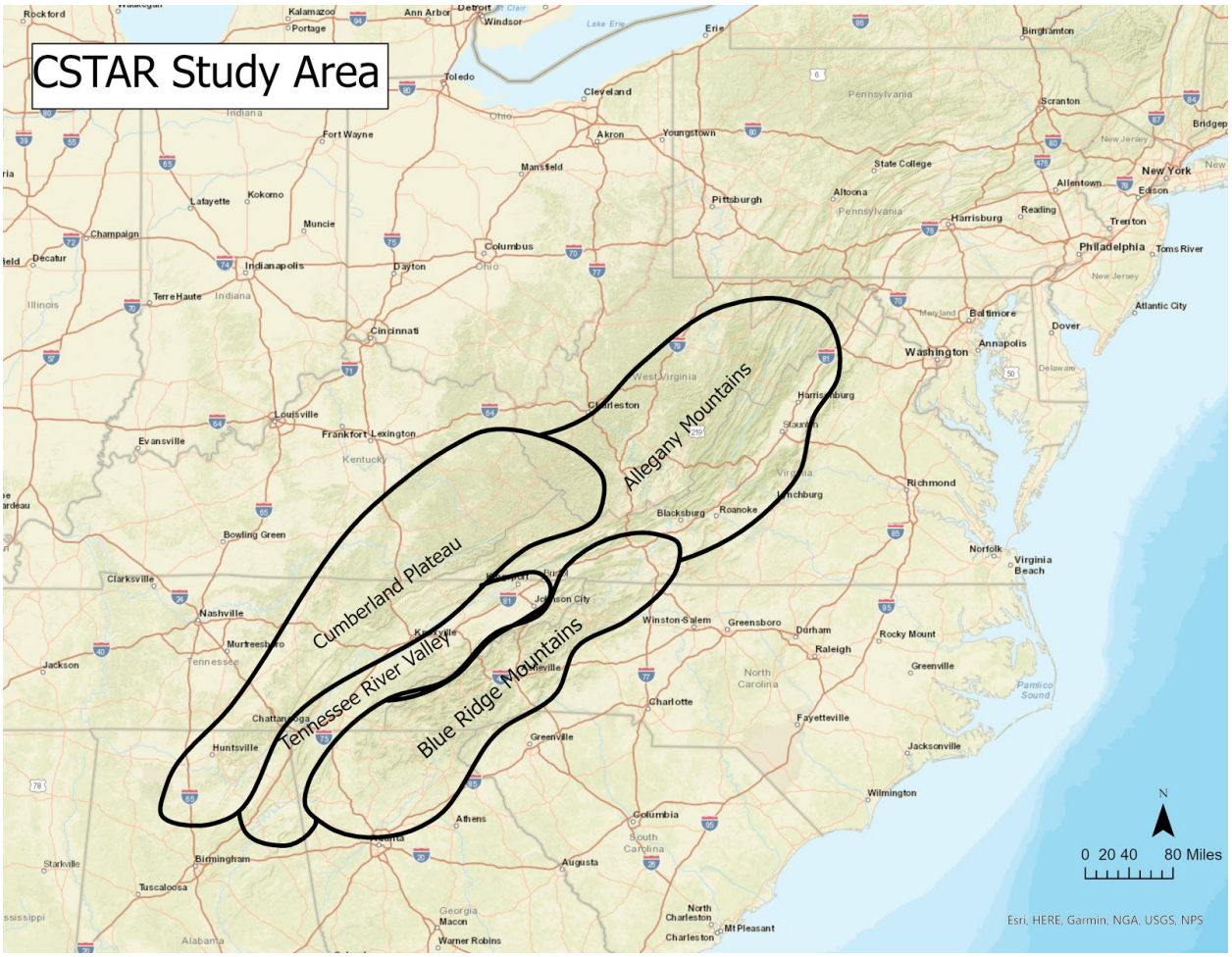

Figure 1.1: A map of the study area and the underlying terrain features mentioned in the study.

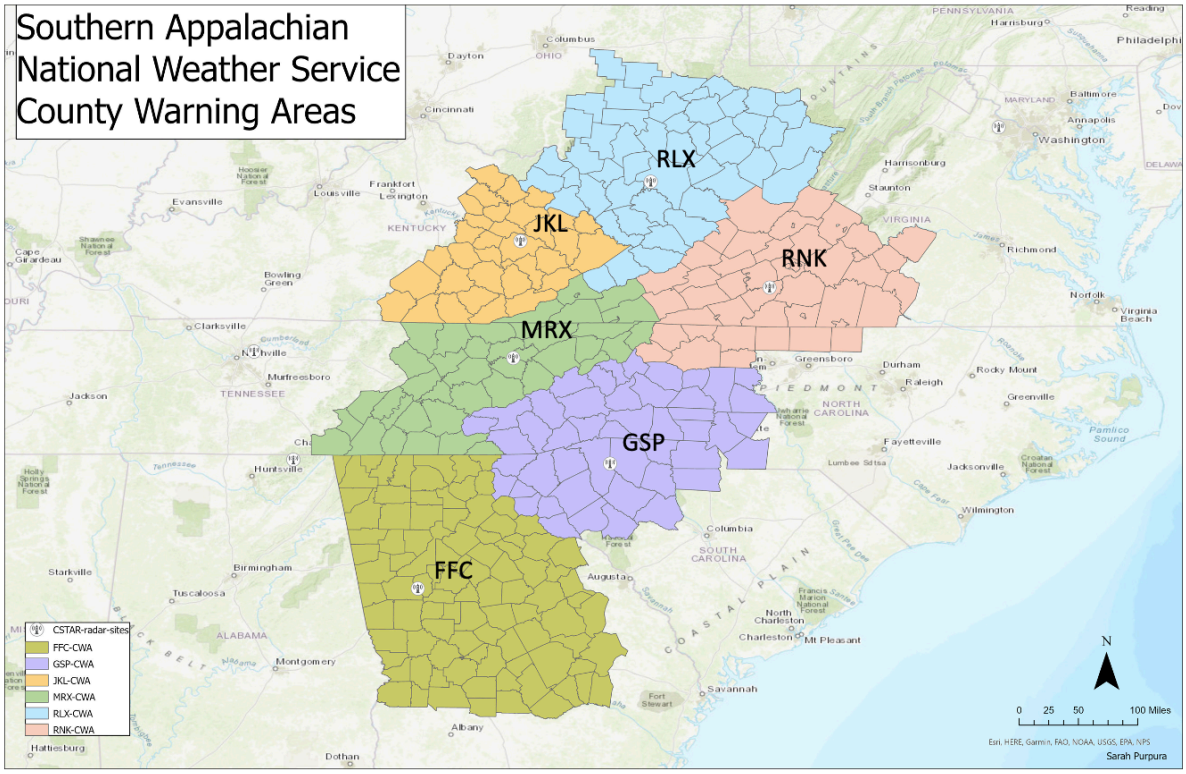

Figure 1.2: The County Warning areas for the Peachtree City, GA, Greenville-Spartanburg, SC, Jackson, KY, Charleston, WV, Blacksburg, VA, and Morristown, TN National Weather Service offices.

CHAPTER 2: LITERATURE REVIEW

2.1 Climatology of Supercells in the Appalachian Mountains

While there is an overall lack of systematic studies of supercells in the Appalachian Mountains, a number of studies have identified the climatological characteristics of supercells within a few subregions of the Appalachians, including the Southern Appalachians, the Greenville-Spartanburg, SC County Warning Area (CWA), and the Blacksburg, VA CWA (cf. Fig. 1.2). Broadly, these studies have focused on the diurnal and annual cycles of supercells in the region, as well as associated severe weather and the synoptic and mesoscale patterns.

The timing of these severe and tornadic supercells follows a trend similar to supercells across the country. A majority of severe weather and significant tornadoes in the Appalachian region tend to occur between 12 pm and 8 pm LST, around the time of peak heating (Figs. 2.1-2.2; Gaffin and Parker 2006; Stonefield and Hudgins 2006; Lane 2008). Studies have also found that significant tornadoes in the region are more likely to occur between April and May, with a higher frequency of tornadoes in April (Figs. 2.3-2.5).

Compared to the Great Plains, supercells, and especially tornadic or significantly tornadic supercells, are fairly rare: the southern Appalachians observe about 1.4 significant tornadoes (EF2 or greater) a year and occur on the southern and western side of the mountains (Gaffin and Parker 2006). The Greenville-Spartanburg, SC CWA has observed approximately 146 tornadoes between 1888 to 2006 (Lane 2008; Fig. 2.6). These tornadoes commonly occur in the Piedmont and foothills of upstate South Carolina, northeast Georgia, and the southern Piedmont of North Carolina. The supercells associated with these tornadoes tend to traverse the Piedmont and foothills, usually initiating in the southern Appalachians and to the east of the Blue Ridge Mountains. This is illustrated in the Blacksburg, VA CWA, in which 132 tornadoes have been

observed from 1950 to 2005, the vast majority of which touched down in southern Virginia and to the east of the Blue Ridge Mountains (Stonefield and Hudgins 2006; Fig. 2.7). The number of significant tornado days, analyzed between 1921 and 1995, dropped considerably from west to east, especially in the Appalachian region (Fig. 2.8). It is evident that the frequency of tornadoes and significant tornadoes in the Appalachian region are low compared to the central United States, but significant tornadoes can still occur in the mountains and can cause significant damage.

A popular approach in past climatological studies has been to examine the synoptic and mesoscale patterns associated with these tornadic and supercell events to aid forecasters in pattern recognition for such rare events. For example, the vast majority (92%) of significant tornado events in the Southern Appalachians were located near a jet streak, largely near the right side, though not necessarily the right entrance region associated with rising motion (Fig. 2.9; Gaffin and Parker 2006). Moving down to the mid-levels, significant tornadoes were further associated with westerly or northwesterly 500 hPa flow in conjunction with either a mid-level closed low or a negatively-tilted trough. However, for tornado outbreaks (5 or more EF2+ tornadoes), the 500 hPa flow tended to be from the south, southwest, or west. Near the surface, boundaries also appeared to be influential for supercells and tornado production, as significant tornadoes were located within 100 km of a moisture or thermal boundary (Gaffin and Parker 2006); this finding is consistent with the well-established relationship of boundaries and Great Plains supercell tornadoes (e.g., Markowski et al. 1998; Rasmussen et al. 2000; Bunkers et al. 2006; Magee and Davenport 2020). Notably, however, in the Greenville-Spartanburg CWA, the location of a cold front had little influence on whether a significant tornado would occur (Lane 2008).

When looking more closely at the storm-scale environments, it was found that wind dynamics (storm-relative helicity [SRH] and bulk vertical wind shear) are more important to significant tornadoes than instability (Gaffin and Parker 2006). Similarly, Lane (2008) also found that instability was not as important as wind dynamics for significant tornadoes, but identified that the lowest 0-3 km of instability (using CAPE) helped distinguish between weak tornadoes and significant tornadoes. It is also deduced that there are fewer tornadoes located in the Great Tennessee River Valley (cf. Fig. 1.1), as LCL heights tend to be higher than the heights observed in the plateaus or mountains. Lower LCL heights are important for tornado development because the lower the LCL, the easier it is for a tornado to reach the surface (e.g., Craven and Brooks 2004). The climatological studies help to paint a picture of the overall pattern as supercells and tornadoes track through the area.

2.2 Idealized Modeling Studies

Idealized models are often used in meteorology to simulate past weather events to understand how these events may have progressed based on varying environmental conditions or terrain. Several studies have used these models to understand how supercells might be impacted as they interact with varying degrees of complex terrain; most notably, studies have focused on testing different escarpment heights (Geerts et al. 2009; Markowski and Dotzek 2011; Lyza and Knupp 2014; Katona et al. 2016; Smith et al. 2016; Scheffknecht et al. 2017).

Using the Cloud Model 1 (CM1; Bryan and Fritsch 2002), idealized terrain, and an idealized environment (Weisman and Klemp 1982, 1984), Markowski and Dotzek (2011) and Smith et al. (2016) tested various terrain configurations to identify orographic effects on supercell development; such configurations included varying the height, width, and shape of the underlying terrain. Overall, it was found that the supercell strengthened (measuring strength by

the updraft and mesocyclone intensities) on the windward side of an escarpment, which led to the supercell weakening as it descended the leeward side (Markowski and Dotzek 2011). The weakening of the supercell was caused by downsloping, which increased the amount of CIN and decreased the amount of relative humidity needed to maintain convection (Fig. 2.10). Smith et al. (2016) then found that enhanced inflow was created by terrain blocking, which, in turn, led to enhanced precipitation (Fig. 2.11). The heavy amounts of precipitation then led to a stronger outflow boundary which sustained the supercell. However, once the cold pool became too strong, it weakened the supercell. Markowski and Dotzek (2011) associated the weakening of supercells to the downsloping flow, while Smith et al. (2016) attributed the weakening of supercells to the strength of the outflow boundary created by heavy precipitation from the given supercell. Even though there is some disagreement about the cause of weakening, both studies are in agreement that the complex terrain aided in supercell strengthening and weakening.

Storm-scale modifications can also be analyzed in relation to realistic terrain variations using idealized modeling. Using the Weather Research Forecast (WRF) model, a supercell on 2 August 2007 in eastern Switzerland was studied (Scheffknecht et al. 2017). This supercell was imposed on the terrain of the Alps Mountains to identify how the supercell would modify as it interacted with realistic terrain. It was found that slope circulations, from small-scale terrain, aided in the upward transport of moisture. This circulation led to a local increase in CAPE and a decrease in CIN, which lengthened the lifetime of the supercell; such terrain-induced variations in the environment are consistent with the simulations in Markowski and Dotzek (2011; Fig. 2.12).

Boundaries also play an important role in supercell and tornado development, particularly in the Great Plains, but have also been established via idealized modeling to be influential near

terrain (Geerts et al. 2009; Smith et al. 2016; Scheffknecht et al. 2017). These boundaries include gust fronts, warm fronts, cold fronts, and occluded fronts which play a role in convergence, upward motion, and vertical shear needed to maintain supercell development (Fig 2.13). This is consistent with previous research on the relationship with boundaries and supercells (e.g., Markowski et al. 1998; Rasmussen et al. 2000; Bunkers et al. 2006; Magee and Davenport 2020).

2.3 Observational Studies

Modeling studies have determined that terrain blocking, slope circulations, and boundaries play an important role in supercell evolution near complex terrain. Importantly, many of these processes have been confirmed in analyses of observed events, particularly for high-end tornadic and outbreak events (Bosart et al. 2006; Schneider 2009; Gaffin 2012; Prociv 2012).

2.3.1 The Great Barrington, Massachusetts, Tornado on 29 May 1995

An EF3 tornado tracked through Great Barrington, Massachusetts on 29 May 1995 and interacted with the complex terrain of the Catskill Mountains, Hudson Valley, and Taconic Range (Bosart et al. 2006; Fig. 2.14). A line of convection was initiated around 1754 UTC and tracked across part of the Catskill mountains. By 2200 UTC, the supercell began to descend into the Hudson Valley. As the supercell moved down into the valley, it became tornadic and rapidly intensified. The supercell reached peak intensification as it ascended the western foothills of the Taconic Range and weakened as it reached peak elevation of the Taconic Range. This finding was similar to Markowski and Dotzek (2011) and Smith et al. (2016), in which supercells strengthened as they ascended the mountain due to upslope flow.

Upper-air soundings around Massachusetts helped to elucidate the environmental factors that led to tornadogenesis as the supercell crossed varying terrain. The observed Albany, NY (ALB) sounding at 1200 UTC, taken roughly 12 hours prior to the tornadic supercell descending into the Hudson Valley, indicated channeling of the south-southeasterly winds in Hudson Valley (Fig. 2.15). Channeling of low-level flow about the terrain, helps to advect warm moist air into these areas while also increasing vertical shear which enhances the potential for supercell development and tornadogenesis (Fig. 2.16). The presence of strong vertical wind shear allows for the development of a mesocyclone, supporting the longevity of a supercell. The advection of warm, moist air destabilizes the atmosphere which allows parcels to rise. The combination of instability and shear are needed for the development and longevity of supercells and tornadoes. Along with flow channeling, a combination of vertical wind shear, instability, and the orientation of the topography may have led to the development of the tornadic supercell.

2.3.2 Tennessee Valley Tornadoes

Schneider (2009) analyzed three tornadic supercell events within the Tennessee Valley to identify potential commonalities that may have led to tornadogenesis. Each tornado was associated with differing terrain configurations, enhancing the difficulty of predicting such events. On 26 April 2007, an EF1 tornado moved from the southwest to the northeast into Tennessee, following the orientation of the terrain. In the Powell River Valley in Virginia, an EF1 tornado was spawned on 4 March 2008 in Virginia. On the 14th of November 2007, in the southern portion of the Tennessee Valley, a long lived supercell produced an EF1 and EF2 tornado. Schneider (2009) determined that higher terrain may have aided in the strengthening of the main storm updraft (supporting tornadogenesis) due to upslope flow, consistent with results of subsequent modeling studies (e.g., Smith et al. 2016; Scheffknecht et al. 2017). It was also

concluded that when a supercell moved from a higher elevation to lower elevation, vorticity stretching occurred which strengthened the supercell, in line with other studies (e.g., Bosart et al. 2006; Prociv 2012). Additionally, supercells that moved through smaller valleys led to enhanced flow channeling and increased helicity, which aided in tornadogenesis, similar to Bosart et al. (2006) and Gaffin (2012). These factors led to the enhancement of the updraft, which in turn, led to the strengthening and longevity of the tornadic supercells.

2.3.3 Super Tornado Outbreak 27 April 2011

Several supercells developed near the opening of the Tennessee River Valley in the southern Appalachian Mountains on 27 April 2011 (Gaffin 2012; Fig. 2.17). Many of these supercells produced damaging tornadoes. The environment was already conducive for the formation of tornadoes, as there were high helicity values and moderate instability within the Tennessee River Valley. Along with the primed environment, strong southeasterly surface winds were present, and channeled through the southeast to northwest oriented valleys located in the southern Appalachians. This flow channeling may have helped to accelerate the flow and in turn might have enhanced the probability of tornado formation due to the pre-existing vorticity.

2.3.4 Blacksburg, Virginia 14 Supercells

Fourteen supercells that interacted with the complex terrain of the Appalachian Mountains within a 64 km radius of the Blacksburg, Virginia radar site were analyzed by Prociv (2012; Figs. 2.18). These supercells spanned from 1998 through 2011 and occurred between April and June. The supercells were examined to determine if terrain variability led to the enhancement or demise of supercells. It was found that terrain aids low-level rotation in supercells due to slopes being shallower and the terrain being less rough. Supercells were also

much weaker on west-facing terrain due to the lack of warm, moist air coming off of the Atlantic Ocean. The strongest supercells occurred in the Piedmont and may be due to the absence of terrain or that the supercells encountered similar environments. However, eight supercells intensified while descending from elevated terrain, suggesting that vertical vorticity stretching was a contributing factor (Fig. 2.19).

2.4 Inflow Environments Using Operational Regional Models

While observational case studies are widely used to understand specific meteorological events, there are often many limitations to the data. One considerable limitation, especially in the Appalachian Mountains, is the lack of radar coverage and aerial upper-air soundings, both spatially (Fig. 2.20) and temporally (i.e., launches only twice per day). To overcome this challenge, high-resolution operational models have been used to provide a more detailed assessment of the mesoscale and synoptic patterns; a select set of case studies utilizing this approach to glean more information about supercell environments as they interact with terrain will be described below.

2.4.1 22 May 2014 Duanesburg, New York Tornadic Supercell

An EF3 tornadic supercell moved through Duanesburg, New York on 22 May 2014 (Tang et al. 2016). This supercell occurred between 1500 UTC and 2000 UTC and traversed the southeastern portion of the Adirondack Mountains, strengthened as it moved into the Mohawk Valley, and dissipated into the Catskill Mountains. The 3 km HRRR was used to analyze the mesoscale and storm-scale modifications of the supercell. The supercell interacted with several boundaries from previous convection which helped to produce sufficient shear to support the supercell. The 0-1 km SRH ahead of the cell was 50-100 m^2/s^2 and low LCLs were present,

which may have also helped with tornadogenesis. Tornadoes, especially significant tornadoes, have been associated with lower LCL heights because this limits the subcloud evaporation which decreases the chance for the mesocyclone to be undercut by the cold outflow (Craven and Brooks 2004). There was also backing of the winds in the valley which created enhanced upslope flow in the Adirondacks and coincided with the strengthening of the supercell (Fig. 2.21). These findings were in agreement with the Schneider (2009), Markowski and Dotzek (2011), and Scheffknecht et al. (2017) studies in which upslope flow was important to the strengthening of supercells.

2.4.2 Tornadic and Non-Tornadic Supercell Outbreak in Southwest Virginia on 28 April 2002

On 28 April 2002, there were several isolated long-lived supercells that developed to the west of the Appalachians and moved east through the mountains into the Piedmont of eastern Virginia and central North Carolina (Keighton et al. 2004). This system produced 4 isolated supercells which produced an EF4 tornado and three weak tornadoes. The EF4 tornado was associated with the northernmost supercell (Fig. 2.22).

The 2000 UTC RUC analysis proximity soundings from eastern Virginia and central North Carolina illustrated notable variability; the CAPE in north-central North Carolina was around 1500 J/kg, while in west-central Virginia CAPE was much higher, around 2500 J/kg. The 0-3 km SRH was between 250 and 400 m^2/s^2 and 0-1 km SRH was between 150 and 200 m^2/s^2, with increased values to the north indicating a more favorable environment to the north. Many of these supercells maintained their structure as they continued to move across the Appalachian Mountains and dissipated east of the Blue Ridge. This would indicate that higher amounts of

shear and SRH are important to sustain supercellular structures as they traverse across complex terrain.

2.5 Summary

Earlier studies have addressed several questions regarding supercells in the Appalachian region. It was found that these supercells follow a similar diurnal and monthly trend to the overall severe weather climatology in the United States (Gaffin and Parker 2006; Stonefield and Hudgins 2006; Lane 2008). Flow channeling and upslope flow appear to be important to the strengthening of supercells as it helps to upwardly transport warm, moist air, which in turn, helps to destabilize the atmosphere (Bosart et al. 2006; Geerts et al. 2009; Gaffin 2012; Prociv 2012; Smith et al. 2016; Tang et al. 2016; Scheffknecht et al. 2017). The lowest 3 km of shear and SRH are also potentially significant parameters whose values would support maintaining supercells across complex terrain (Keighton et al. 2004; Lane 2008; Tang et al. 2016).

These previous research studies have posed several unanswered questions; such as, how does the environment change as supercells move across varying terrain features? What are the key environmental parameters that lead to tornadogenesis as supercells traverse complex terrain?

This study uses 62 observed supercells that interact with complex terrain within the Peachtree City, GA, Greenville-Spartanburg, SC, Jackson, KY, Charleston, WV, Blacksburg, VA, and Morristown, TN National Weather Service CWAs. The goal of this study is to be able to enhance short-term forecasts and better understand how supercells interact with complex terrain. This project will 1) identify how the inflow environments of supercells are modified as they interact with terrain, and 2) identify environmental differences that support crossing and non-crossing supercells.

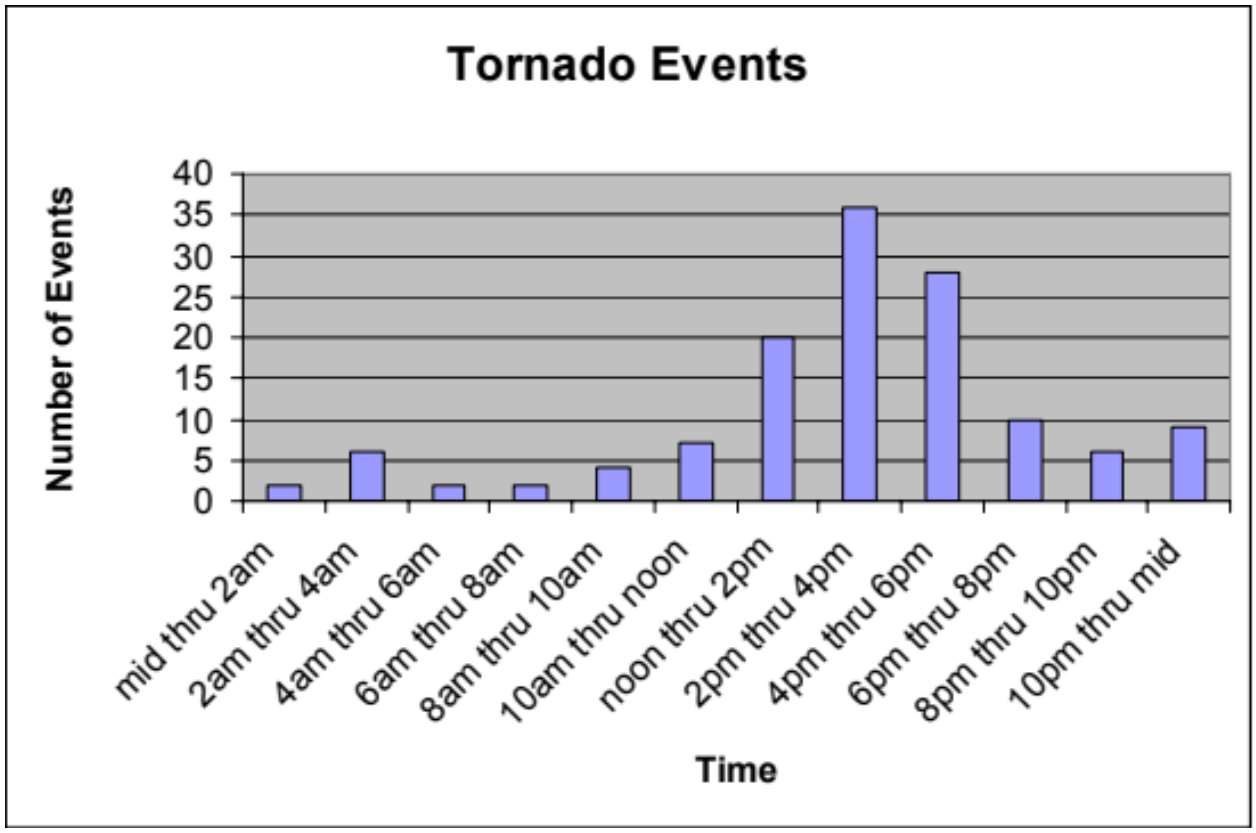

Figure 2.1: Tornado events by hour between 1950-2005 in the Blacksburg, VA CWA (from Stonefield and Hudgins 2006).

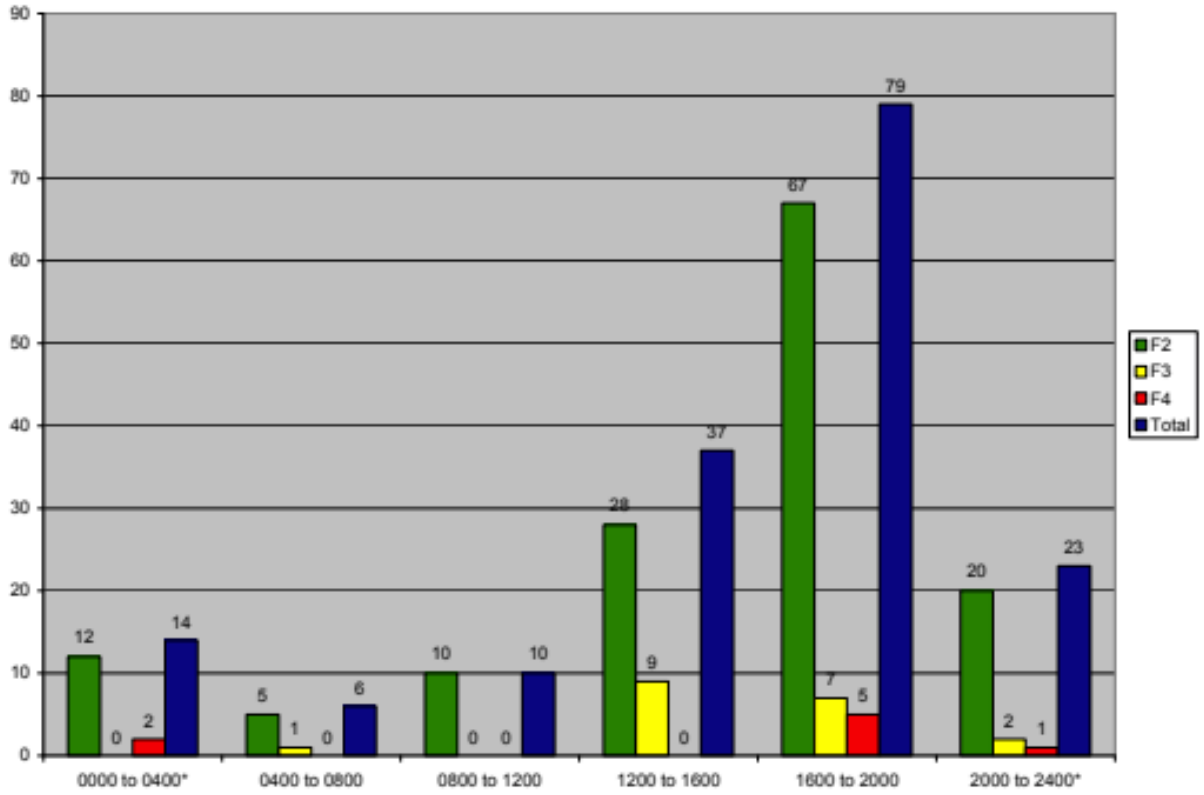

Figure 2.2: Diurnal distribution of tornadoes between 1800-2006 in the Greenville-Spartanburg, SC CWA (from Lane 2008).

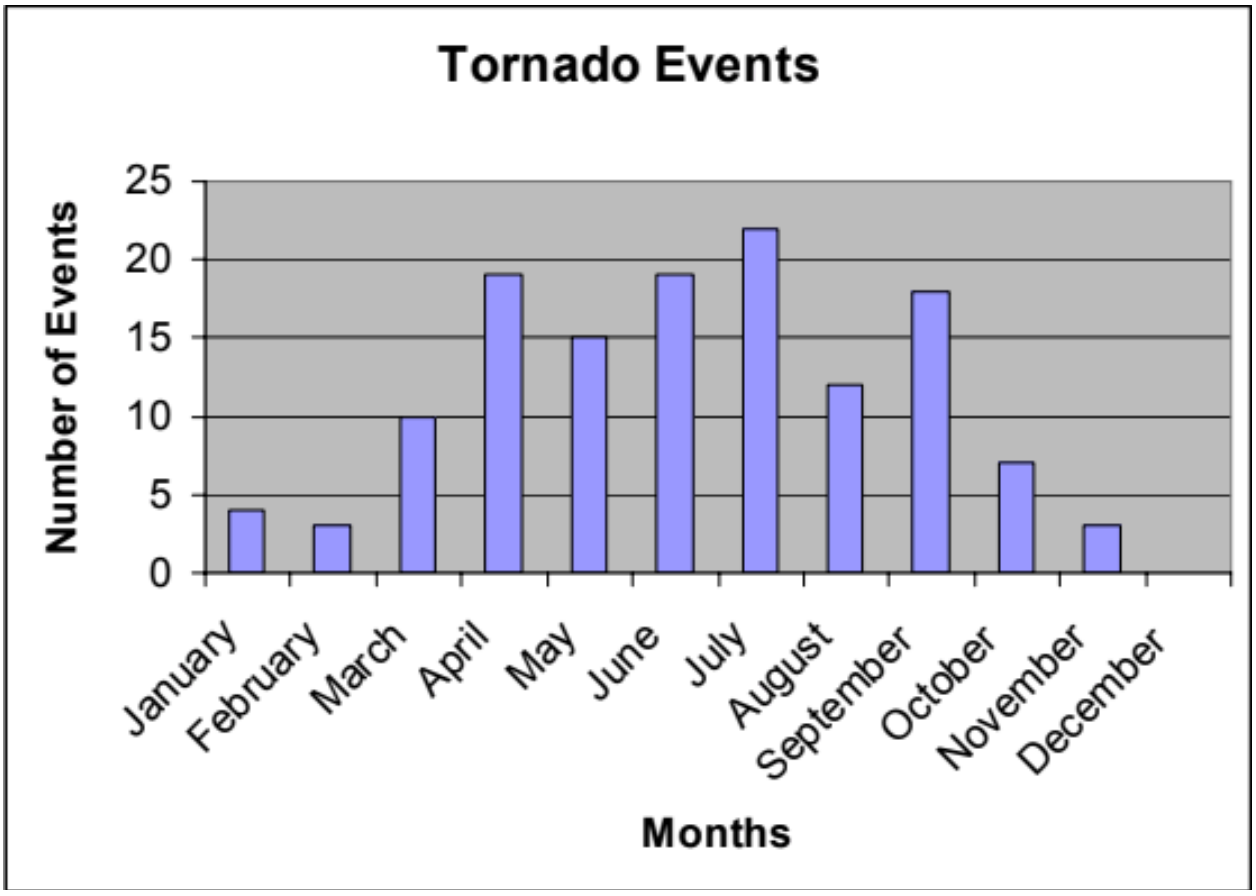

Figure 2.3: Tornado events by month between 1950-2005 in the Blacksburg, VA CWA (from Stonefield and Hudgins 2006).

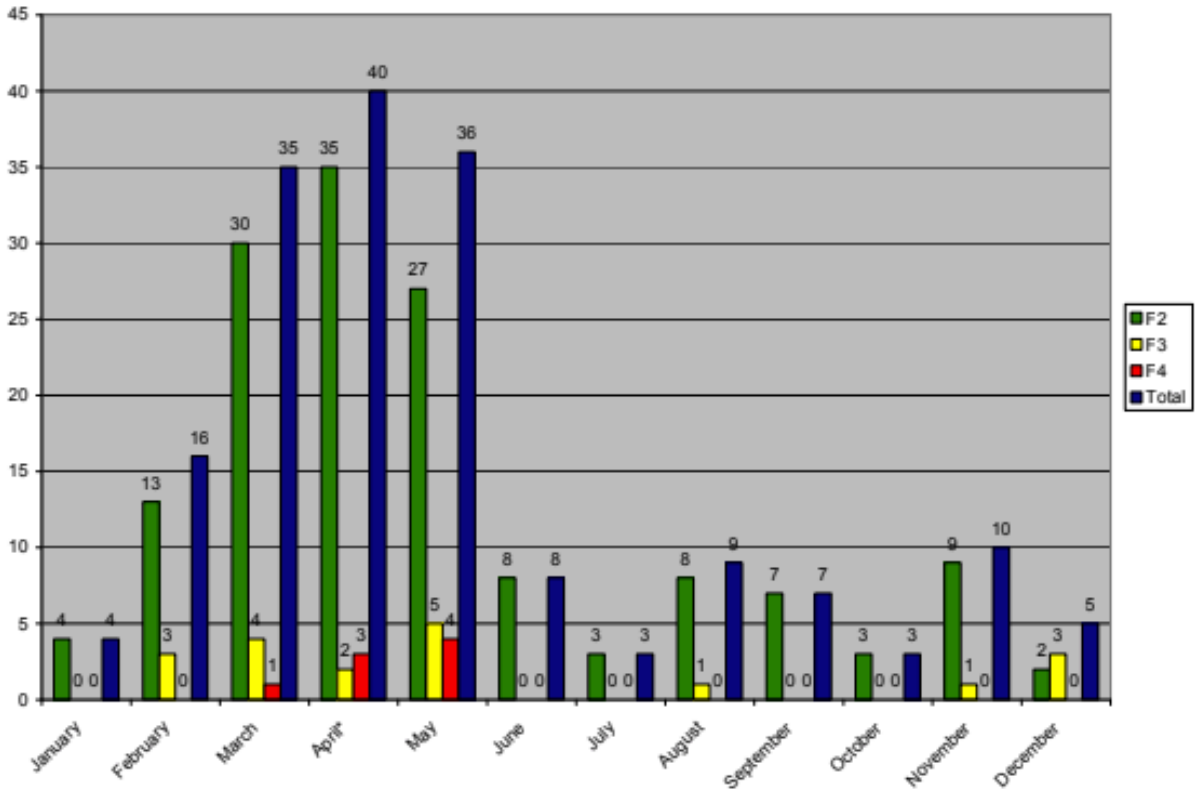

Figure 2.4: Monthly distribution of tornadoes between 1800-2006 in the Greenville-Spartanburg, SC CWA (from Lane 2008).

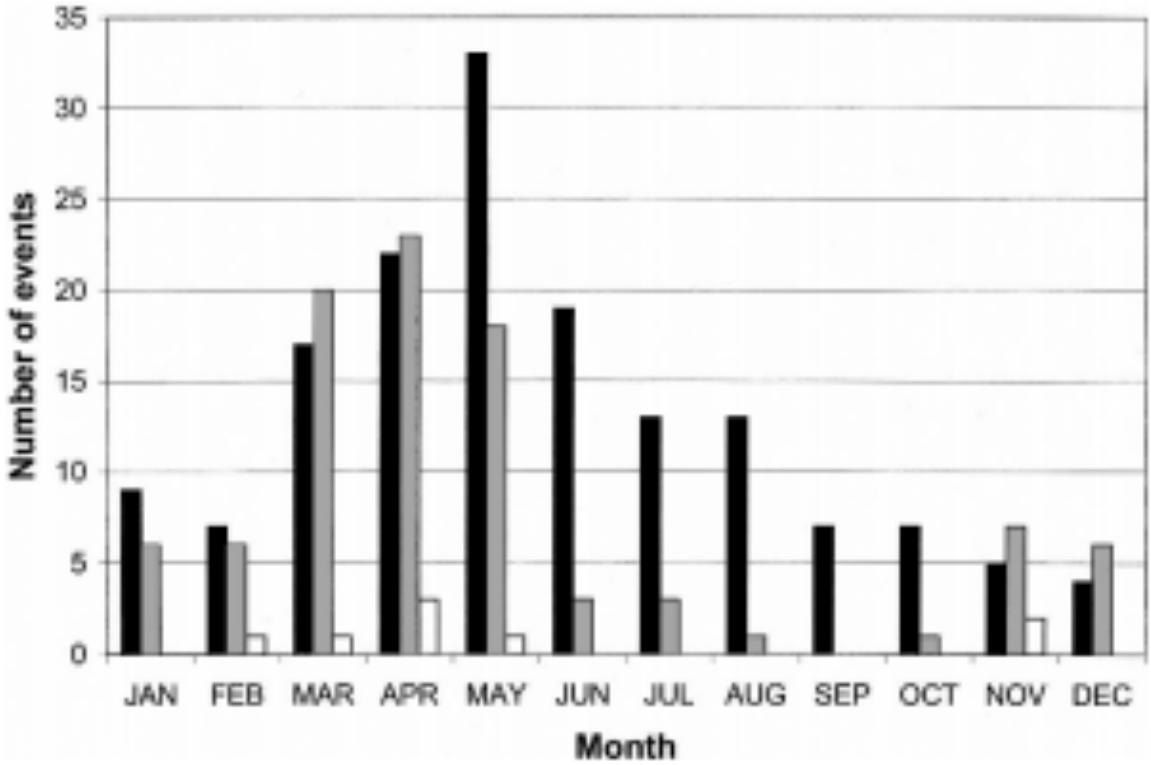

Figure 2.5: The numbers of outbreak (white bars), significant (gray bars), and weak (black bars) tornado events across the southern Appalachian region by month (from Gaffin and Parker 2006).

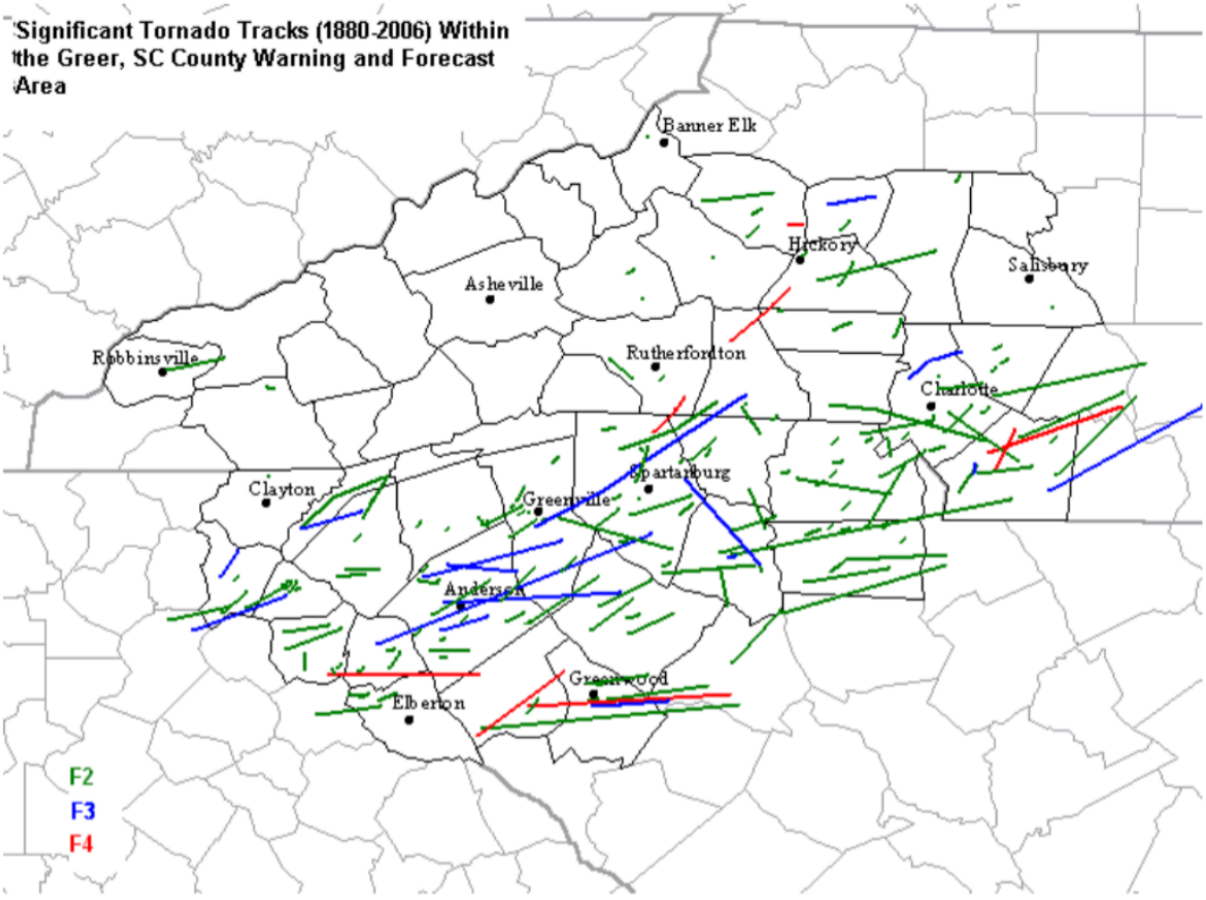

Figure 2.6: Significant tornado tracks between 1880 and 2006 in the GSP CWA (from Lane 2008).

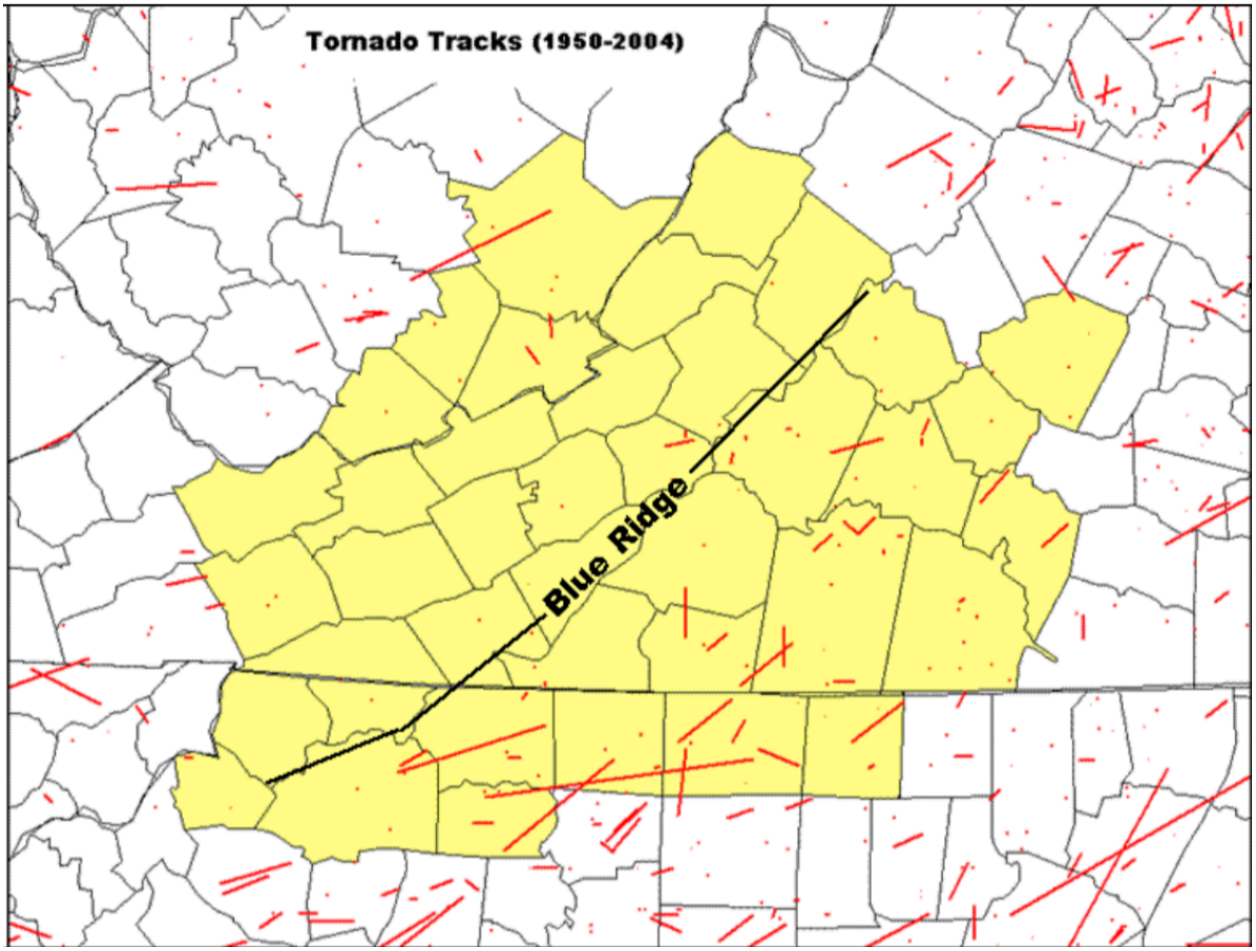

Figure 2.7: Tornado tracks between 1950 and 2004 within the Blacksburg, VA CWA (yellow) (from Stonefield and Hudgins 2006).

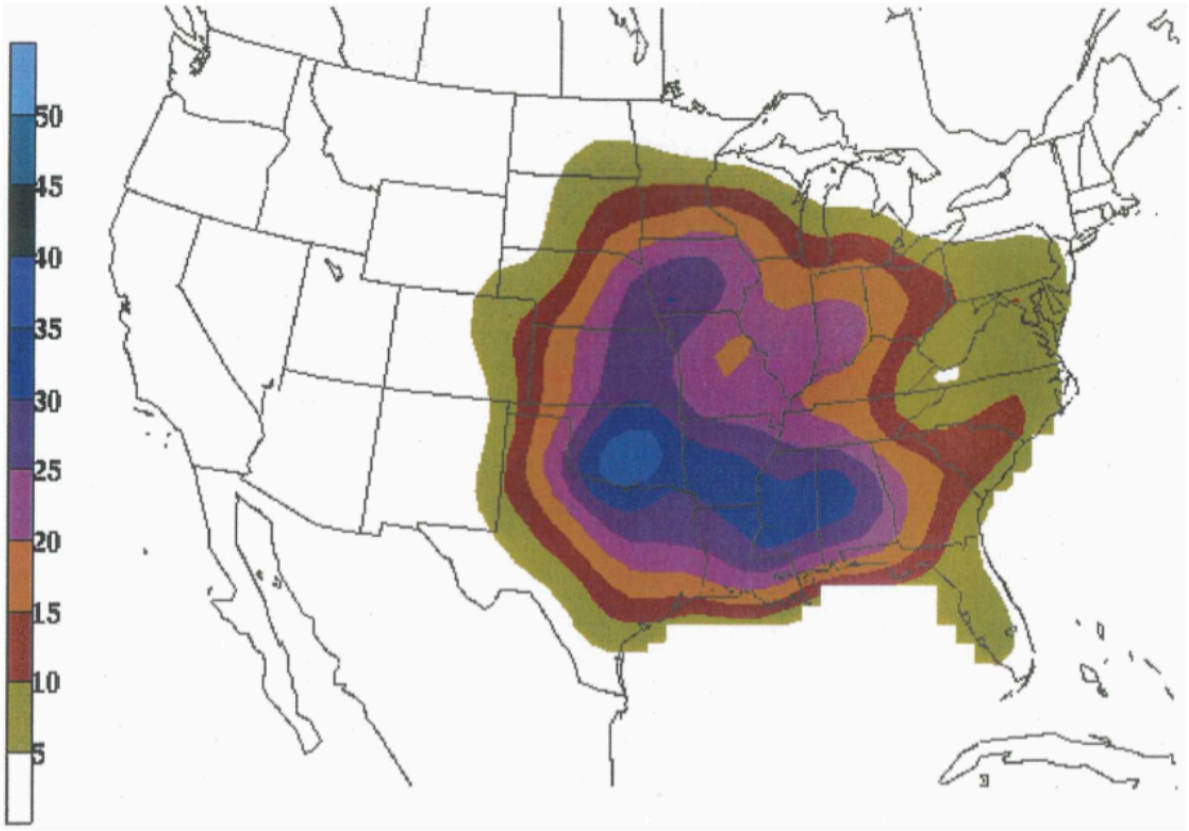

Figure 2.8: Number of significant tornado (EF2+) days between 1925 and 1995 (from Concannon et al. 2000).

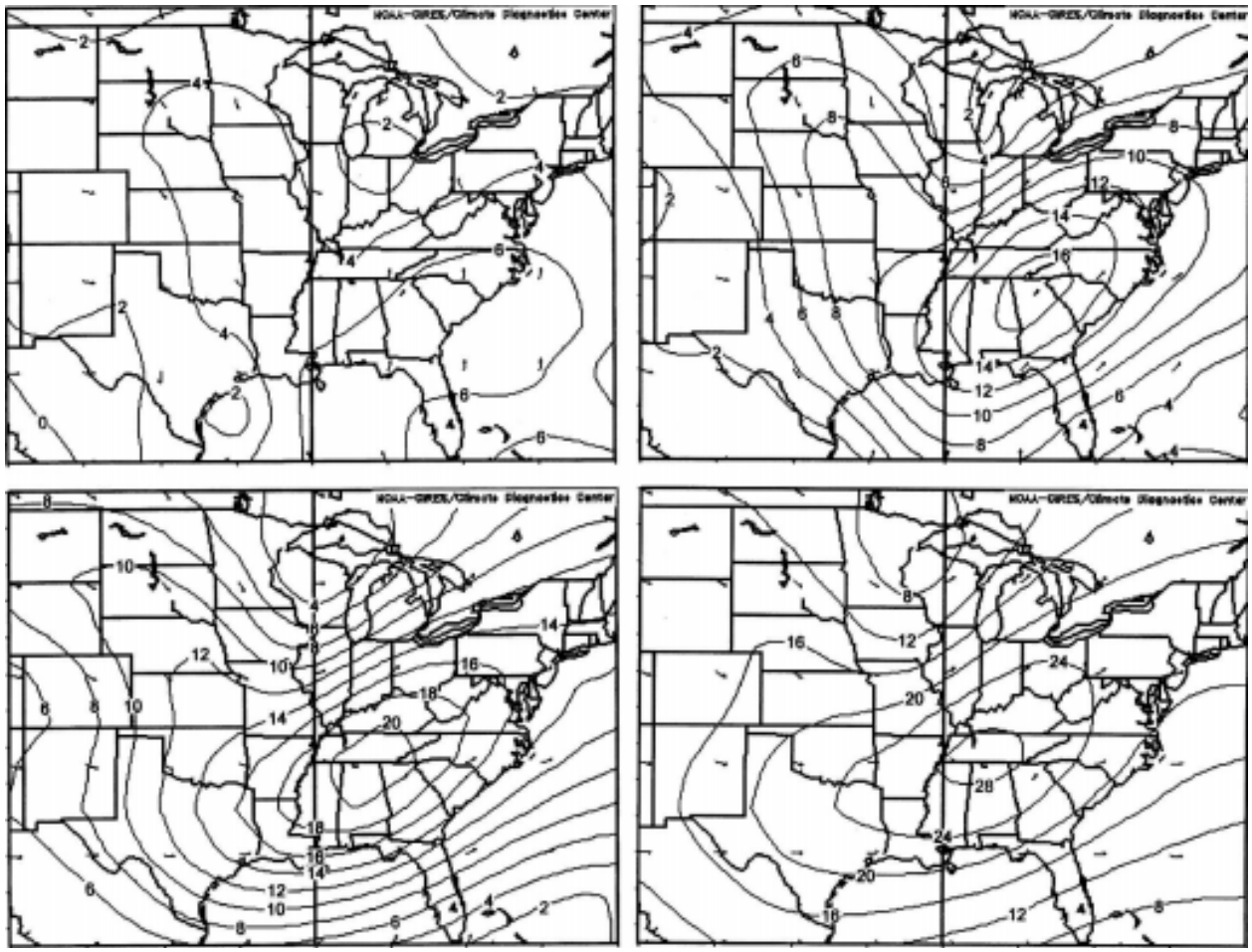

Figure 2.9: Composite maps of significant tornado events in the southern Appalachians, surface wind speeds m/s (top left), 850 hPa wind speed (m/s) (top right), 700 hPa wind speed (m/s) (bottom left), and 500 hPa wind speed (m/s) (bottom right) (from Gaffin and Parker 2006).

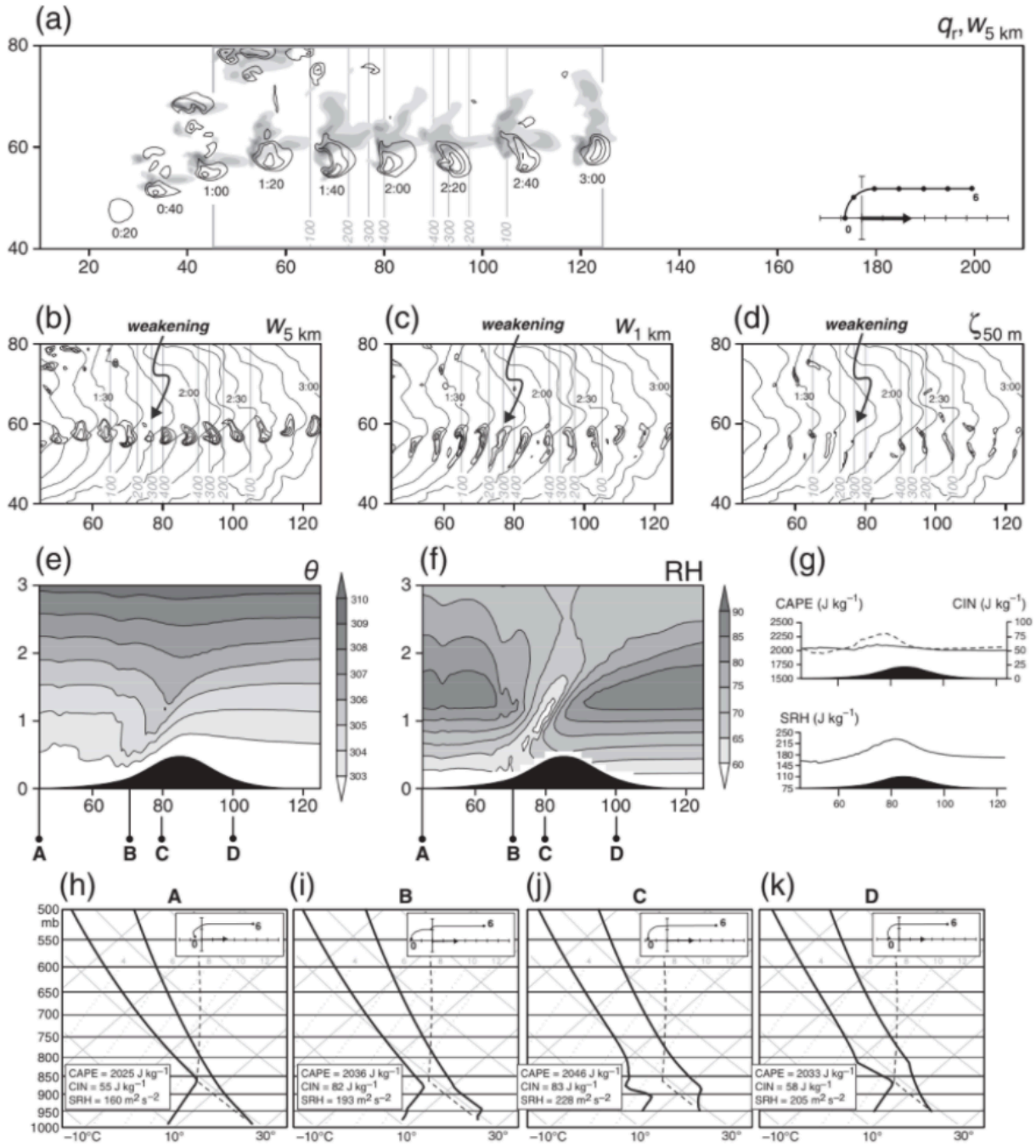

Figure 2.10: Model output of a simulation of a case using a 500 meter tall hill. (a) representing the precipitation and vertical motion produced by the supercell every 20 minutes. (b), (c), and (d) representing the vertical velocity at a height of 5 km, 1 km, and 50 m above ground respectively. (e) and (f) cross sections of potential temperature and relative humidity respectively. (g) Horizontal profiles of CAPE, CIN, and SRH. (h)-(k) Skew T-log p diagrams at the four different locations of the supercell A-D (from Markowski and Dotzek 2011).

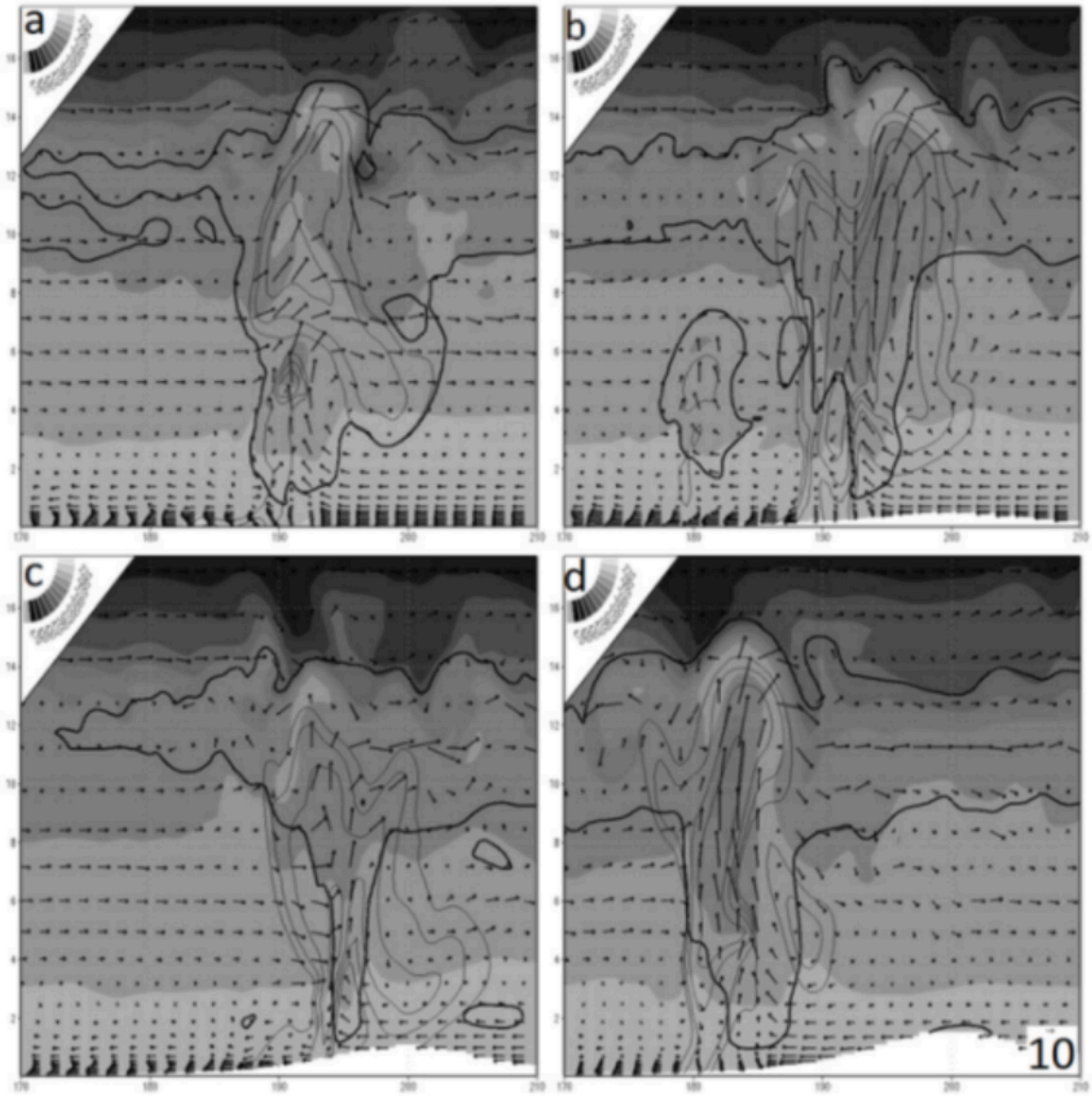

Figure 2.11: Cross sections of potential temperature, reflectivity, cloud outline, and wind vectors with theta shaded at 180 minutes of four different cases. (a) case with no mountain, (b) case with 500 meter tall mountain, (c) case with 1000 meter tall mountain, and (d) case with 1500 meter tall simulations (from Smith et al. 2016).

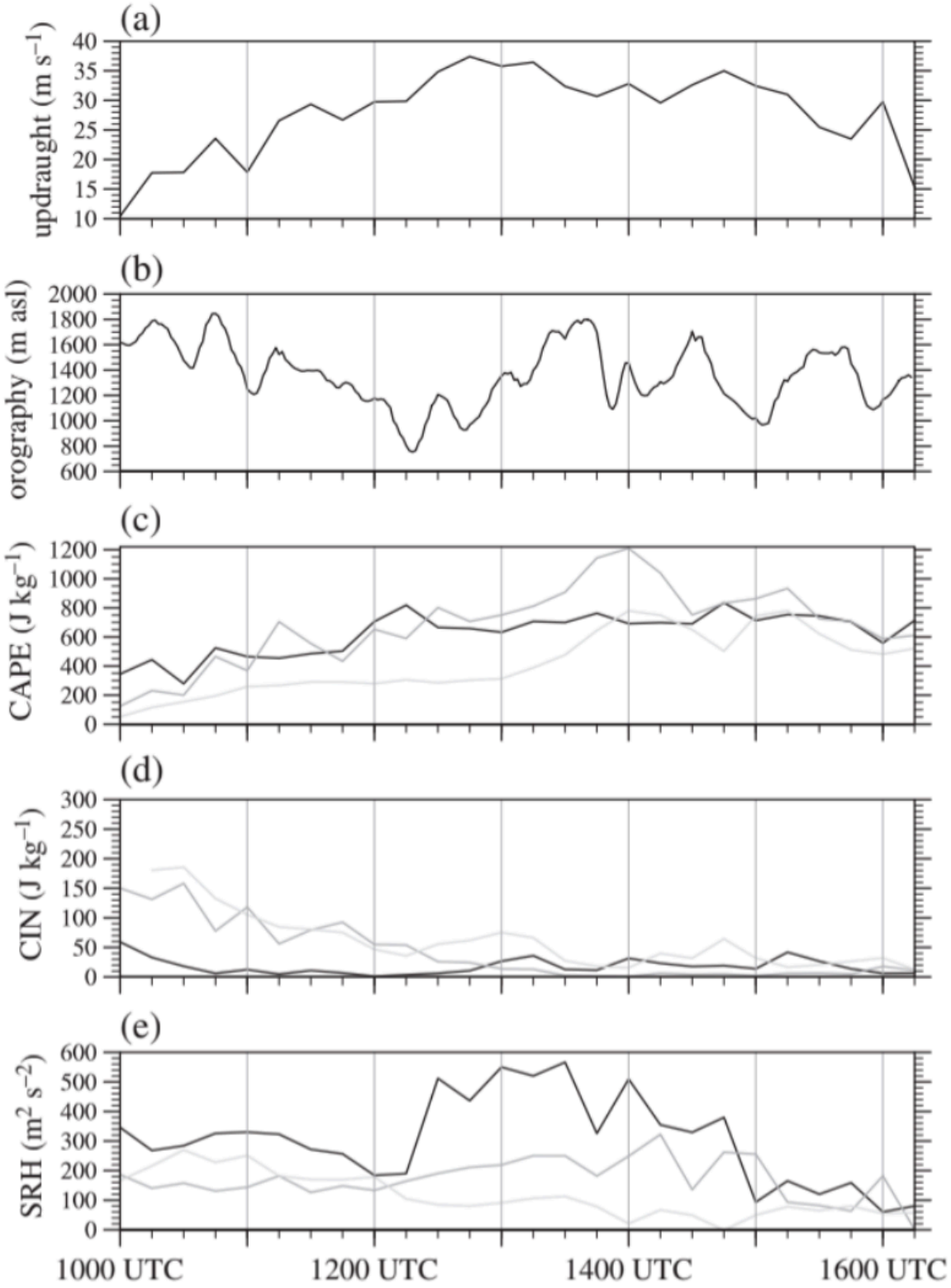

Figure 2.12: Time series of a) updraft strength, b) the elevation the supercell encountered, c) CAPE, d) CIN, and e) SRH. The three different lines in c, d, and e indicate the conditions of varying times before storm arrival. Black is 15 minutes before arrival, dark grey is 60 minutes before arrival, and light grey is 180 minutes before arrival (from Scheffknecht et al. 2017).

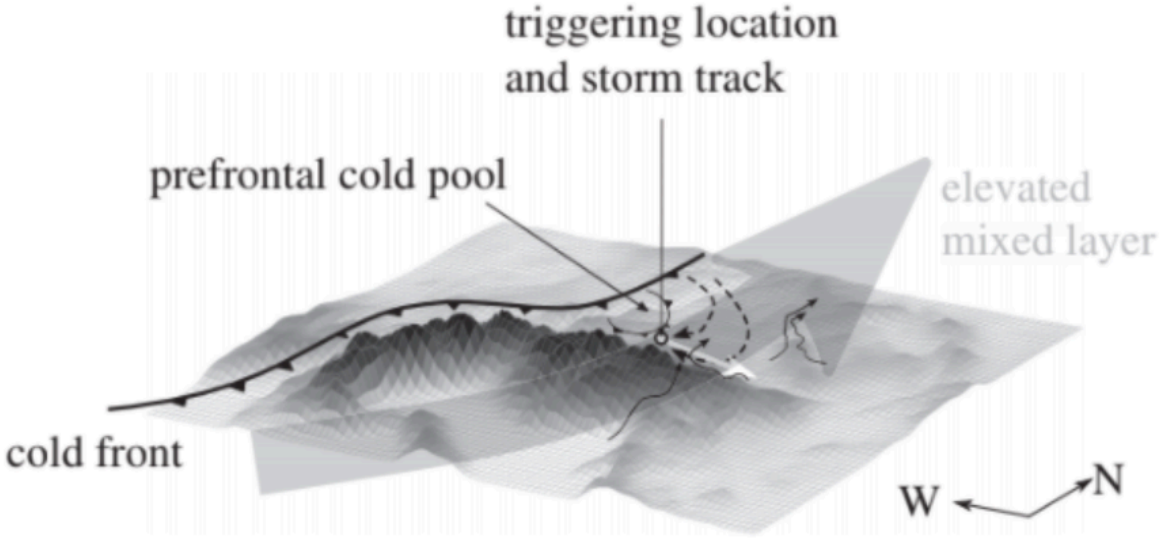

Figure 2.13: Schematic illustrating the synoptic scale surface pattern and terrain influencing the initiation of the development of the supercell north of the Alps on 2 August 2007 (from Scheffknecht 2017).

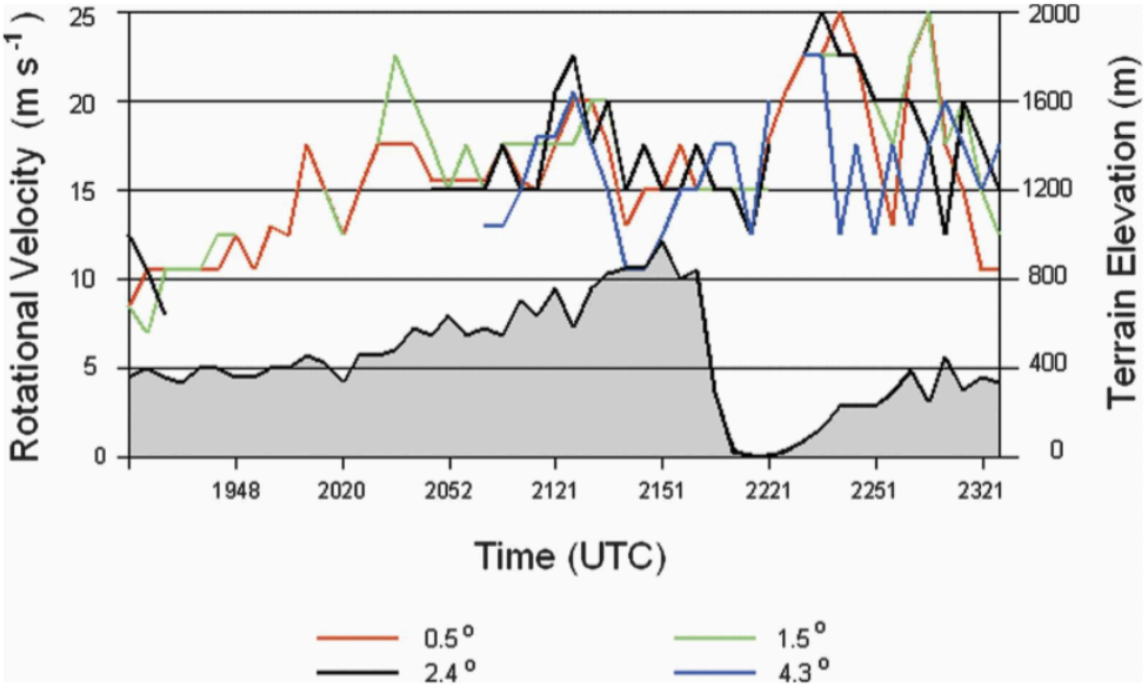

Figure 2.14: Time series of rotational velocity, using different beam angles, of KBGM and KENX between 1913 and 2321 UTC on 29 May 1995 following the track of the supercell in relation to the terrain (from Bosart et al. 2006).

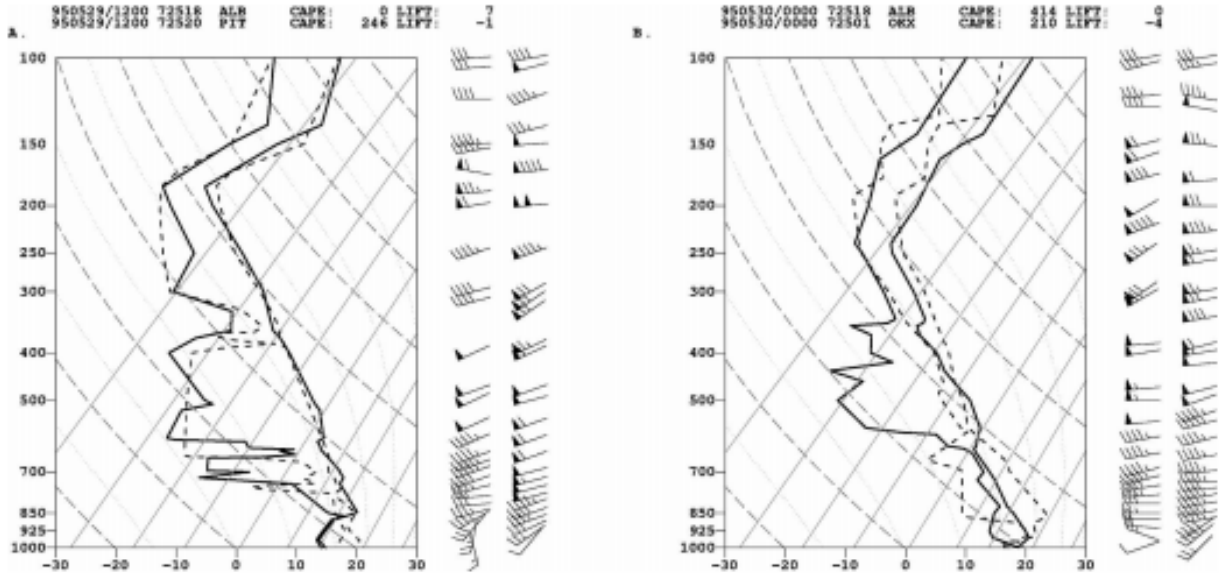

Figure 2.15: Observed soundings at 1200 UTC at 29 May 1995 (left) at ALB (solid) and PIT (dashed) and 0000 UTC at 30 May 1995 (right) at ALB (solid) and PIT (dashed) (from Bosart et al. 2006).

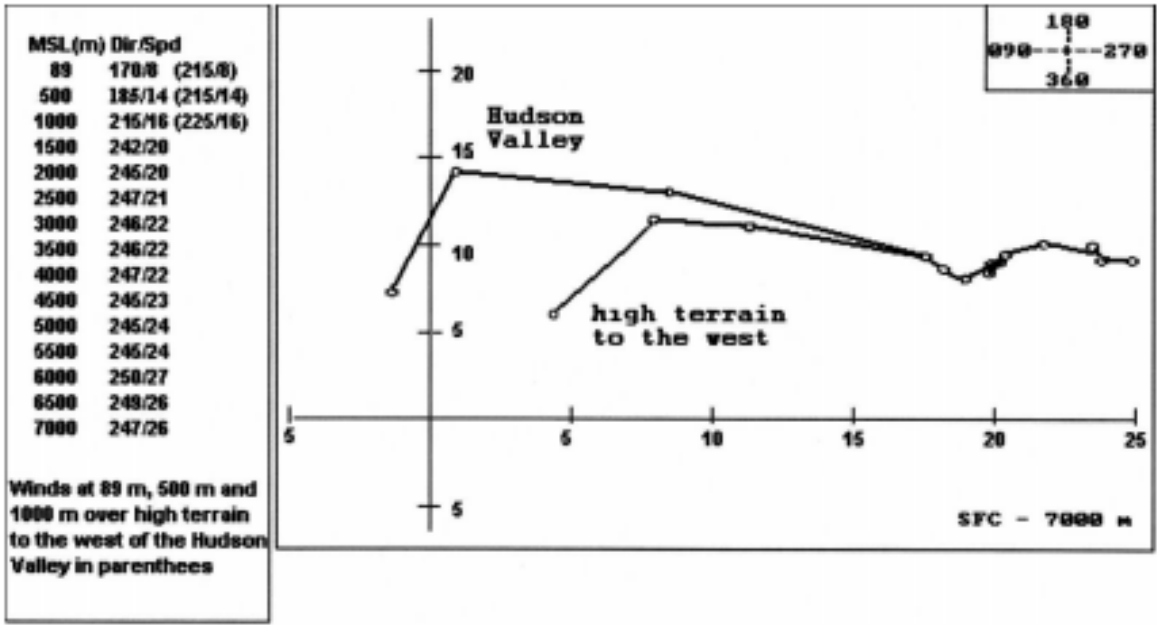

Figure 2.16: Estimated hodograph for the Hudson Valley and higher terrain to the west in the Catskills based off of the 1200 UTC 29 May 1995 ALB observed sounding (from Bosart et al. 2006).

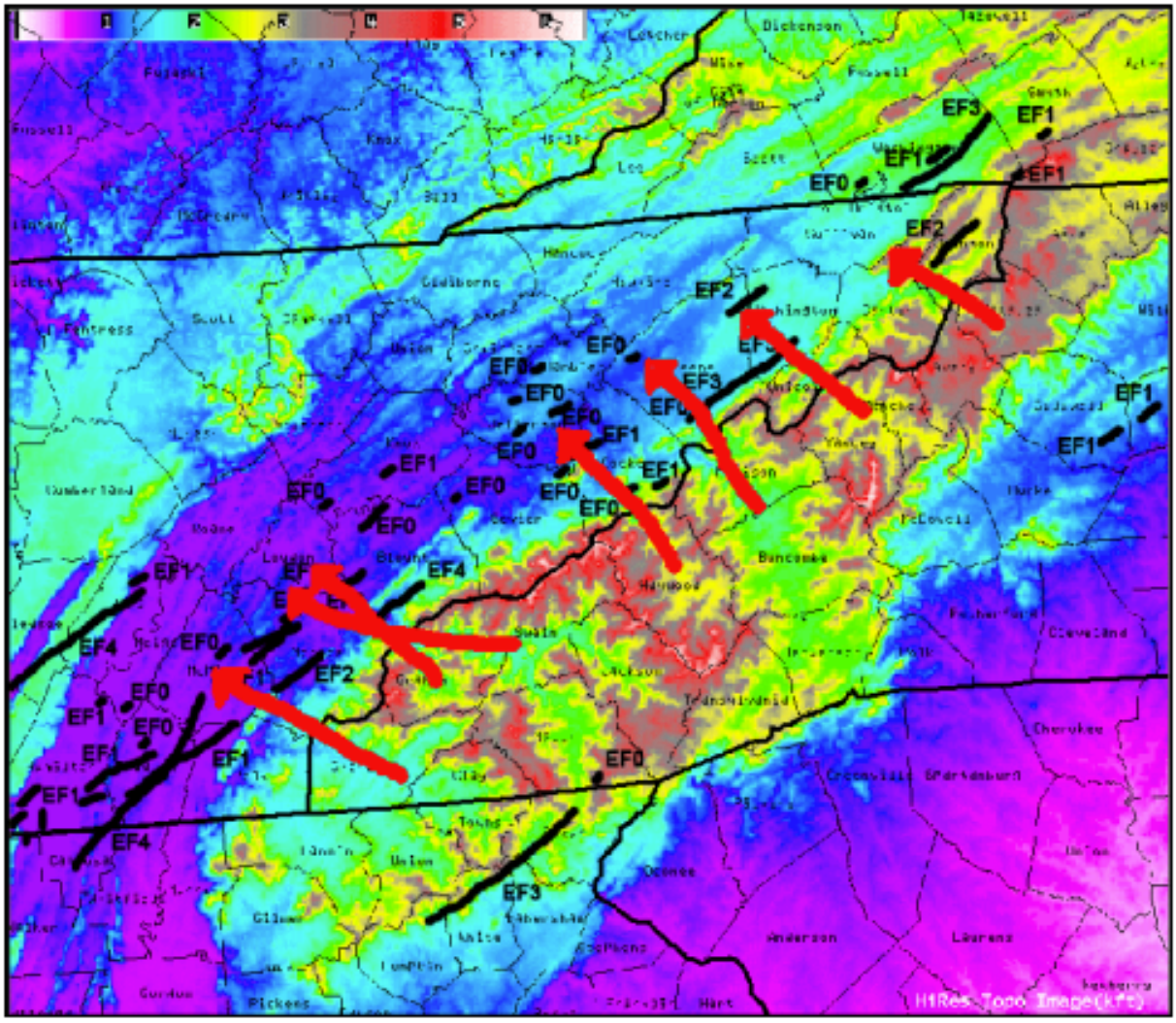

Figure 2.17: The tracks and intensities of the tornadoes that were produced during the 27-28 April 2011 Outbreak across the southern Appalachians (black lines) and the likely path of the southeasterly winds channeling through the northwest to southeast valleys (red arrows) (from Gaffin 2012).

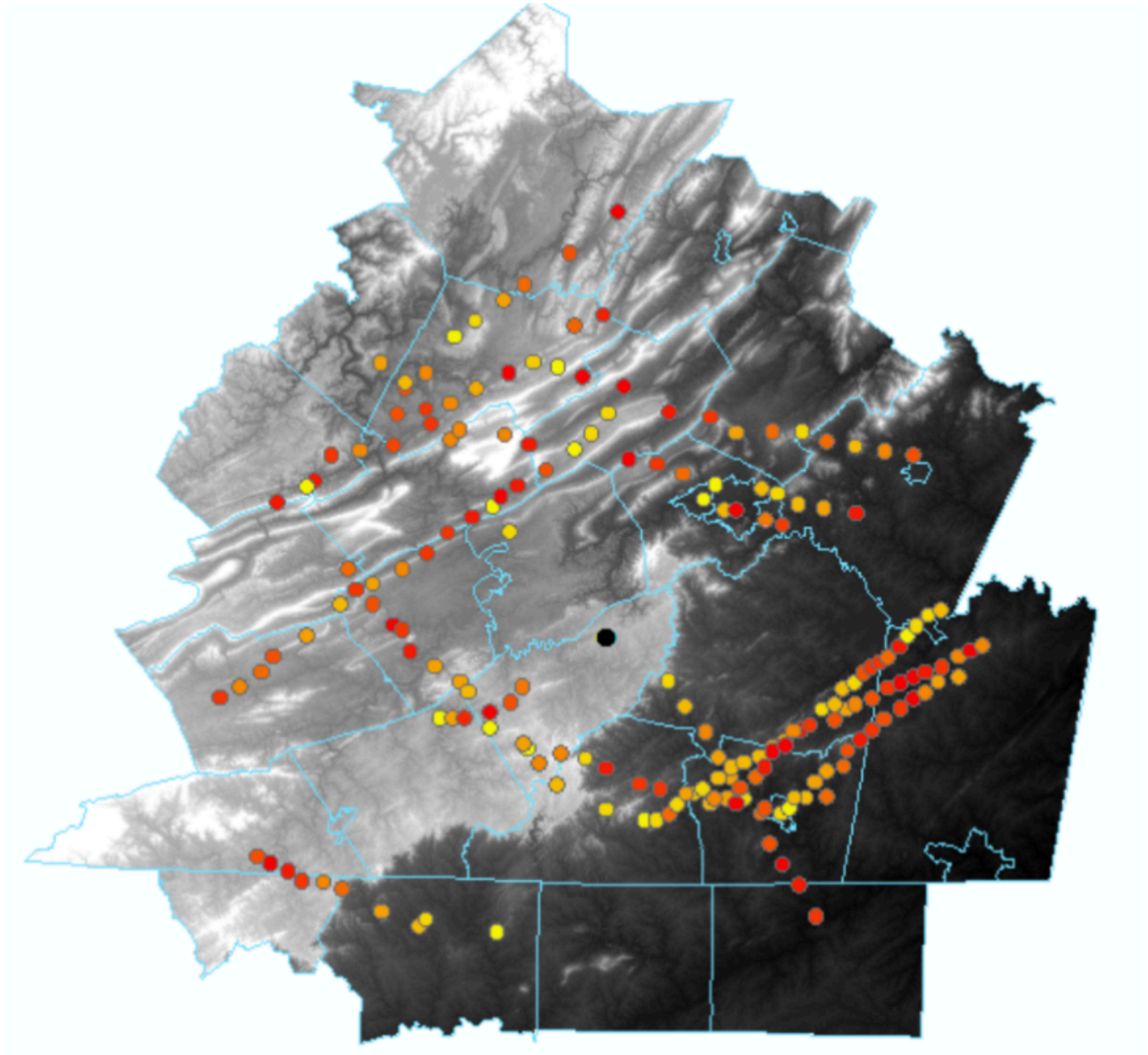

Figure 2.18: The tracks of the 14 supercells within the Blacksburg, VA CWA. The symbology changes from yellow to red when rotational velocity increases (from Prociv 2012).

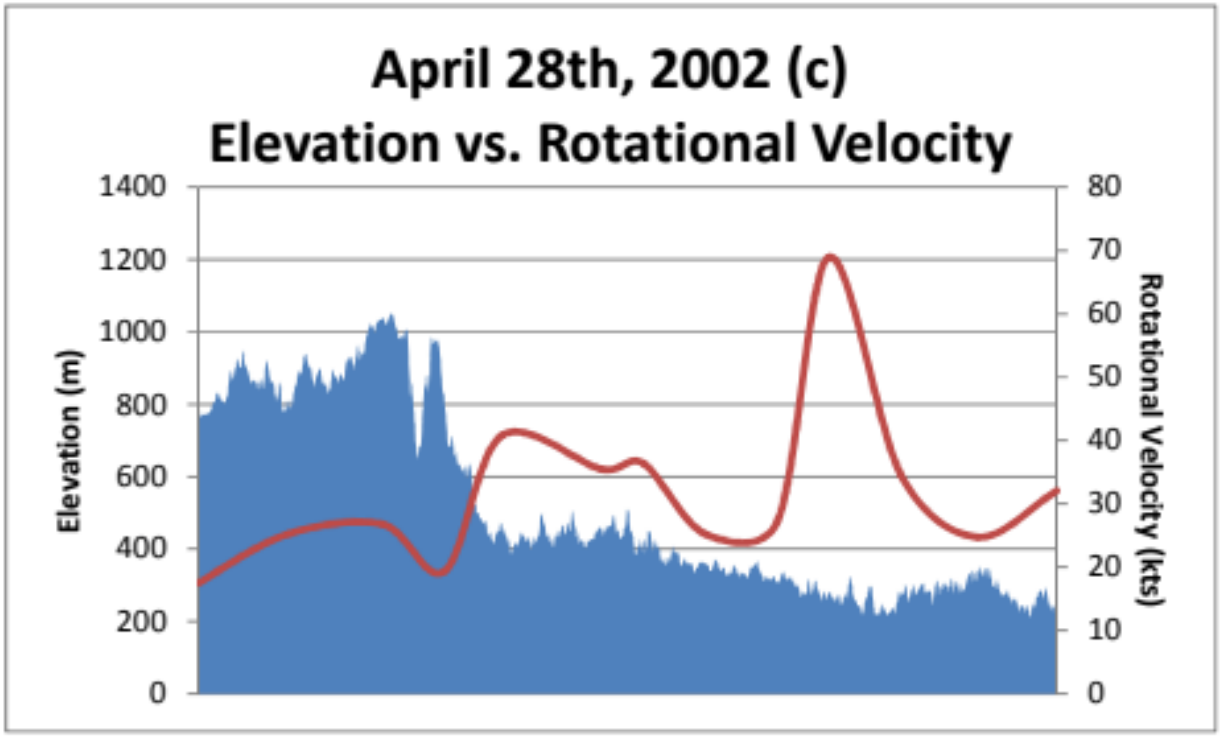

Figure 2.19: Profile of terrain compared to the rotational velocity (kts) from the 28 April 2002 near Blacksburg, VA (from Prociv 2012).

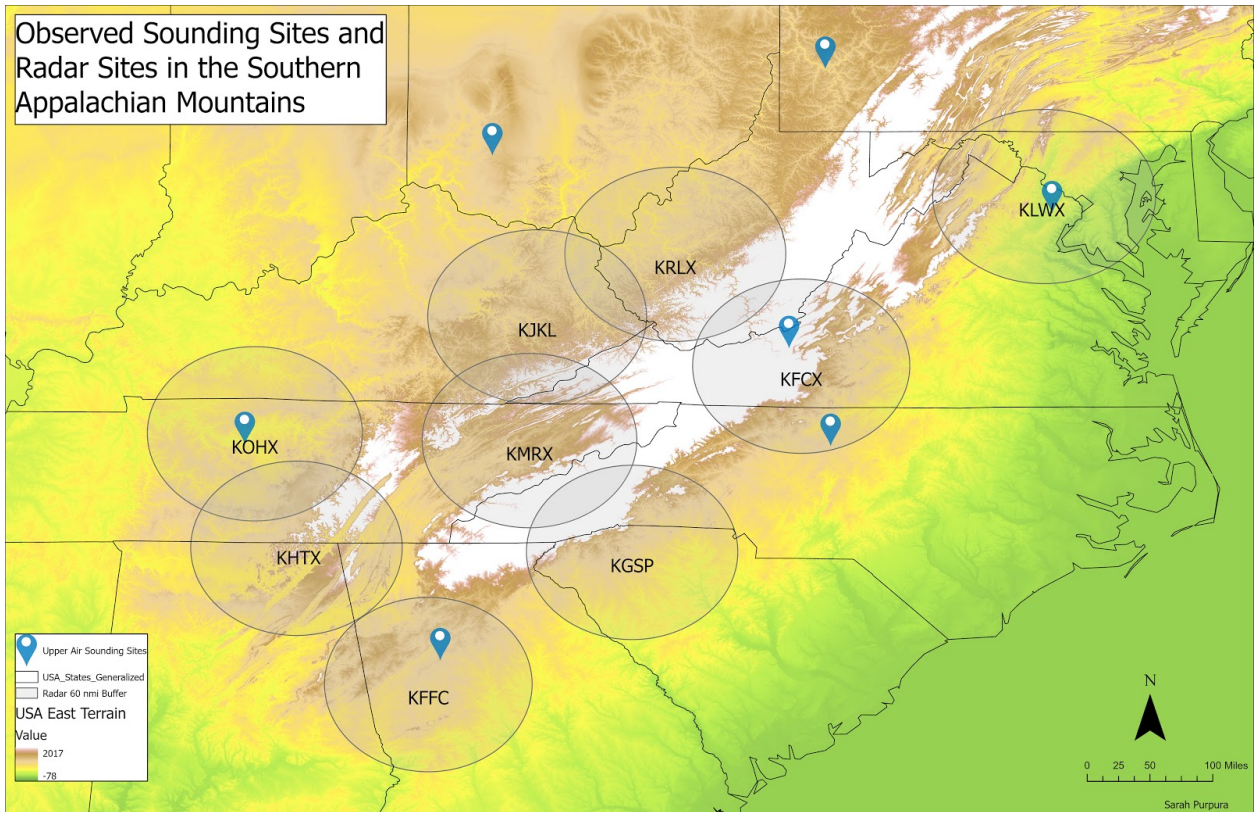

Figure 2.20: Observed sounding sites and the radar sites in the case study domain terrain features.

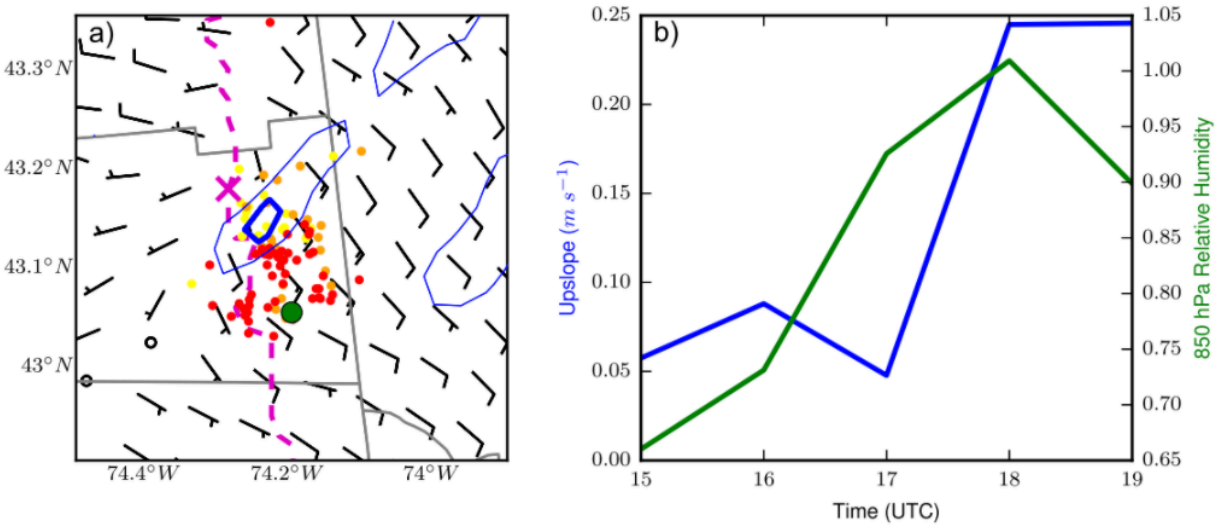

Figure 2.21: (a) 1800 UTC HRRR analysis of the 80 meter wind (barbs), upslope flow (blue lines), yellow, orange, and red dots indicating lightning flashes between 1800-1820, 1820-1830, 1830-1840 UTC respectively, and the track of the mesocyclone (purple dashed lines). (b) The upslope flow from the 1500-1900 UTC HRRR analysis (blue) and relative humidity at 850 hPa (green) (from Tang et al. 2016).

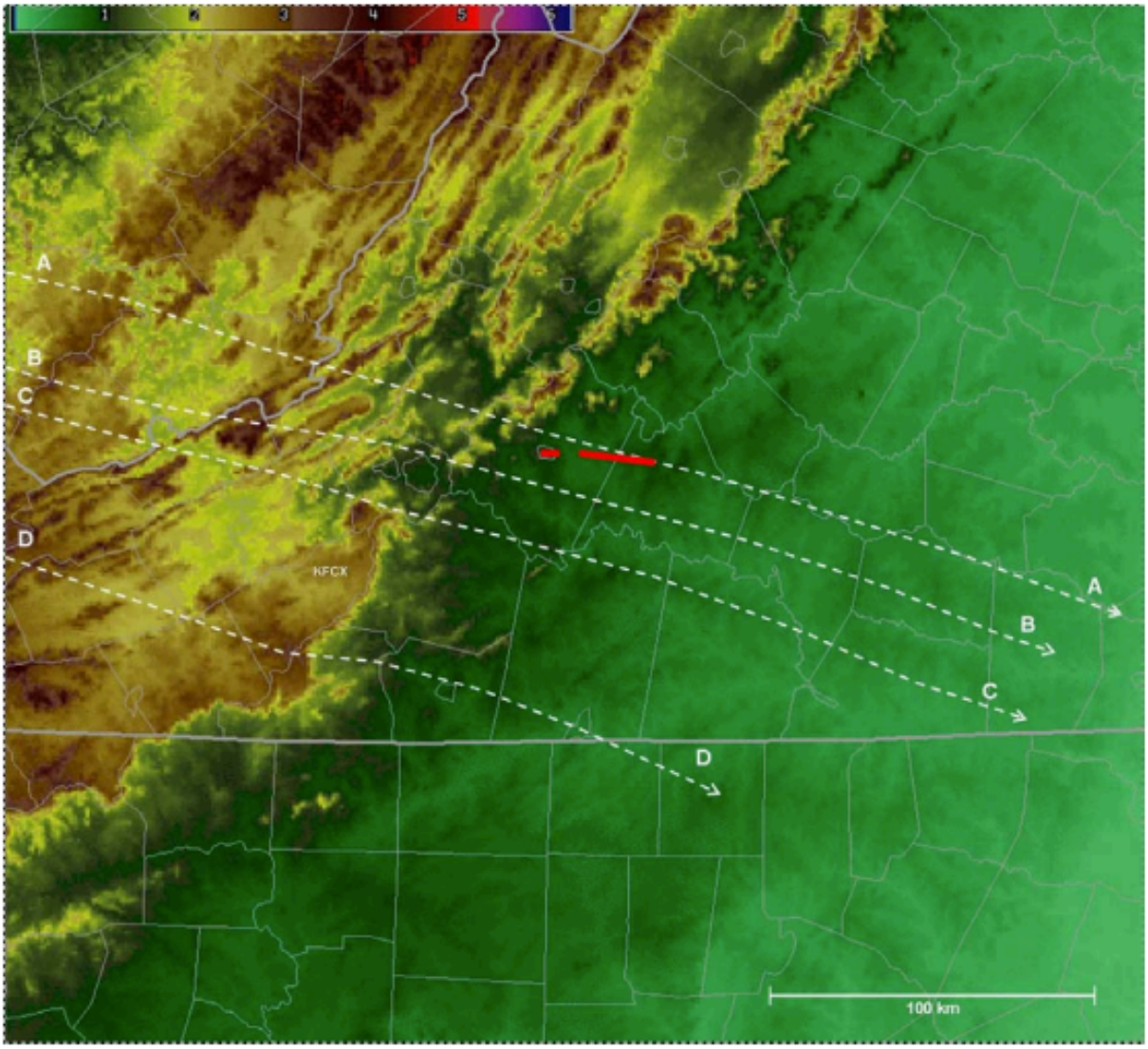

Figure 2.22: Four supercell tracks that occurred on 28 April 2002 and developed to the west of the Appalachian Mountains and moved in the Piedmont of North Carolina and Virginia (white dashed lines) and the track of the EF4 tornado (red lines) (from Keighton et al. 2006).

Chapter 3: Data and Methods

3.1 Radar Interpretation

The dataset used in this study originated from a list of 75 candidate case dates of isolated supercells interacting with the Appalachians between 2000 and 2019. These dates were identified by examining Storm Prediction Center (SPC) tornado reports within the central and southern Appalachians. The reports were further scrutinized using local and national radar data to only retain those associated with supercell thunderstorms, and then limited to those where convection was initiated on the upstream side of the mountains. Finally, following discussions with central and southern Appalachian WFOs, the event dates were further limited to between 2009 and 2019 when RUC/RAP hourly analyses were readily available.

To identify individual supercells on each potential date, storms were manually tracked using GR2Analyst with data from the NCEI NOAA NEXRAD Level II archive, starting in 2019 and working in reverse chronological order. Isolated tornadic supercells, isolated non-tornadic supercells, and isolated non-severe supercells were manually tracked across individual radar volume scans (approximately every 5 minutes) from initiation to dissipation, or when the supercell became linear or merged with other convection. For a supercell to be considered isolated, the storm had to be approximately a storm's width away from other convection (e.g., Bunkers et al. 2006; Gropp and Davenport 2018). The presence of a rotating updraft was identified using base velocity and normalized rotation (NROT). This process identified 142 isolated supercells. However, an additional supercell lifetime restriction of at least 2 hours was imposed to ensure that temporal and spatial variability could be measured reasonably in the model analysis data; this limitation decreased the total number of isolated supercells to 62 (see further discussion in section 3.3).

During each volume scan throughout the supercell's lifetime, a few key characteristics were collected. These parameters include: the time, the angle of the beam, the distance the supercell was from the radar, the elevation of the beam, the longitude and latitude of the supercell, the severe weather reports at each point, and whether the supercell dissipated or became linear. The time, latitude and longitude of the supercell mesocyclone during each scan was included to identify where the supercells were located. Severe weather reports and the dissipation or linearization points were also collected to determine where the supercell produced severe weather and when it reached its demise in relation to the terrain.

To track the supercells, the KMRX, KRLX, KFCX, KFFC, KGSP, KJKL, KBMX, KHTX, KDGX, and KGWX radar sites were used (Fig. 3.1). The database was limited to supercells that passed within 60 nmi of a radar (to minimize mesocyclone size and location errors associated with the conical radar volume geometry; Prociv 2012), but the entirety of each supercell lifecycle (i.e., from initiation to dissipation or linearization beyond 60 nmi from any radar) was tracked using a combination of Doppler winds and radar reflectivity. For each volume scan, the supercell location was determined as either the center of base-level mesocyclone rotation (if present) or the center of base-level radar reflectivity. The supercells were manually tracked, which may have reduced the accuracy of the center point of the supercell due to an element of human error.

Out of the 62 supercells, 15 passed through KMRX, 12 passed through KRLX, 14 passed through KFCX, 5 passed through KFFC, 7 passed through KGSP, and 23 passed through KJKL within a 60 nmi radius (Table 1). Using elevation change, extracted from a Digital Elevation Model (DEM) described in the next section, the altitude of each supercell throughout its lifetime was analyzed and plotted as a time series. From these time series and supercell tracks, the

supercells that crossed or did not cross the Appalachian Mountains were determined. A crossing supercell (***crosser***) had to have a distinct "up and over" pattern in the time series, indicating it traversed significant terrain. A crossing supercell also had to cross the entirety of either the Cumberland Plateau, Blue Ridge Mountains, or the Allegheny Mountains. The remaining supercells were considered ***non-crossers***. Among the non-crossers, four subsets emerged: 1) the supercell started at low elevation and dissipated or became linear at low elevation (LL), 2) the supercell started at low elevation and dissipated or became linear at high elevation (LH), 3) the supercell started at high elevation and dissipated or became linear at low elevation (HL), or 4) the supercell started at low elevation, died at low elevation, and interacted with complex terrain (by exhibiting the "up and over pattern" associated with crossers) but did not cross the entirety of any of the three prominent terrain features to be considered a crosser (CT) (Figure 3.2). A "low elevation" was considered below 500 meters and a "high elevation" was considered above 500 meters (i.e., in line with heights tested in Markowski and Dotzek 2011).

3.2 GIS

ArcPro was used for the analysis and plotting of the supercells. The use of ArcPro aided in finding the elevation of the points of the low-level mesocyclone, collected every 5 minutes via radar, to analyze where the supercells tracked in relation to complex terrain. The maps created were set at the WGS 84 Mercator projection.

Using the latitude and longitude of the points of the low-level mesocyclone, a shapefile of points were created and plotted using the tool "xy to point". Another shapefile was created with lines of the supercell tracks using the "xy to line" tool. Using the Eastern US Elevation DEM and the point shapefile, the extract by multipoints tool was used to get the elevation at each point of the life cycle. Terrain features were determined using a 30-m (1-arc-second) DEM

obtained from the USGS online data portal. From there, the table that contained the points and the elevation were combined and exported to an excel spreadsheet using the "table to excel" tool.

3.3 RAP and RUC Data

To overcome issues with limited radar and upper-air observations in the Appalachian Mountains, the hourly 13 km RAP and RUC (Benjamin et al. 2004; Benjamin et al. 2016) was used to identify storm-scale environmental information associated with each supercell. The NCEI THREDDS server and NCEI AIRS was used to gather the RAP and RUC data for the supercells. For each supercell, three inflow soundings were collected throughout its lifetime at key points during its interaction with complex terrain, including: 1) the initiation point of a supercell or when the supercell became discrete (upstream), 2) the point of highest elevation the supercell crossed (peak), and 3) the point of dissipation or when the supercell became linear (downstream; Figs. 3.3-3.4). As a result of some missing RAP and RUC data, only 59 out of the 62 supercells environments were analyzed; this change resulted in 36 non-crossers and 23 crossers for analysis. The soundings were pulled during the hour of the initiation, peak elevation, and the dissipation or linear stage of the supercell. If the supercell sounding was to be pulled between the 45-59 minutes of the hour, the next hour would be used. If the highest elevation of the supercell occurred at the dissipation or linear phase of the supercell, then the next highest elevation was used. Each sounding that was pulled were at least 4 volume scans away (about 20 minutes) from the other to guarantee a spatial difference between the three soundings.

For each supercell, a series of parameters were calculated to quantify the thermodynamic and kinematic environments at different stages of its interaction with terrain; these parameters were determined based on both prior research on severe convective storms, as well as in

collaboration with Appalachian-region NWS offices. Python was used to siphon in the RAP and RUC data and then calculate 30 different parameters using MetPy and SharpPy (May 2016; Blumberg et al. 2017). The lifted condensation level (LCL), level of free convection (LFC), and equilibrium level (EL) were calculated as the variations of these levels can potentially indicate favorability for tornadogenesis (e.g., Thompson et al. 2003; Craven and Brooks 2004). The 0°C height, -20°C height, the wetbulb zero height were also calculated as these parameters help to determine if severe hail would occur (Lenning et al. 1998). Bulk vertical wind shear and storm relative helicity (SRH) were calculated over several layers, including 0-1, 0-3, and 0-6 km shear, and 0-1 and 0-3 km SRH; these parameters play an important role in supporting the development and maintenance of a rotating updraft (e.g., Davies-Jones 1984; Rotunno and Klemp 1985; Moller et al. 1994; Thompson et al. 2003; Thompson et al. 2007). Variations in convective available potential energy (CAPE), and convective inhibition (CIN) were calculated as these parameters also play a key role in supercell development (Moller et al. 1994; Thompson et al. 2003; Thompson et al. 2007). The variations in CAPE and CIN calculated were: surface based, mixed layer, and most unstable CAPE (SBCAPE, MLCAPE, and MUCAPE, respectively), and surface based, mixed layer, and most unstable CIN (SBCIN, MLCIN, and MUCIN, respectively). Lapse rates were also calculated to identify instability within a layer (0-1 km, 0-2 km, 0-3 km and 0-6 km). The significant tornado parameter and supercell composite parameters (STP and SCP, respectively) were also calculated as these parameters were found to be the best predictor in cell type (Thompson et al. 2003). The surface equivalent potential temperature (θ_e), the mid-level θ_e, and the average 700-400 hPa relative humidity were used to identify the moisture content of the environment. The SHERBS3 parameter was calculated using the 0-3 km lapse rate, surface-3 km lapse rate, and the 700-500 hPa lapse rate to identify the potential for

significantly severe weather production within high shear low CAPE environments, which are particularly common in the southeastern United States (Sherburn and Parker 2014). Lastly, downdraft CAPE (DCAPE) was calculated as this parameter can help to predict severe winds (Sumrall et al. 2020). Note that if the sounding was convectively contaminated, parcel moistening over a large depth in a short amount of time, an earlier hour was used up to 4 hours before the supercell occurred at the point, which may alter the calculations for CAPE, CIN, and $_{e}$ parameters.

While these hourly mesoscale operational models help to fill in the observational gap in the Appalachian region, there are limitations that have to be considered. When using hourly model data, the farther away from 0000 and 1200 UTC, the less accurate the predictions become since models are rooted in observations (Benjamin et al. 2004). Also, hourly sounding data may not necessarily reflect rapid environmental changes that influenced the supercell evolution depicted in the scan-by-scan radar volumes (every 5 minutes). Lastly, the hourly soundings may not fully capture the environment at the exact time when a supercell passed by a point.

Table 1: Each date that a supercell passed through the different National Weather Service CWA's. Includes the number of crossing and non-crossing supercells as well as the total number of supercells that passed through the CWA's.

Radar Site	Dates	Crossers	Non-crossers	Total
KMRX	8 May 2009 28 April 2014 27-28 April 2011 27 July 2014	13	2	15
KFCX	8 May 2009 9 May 2009 8 April 2011 27-28 April 2011 9 April 2015 25 June 2015 28 April 2015	10	4	14
KRLX	27-28 April 2011 9 April 2015 25 June 2015 1 May 2016	4	8	12
KFFC	27-28 April 2011 11 April 2013	3	2	5
KJKL	27-28 April 2011 27 July 2014 1 May 2016 14 April 2019	5	18	23
KGSP	8-9 May 2009 27 July 2014 25 April 2015 25 June 2015 1 May 2016	5	2	7

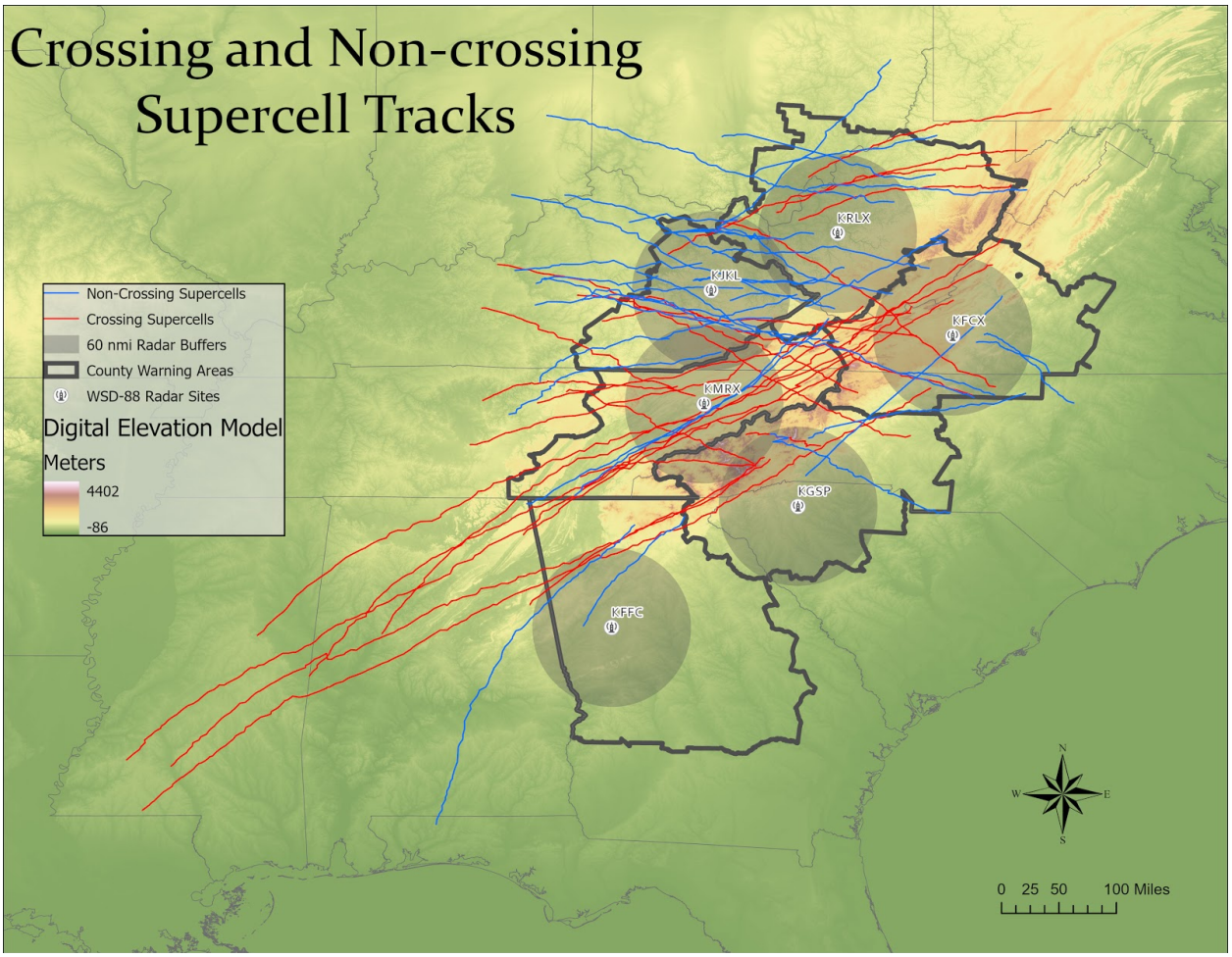

Figure 3.1: A map of crossing and non-crossing supercells within this study are with a 60 nmi buffer around the radar sites.

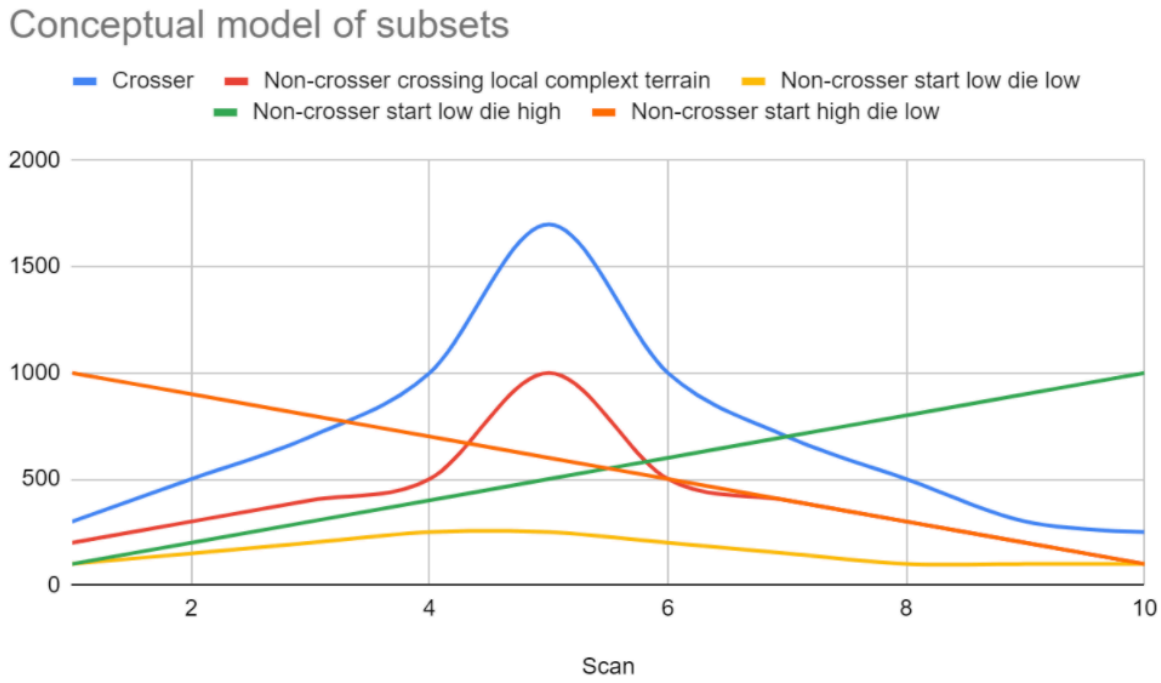

Figure 3.2: A conceptual model of how crossers and non-crossers are defined.

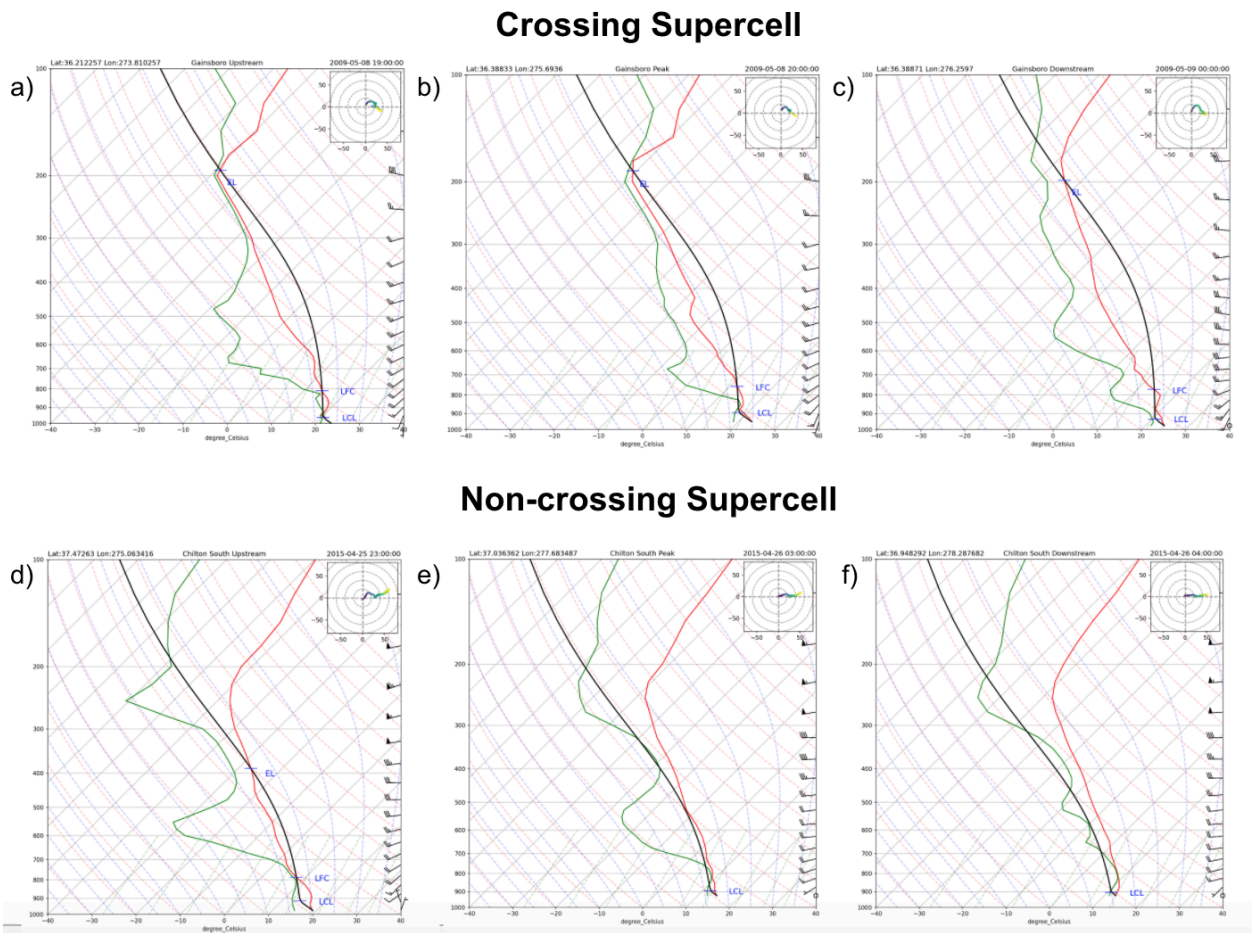

Figure 3.3: Examples of the sounding images produced. (a)(d) RUC/RAP proximity sounding pulled from the initiation point, (b)(e) RUC/RAP proximity sounding pulled from the peak elevation point, and (c)(f) RUC/RAP proximity sounding pulled from the dissipation for a crossing and non-crossing supercell respectively.

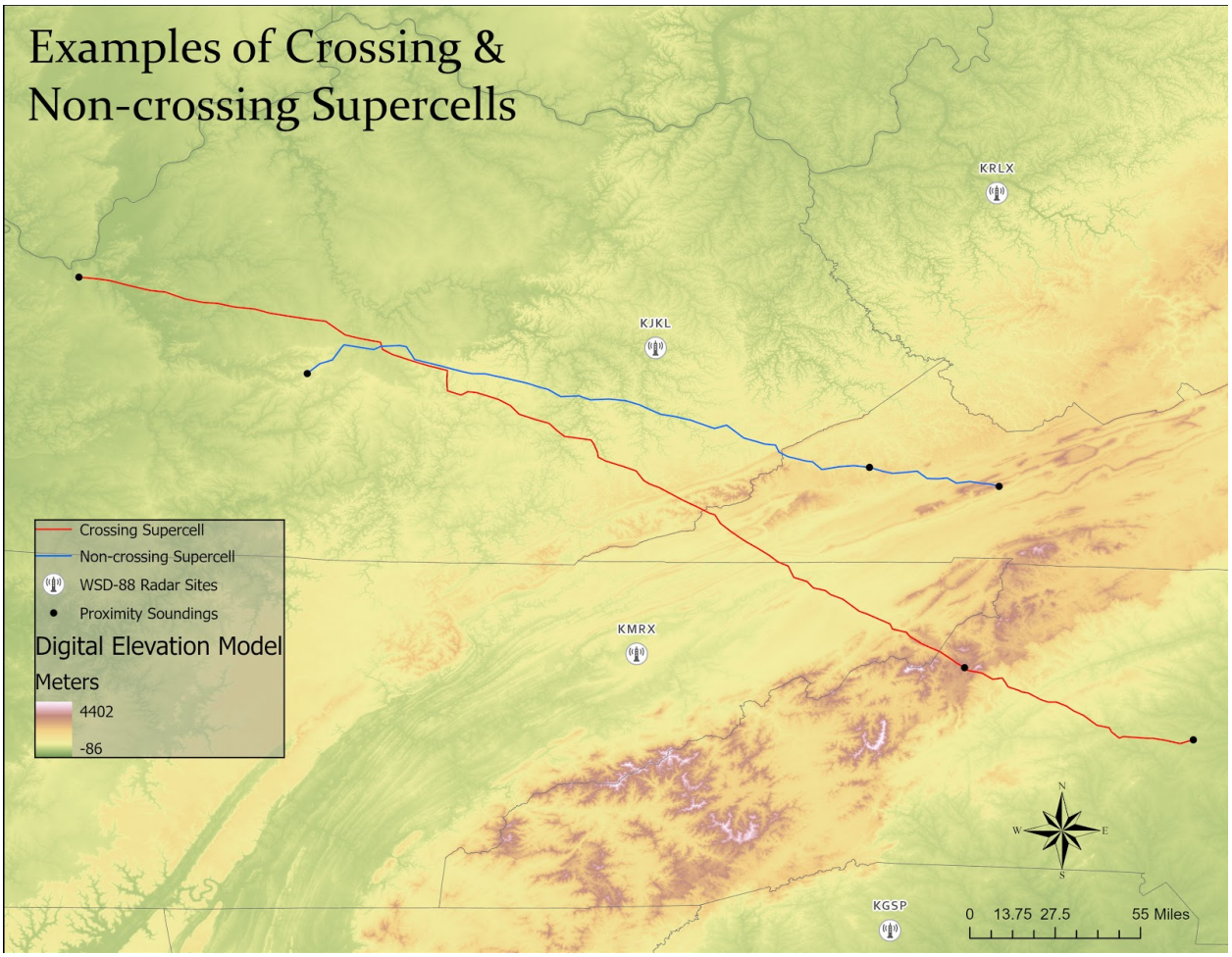

Figure 3.4: Examples of a crossing supercell (red track) and a non-crossing supercell (blue track). The black circles represent where a sounding was pulled for the upstream peak, and downstream sounding.

CHAPTER 4: RESULTS

4.1: Climatology

Due to the rarity of isolated supercells in the Appalachian Mountains, very little is understood about their structure and evolution. The goal of this study is to understand how isolated supercells interact with complex terrain to more accurately predict the occurrences of these supercells. The inflow environments of each supercell were collected at the upstream, peak, and downstream points (Figs. 3.3-3.4). This study will focus on identifying how the inflow environment of a supercell changes in relation to terrain, and its subsequent effects on overall storm maintenance. The important environmental parameters that lead to tornadogenesis and severe weather as supercells move along complex terrain will also be explored.

The 62 supercells in this dataset ranged from April through July between 2009 and 2019. The majority of these supercells occurred in April and May, which is consistent with previous climatologies in the region (Fig. 4.1; Gaffin and Parker 2006; Stonefield and Hudgins 2006; Lane 2008). When separating frequency of events based on storm maintenance, a similar trend of peak occurrence in April and May is also evident, regardless of crossing status (Fig. 4.2).

Notably, the supercells in this study tended to occur in temporal clusters (Table 2). Key events that produced at least 5 supercells included 27-28 April 2011, 1 May 2016, 27 July 2014, 9 April 2015, 8 May 2009, and 25 April 2015. As a result, forecasters should be prepared to address short-term forecasting challenges associated with multiple supercells occurring on a single day.

The time of day that supercells formed or dissipated varied somewhat between storm categories. The majority of supercells initiated in the afternoon and evening hours, though crossing supercells tended to initiate a few hours earlier and reach their demise several hours

later than non-crossing storms (Fig. 4.3). These findings were consistent with other climatological studies of supercells in the Appalachian Mountains (Gaffin and Parker 2006; Stonefield and Hudgins 2006; Lane 2008), and broadly make sense, given that peak heating in the afternoon helps support supercell development.

The severe hazards rate of production by the supercells were reported (Figs. 4.4-4.5). Hail was the most common severe threat (observed in 55 out of 62 storms) among all supercells, followed by severe wind (26 out of 62). Tornadoes were the least common severe threat, with only 16 tornadic supercells. When separating into crossers and non-crossers, the trend still remained with hail being the most common severe threat and tornadoes being the least common severe threat. However, the crossers had a higher rate of producing severe wind and tornadoes compared to the non-crossers. These findings are in agreement with similar studies of analyzing severe weather in the Appalachian region (Gaffin and Parker 2006; Stonefield and Hudgins 2006; Lane 2008).

It is important to note that about 19% of the total supercells were produced from the 27-28 April 2011 outbreak. The overall monthly frequency of supercells did not change when the outbreak supercells were removed, however, the frequency of crossing supercells in April decreased, approaching the May frequency of crossing supercells (Fig. 4.6). The crossers also tended to initiate at either 1600 or 1900 UTC, and this trend did not change as when the outbreak was removed from the dataset (Fig. 4.7). Lastly, the severe report frequencies decreased when the outbreak was taken out of the dataset, but the overall trends remained (Fig. 4.8). Since this outbreak produced a bulk of supercells used in this project, it is crucial to acknowledge how these supercells may skew the data.

4.2 RUC/RAP Analysis

Out of the total 62 supercells, there was only RAP and RUC data available for 59 of the supercells. These results only include the 59 supercells, with 23 crossing supercells and 36 non-crossing supercells.

4.2.1 Synoptic Analysis

The synoptic setup of each case date was analyzed to determine if there were patterns that corresponded with crossing or non-crossing supercells in the Appalachian Mountains. Four sets of maps were created to identify the syntopic patterns; the 250 hPa, 500 hPa, 850 hPa, and surface patterns were analyzed.

The location of the 250 hPa jet streaks are important for supercellular development, as about 84% of storm reports were associated with jet streaks (Clark et al. 2009). Storms tended to occur on the right side of the jet streaks, favoring the right entrance region. Gaffin and Parker (2006) identified a similar relationship between the location of the jet streak and storm development. A similar trend emerged when analyzing the 62 supercells within this study; about 75% of the supercells in the Appalachians occurred on the right side of the jet streak (Figs. 4.9a-4.10a; Table 3).

At the 500 hPa level, patterns emerged in relation to the direction of the flow and the position of the trough. A majority (68%) of the supercell tracks tended to follow the 500 hPa flow (Figs. 4.9b-4.10b; Table 4). When the supercells were separated between crossers and non-crossers, this trend still remained. This would indicate that the steering flow is important to the motion and direction of supercells, which is consistent with Gaffin and Parker (2006). Furthermore, this same study demonstrated that significant tornadoes in the Appalachian Mountains have been associated with either a negatively tilted 500 hPa trough or a 500 hPa

closed low, which is consistent with the patterns associated with crossing supercells, with a majority of crossing supercells in conjunction with a negatively tilted trough and/or a closed 500 hPa low (Fig 4.9b; Tables 5-6). Non-crossing supercells tended to occur under a positively tilted 500 hPa trough and a closed 500 hPa low (Fig. 4.10b).

In all of the cases, a low level jet was present, with winds from the south or southwest and greater than 30 knots, and relative humidity over 70% (Fig. 4.9-4.10c). The low level jet would reach much of the southern Appalachian Mountains and this likely led to an increase in low-level shear and SRH in the southern regions of the study area. The increased moisture from the Gulf of Mexico, also likely aided in the increase of CAPE in the Southern Appalachians. These parameters are potentially important in distinguishing between crossing and non-crossing supercells, and will be discussed further in the next section.

The location of the surface low pressure also appeared to be connected to significant tornadoes in the Appalachian region. A majority of the significant tornadoes that occurred within the Greenville-Spartanburg CWA took place around the same time as a surface low pressure that was located in the Great Lakes region (Lane 2008). Similarly, out of all of the supercells that were analyzed, about 42% of the supercells (both crossing and non-crossing) occurred around the same time as a surface low pressure in the Midwest (Table 7). Over 50% of the crossing supercells were associated with a surface low pressure in the Midwest and 20% associated with a surface low in the Northeast (Figs. 4.9d-4.10d).

Additionally, the presence of nearby surface boundaries were important in these case dates for storm initiation. All of the events were accompanied by either a cold front, stationary front, or outflow boundary (Table 8; Figs. 4.11-4.13). Over half (56%) of the crossing supercells initiated ahead of a cold front and the supercells moved eastward with the front. About half

(54%) of the non-crossing supercells were accompanied by a stationary front, initiated at the time of an outflow boundary, and the supercells followed the boundary. Figures 4.14-4.15 represent a conceptual summary of the above findings.

There were also stark differences between the patterns as the months shifted. The flow tended to be more amplified during events that occurred in April, whereas the flow was more zonal during May, June, and July. This shift in synoptic patterns may have led to the weakening of shear and SRH, discussed further in section 4.2.3.3 (Fig. 4.16).

4.2.2 Composites

Composite soundings and hodographs were created using all of the crossing and non-crossing supercell environments at each of the three points (upstream, peak, and downstream; Fig. 4.17). On the whole, one of the first notable features is the overall similarity in instability profiles between crossers and non-crossers, suggesting that this is less likely to be a distinguishing parameter between these categories. The upstream points of both crossing and non-crossing supercells had more CAPE than the other two points, likely due to the initiation of the supercells occurring during peak heating (Fig. 4.3). While the upstream points indicated the highest amount of instability, the downstream points for both the crossers and non-crossers seemed to have had the highest amount of CIN, consistent with supercells tending to dissipate or become linear later in the evening, after peak heating. It is interesting to note that the non-crossing composites seemed to have more dry air in the mid-levels than the crossing composites, which would indicate higher amounts of instability; however, this is not found with regards to CAPE.

Another clear trend in the composites is that there was more directional shear with the crossers, while the shear magnitude was stronger for the non-crossers (Fig. 4.17). This indicates

that shear plays an important role in maintaining supercellular structure as it moves across complex terrain. These findings indicate that shear is potentially a distinguishing factor between crossers and non-crossers rather than instability and will be discussed further in the next section.

Similar trends were found when comparing the composite soundings and hodographs of the supercells based off of the month in which they occurred. April's crossers had more directional shear, while the non-crossers had more speed shear. The April soundings also indicated that the upstream points had more CAPE than the peak and downstream points for both the crossers and non-crossers (Fig. 4.18). Additionally, the non-crossers were drier in mid-levels than the crossers. This is to be expected as about 55% of the supercells that were analyzed occurred during the month of April and likely skewed the data.

Similarly, the May soundings indicated that the crossing and non-crossing upstream points had the largest amount of CAPE (Fig. 4.19). The non-crossers in May also had drier mid-levels than the crossers. However, in May there was also little distinction between the crossers and non-crossers with respect to the directional and speed shear. CAPE also tended to be larger for the non-crossers than the crossers. This could be attributed to more non-crossing supercells (70%) that were analyzed in May than crossing supercells (30%). The July soundings and hodographs were similar to the May soundings (Fig. 4.20). The CAPE was larger for the non-crossing supercells, as well as larger at the upstream points for both the crossers and non-crossers during the July supercells. There was also very little distinction between the directional and speed shear when comparing the crossing and non-crossing supercells. These findings may indicate that SRH and shear are not good parameters to use to identify whether or not a supercell will cross the Appalachians during May and July. It is important to note that composites of the

June supercells were not created as there were only non-crossing supercells analyzed, and due to the nature of the data the crossing and non-crossing supercells were unable to be compared.

Additional composite soundings were created separating supercells that produced severe hail, severe wind, and tornadoes for crossers and non-crossers at each of the three points. Similar to all of the supercells, the upstream points had more CAPE than the peak and downstream points for all of the three severe weather types (Figs. 4.21-4.23). These composites also indicated that the supercells that produced severe hail had less directional shear when compared to the supercells that produced severe wind and tornadoes. The supercells that produce tornadoes had more directional shear than the supercells that produced severe wind and severe hail (e.g., Davies-Jones 1984; Rotunno and Klemp 1985; Moller et al. 1994; Thompson et al. 2003; Thompson et al. 2007). Similar to the hodographs of all of the crossing and non-crossing supercells, the crossing supercells tended to have stronger directional shear and the non-crossers tended to have stronger speed shear across all three severe weather types.

It is necessary to acknowledge that the 27-28 April 2011 outbreak consists of about 19% of the supercells within the data and likely skewed the data when comparing different samples. When the outbreak was removed, the crossers tended to have less directional and speed shear across all of the subsets (Fig. 4.24). The shear and SRH were the only parameters that changed when the outbreak was taken out. This would suggest that there was strong dynamical forcing that played a role in the outbreak and that this strong of forcing is not common across the Appalachian Mountains, and is consistent with previous studies (e.g., Gaffin 2012; Lyza and Knupp 2014).

4.2.3 Statistical Analysis of Forecasting Parameters

When comparing crossing and non-crossing supercells, statistical analyses were used to quantify the significance of the patterns identified in the composite soundings and hodographs. After establishing that the data was normally distributed, a two sample t-test was used to identify if the distributions of the forecasting parameters were statistically different between the crossers and non-crossers.

To confirm whether a statistically significant result could be considered physically significant, the margin of errors identified in Thompson et al. (2003) when comparing 0-h RUC proximity soundings to observed soundings, were used. Differences in mixed-layer and most unstable CAPE were physically significant if the average difference between distributions was greater than 250 J/kg, and over 300 J/kg for SBCAPE. The margin of errors for shear and SRH were 2 ms^{-1} and 16 m^2s^{-2} respectively, and was used to identify if these parameters were physically significant. Additionally, the average 850-400 hPa temperature errors were about 0.5°C, thus a physically significant difference in distributions for lapse rates were values over 2°C/km.

4.2.3.1 Comparison of All Supercells

All of the supercells were compared based off of their ability to maintain structure as they crossed the Appalachian Mountains or not. When using the two sample t-test on this subset of data, several parameters emerged indicating that the crossing and non-crossing distributions were statistically or physically significantly different (Table 9). One of these sets of parameters was the 0-1 km and 0-3 km SRH. The SRH for the crossers tended to be larger than the non-crossers and increased as supercells moved from the upstream point, when comparing the average change (Fig. 4.25). This key difference may be due to terrain effects such as flow channeling (e.g., Bosart et al. 2006; Gaffin 2012; Prociv 2012) as a function of crossers having more interaction

with terrain than the non-crossers. Importantly, larger SRH would help to support supercell updraft maintenance (e.g., Rotunno and Klemp 1985).

The 0-1 km and 0-3 km bulk shear had similar trends to the 0-1 km and 0-3 km SRH trends, with the crossers having higher values of shear than the non-crossers (Fig. 4.26). The SRH and shear increased from the upstream to peak points for both the crossers and non-crossers, when comparing the average delta change. However, the distributions of the 0-6 km shear between crossers and non-crossers had very little difference. This would indicate that the lowest 3 km are the most important layer in distinguishing the difference between crossers and non-crossers and is consistent with previous studies (e.g., Gaffin and Parker 2006; Lane 2008).

The LCL, LFC, and EL heights tended to be lower for the non-crossing supercells compared to the crossing supercells (Fig. 4.27). The LCL pressure decreased at the peak for both of the crossers and non-crossers, associated with decreased relative humidity at higher elevations (e.g., Markowski and Dotzek 2011), with similar distributions at the upstream and downstream points. Similar distribution patterns were found for the LFC heights, with the largest difference between the crossers and non-crossers at the peak points. The separation between crossers and non-crossers at the peak point might not be significant for forecasters, but rather a reflection of crossing supercells encountering higher terrain, thus lower relative humidities that result in higher LFC heights. The distribution of the EL heights had very similar values for the upstream, peak, and downstream points. However, the non-crossing pressures tended to be higher than the crossers. Again, this is likely due to lower moisture associated with higher terrain.

The overall CAPE trends were the same no matter which parcel was used for instability (surface based, mixed layer, or most unstable), with the largest difference between crossing and non-crossing supercells found at the upstream points (Fig. 4.28). The crossers tended to have

larger CAPE at the upstream and downstream points compared to the non-crossers, while the non-crossers tended to have increased CAPE at the peak point when compared to the crossers. Since these events tended to initiate in the afternoon hours (Fig. 4.3), it makes sense that CAPE values would be the highest at the upstream points, and was consistent with the findings using the average delta change. These findings would indicate that instability does not appear to be a good discriminator of crossing and non-crossing supercells.

As noted in the composite soundings, the non-crossers tended to be drier in the mid-levels than the crossers. This was verified using the statistical analyses, which indicated that the surface θ_e, mixed-layer θ_e, and the average 700-400 hPa relative humidity tended to be larger for the crossing supercells (not shown). This might suggest that the dry air may act to enhance the downdraft in non-crossers, and perhaps hasten demise (e.g., Gilmore and Wicker 1998), though this linkage may not be straightforward (e.g., James and Markowski 2010). It is also possible that the dry air aloft enhances entrainment of dry air into the updraft, thus leading to demise (e.g., Honda and Kawano 2015; Davenport and Parker 2015).

The distribution of the 0°C and -20°C heights for both the crossers and non-crossers tended to increase from the upstream points to the downstream points, with the mean heights being higher for the crossing supercells (Fig. 4.29). The mean wet bulb-zero heights were also higher for the crossing supercells compared to the non-crossing supercells. However, the crosser heights increased dramatically at the peak point, while the non-crossers gradually and minimally increased overtime. While these trends suggest that non-crossers are more likely to produce severe hail (Lenning et al. 1998; Witt et al. 1998), this result is not consistent with the observed rates of severe hail reports (Fig. 4.4).

4.2.3.2 Comparison of Severe Weather Production by Supercells

Supercells were separated based on their associated severe weather reports and were compared against one another. When statistically comparing different report types, similar trends emerged from the composite soundings and hodographs as those discussed in section 4.2.2. Tornado-producing supercells tended to have larger 0-1 km and 0-3 km SRH values, while hail-producing supercells had the smallest values of SRH (Fig. 4.30; 0-3 km SRH not shown). Similar results were found with regards to the 0-1 km and 0-3 km bulk shear (Fig. 4.31; 0-3 km and 0-6 km shear not shown). This would indicate that tornado and severe wind-producing supercells had stronger dynamical forcing, which is consistent with previous studies (e.g., Thompson et al. 2003). Additionally, this finding supports what was found in section 4.2.3.1, in which the increase in low-level SRH and shear may be due to terrain effects as the majority of wind (58%) and tornado (75%) producing supercells were crossers.

CAPE tended to be less of a distinguishing factor between the severe types than shear and SRH. Crossing supercells that produced severe hail tended to have less CAPE compared to the crossing supercells that produce severe wind or tornadoes (not shown). However, the distributions between the crossing supercells that produced severe wind and tornadoes were not statistically or physically significant. This would indicate that the severe wind and tornado producing crossing supercells have similar thermodynamic profiles and it may be harder to forecast these two severe types. Non-crossing supercells had different results with regards to the severe types. Hail-producing supercells had the largest CAPE and the supercells that produce tornadoes had the smallest CAPE. However, this might not be significant as the sample sizes between the non-crossing supercells and severe types were vastly different, with 32 supercells producing severe hail and only 10 and 4 supercells producing severe wind and tornadoes,

respectively. This would again suggest that CAPE is not a good parameter to use when determining if supercells will cross the Appalachians and what kind of severe weather it may produce.

Additionally, the distribution of the 0°C heights, -20°C heights, and wet-bulb zero heights tended to be lower for the supercells that produced severe hail than the supercells that produced severe wind or tornadoes (Figs. 4.32-4.34). This is consistent with the findings of Lenning et al. (1998) and Witt et al. (1998), in that lower heights increased the likelihood of hail reaching the surface. These parameters may be important in determining if the supercells in the Appalachian Mountains will produce severe hail.

4.2.3.3 Comparison of Time of Year

As noted in section 4.2.1, the synoptic patterns changed as the months shifted. These changes were also evident in the storm-scale environments (Table 10). In both the crossing and non-crossing supercells, the bulk shear and SRH tended to decrease over time. This is likely due to the pattern becoming more zonal from April through July. The opposite is true for CAPE, as it increased from April through July, and presumably due to the increase in radiational heating during the summer months. The supercells also tended to be drier as the months shifted into summer. The combination of lower shear and lower moisture content might indicate why the number of supercells drops after April (Fig. 4.1), as rotation and moisture is needed to produce and maintain supercells.

4.2.3.4 Weather Forecast Offices

The supercells were further separated based on which WFO they occurred in. Several supercells traversed multiple WFO CWAs and were counted in each individual subset. Similar

characteristics were observed as described in section 4.3.2.1, in which crossing supercells tended to have stronger bulk shear and SRH (Table 11). This was the case for 4 out of the 6 WFOs (FCX, FFC, GSP, and RLX). It is interesting to note that the other two offices (JKL and MRX) are located (at least partially) on the windward side of the Cumberland Plateau, which might indicate that supercells that cross the Blue Ridge require stronger dynamical forcing than supercells that cross the Cumberland Plateau. Similar to section 4.3.2.1, the SRH and shear tended to increase as the supercell reached the peak point and then decrease as it dissipated or became linear at the downstream point. This supports the findings in the previous sections, in which terrain likely plays a role in the increase of shear and SRH needed to maintain the supercellular structure as it traverses complex terrain.

In addition, CAPE tended to be larger for crossing supercells in 5 of the 6 CWAs (FCX, FFC, GSP, JKL, and MRX), while the non-crossers tended to have more CAPE in the RLX region (Table 12). This may be due to the CWA being located the farthest north and the low level jet remaining more in the southern Appalachian mountains. The low level jet was likely a driver of increased CAPE as it was present in all of the events, and presumably advected moisture into the southern WFOs. Similar to section 4.3.2.1, CAPE was largest at the upstream points and was likely due to the supercells occurring during peak daytime heating.

It is important to note that categorizing supercells by WFO regions lowered the sample size used to calculate the statistical analysis. This likely led to bias and may have limited the effectiveness of identifying the true variance between parameters. Additionally, these subsets are highly skewed towards the 27-28 April 2011 outbreak, since all of these supercells traversed multiple CWAs.

4.2.4 Case Study

Six representative supercells were identified to compare the environmental evolution of the crossing and non-crossing supercells. One crossing supercell and one non-crossing supercell that spanned about the same length of time were taken on three different dates: 9 April 2015, 8 May 2009, and 27 July 2014. A RUC or RAP sounding was produced every hour during these supercells to identify how the parameters change as terrain changed.

Similar to what was discussed in the previous sections (4.2.2 and 4.2.3), as the supercell reached higher elevation, the lowest 3 km of bulk shear and SRH increased (Figs. 4.35-4.36). All three crossing supercells had larger values of SRH and shear when compared to the non-crossers. This would support the finding discussed earlier, in that the increase in low-level shear and SRH is likely due to terrain effects. CAPE appeared to have the opposite effect to shear, with CAPE decreasing as elevation increased (Fig. 4.37). Overall, the trends identified in these case studies support the findings discussed in sections 4.2.2 and 4.2.3, in that wind dynamics might be better parameters to use than CAPE, when determining if these storms will maintain supercellular structures as they traverse complex terrain (e.g., Bosart et al. 2006; Gaffin 2012; Prociv 2012).

The 9 April 2015 crossing supercell had more bulk shear and SRH when compared to the 8 May 2009 and 27 July 2014 supercells. This is the opposite of what was found in section 4.2.3.3, in which the SRH and shear tended to decrease over time. This may be due to the 9 April 2015 supercell traversing the Allegheny Mountains and the other supercells crossing the Cumberland Plateau and Blue Ridge Mountains, which is steeper in elevation. This would indicate that higher elevations play a role in increasing low-level SRH and shear, and would back the findings in the previous sections and in earlier studies (e.g., Bosart et al. 2006; Gaffin 2012; Prociv 2012).

Across all of the cases, the lowest 3 km of SRH, shear, and CAPE increased during the same hour that severe weather was produced. This may help forecasters to identify if severe weather might occur. However, it is important to note that only 6 out of the 62 supercells were analyzed and that this pattern might not indicate when severe weather will occur for every supercell in the Appalachian Mountains. Additionally, the severe weather tended to be reported in the valleys. This might suggest that severe weather is more likely to occur in lower elevations or it could be due to valleys being more heavily populated, leading to report bias (e.g. Doswell and Burgess 1988).

Table 2: The number of supercells, crossers and non-crossers, produced on each date.

Date of Events	Crosser	Non-crosser	Total
27-28 April 2011	9	3	12
1 May 2016	1	9	10
27 July 2014	4	4	8
9 April 2015	4	3	7
8 May 2009	3	3	6
25 April 2015	0	5	5
28 April 2016	0	4	4
25 June 2015	0	3	3
28 April 2014	2	0	2
11 April 2013	0	2	2
9 May 2009	1	0	1
8 April 2011	1	0	1
14 April 2019	0	1	1

Table 3: The number of supercells that occurred on the right side of a 250 hPa jet set and supercells that occurred without close proximity (over 300 km away) to a 250 hPa jet streak.

	Located on right side of the jet streak	**Not located near the jet streak**
Crossers	20 (80%)	5 (20%)
Non-Crossers	27 (72%)	10 (27%)
Total	47 (75%)	12 (19%)

Table 4: The number of supercells that followed or did not follow the 500 hPa flow.

	Tracks follow 500 hPa flow	**Tracks does not follow 500 hPa flow**
Crossers	16 (64%)	9 (36%)
Non-Crossers	26 (70%)	10 (29%)
Total	42 (68%)	19 (30%)

Table 5: The number of supercells associated with a positive, negative, or neutral 500 hPa trough.

	Positive 500 hPa tilted trough	**Negative 500 hPa tilted trough**	**Neutral 500 hPa tilted trough**
Crossers	12 (48%)	16 (64%)	0 (0%)
Non-Crossers	27 (72%)	6 (16%)	1 (2%)
Total	39 (62%)	22 (35%)	1 (1%)

Table 6: The number of supercells associated with or not associated with a 500 hPa closed low.

	Closed 500 hPa low pressure	**Not closed 500 hPa low pressure**
Crossers	20 (80%)	5 (20%)
Non-Crossers	25 (67%)	12 (32%)
Total	45 (72%)	17 (27%)

Table 7: The locations of the surface low associated with supercells.

	Northeast	**Midwest**	**Great Plains**	**South**	**East Canada**	**No low present**
Crossers	5 (20%)	13 (52%)	3 (12%)	1 (4%)	3 (12%)	3 (12%)
Non-crossers	4 (10%)	13 (35%)	0 (0%)	9 (24%)	3 (8%)	5 (13%)
Total	9 (15%)	26 (42%)	3 (5%)	10 (16%)	6 (10%)	8 (13%)

Table 8: The type of surface boundaries associated with crossing and non-crossing supercells that acted as the initiation mechanism.

	Cold Front	**Outflow Boundary (Stationary Front Within 100km)**	**Stationary Front**
Crossers	14 (56%)	7 (28%)	4 (16%)
Non-Crossers	13 (35%)	20 (54%)	3 (18%)
Total	27 (44%)	27 (43%)	7 (11%)

Table 9: Statistically significant parameters of all of the crossing and non-crossing supercells at the upstream, peak, and downstream points.

Upstream					**Peak**					**Downstream**				
Parameter	Mean Crosser	Mean Non-crosser	T Stat	P-value	**Parameter**	Mean Crosser	Mean Non-crosser	T Stat	P-value	**Parameter**	Mean Crosser	Mean Non-crosser	T Stat	P-value
0℃ Height:	4203.2	3821.6	3.2	0.0020	**0℃ Height:**	4204.3	3834.0	3.3	0.0014	**0℃ Height:**	4209.0	3802.3	3.5	0.00086
Surface Potential Temperature:	343.9	337.1	2.8	0.0058	**1km Shear**	16.3	10.9	3.1	0.0022	**3 km Shear:**	24.0	18.8	2.8	0.0062
MLCAPE	1814.0	1197.5	2.7	0.0072	**Average Mid-level RH:**	68.6	50.3	3.0	0.0032	**-20℃ Height:**	7318.6	7027.3	2.5	0.014
Mixed-layer Potential Temperature:	342.0	335.8	2.7	0.0090	**LFC:**	744.9	818.7	-3.1	0.0034	**1km Shear:**	15.7	11.5	2.4	0.017
SBCAPE:	2114.9	1442.3	2.6	0.010	**LCL:**	866.6	894.3	-3.0	0.0034	**3km SRH:**	142.0	101.2	2.3	0.020
EL:	206.6	258.7	-2.6	0.01	**1km SRH:**	97.4	56.5	2.9	0.0041	**WBZH:**	3988.6	3561.7	2.2	0.027
1km Shear:	15	10.4	2.6	0.011	**3km Shear:**	23.4	18.6	2.8	0.0067	**LCL:**	891.5	914.5	-2.2	0.030
MUCAPE:	2166	1576.7	2.42	0.018	**-20℃ Height:**	7323.9	6999.0	2.7	0.0091	**Average Mid-level RH:**	72.0	60.3	2.1	0.033
-20℃ Height:	7221.8	6938.9	2.2	0.029	**3km SRH**	145.0	98.8	2.5	0.013	**1km SRH:**	91.2	61.4	2.1	0.042
1km SRH:	85.1	55.2	2.2	0.030	**WBZH:**	3743.7	3413.0	2.4	0.016					
SBCIN:	-11.5	-32.0	2.1	0.038	**DCAPE**	1535.3	1427.0	2.3	0.022					

Table 10: Months associated with supercells ranked based on the strength of bulk shear, SRH, and SBCAPE separated by crossing and non-crossing supercells (blue line), for the upstream, peak, and downstream points.

Upstream							**Peak**					**Downstream**				
Month	**n**	**Mean 0-1km Shear**	**Mean 0-3km Shear**	**Mean 0-1km SRH**	**Mean 0-3km SRH**	**Mean SBCAPE**	**Mean 0-1km Shear**	**Mean 0-3km Shear**	**Mean 0-1km SRH**	**Mean 0-3km SRH**	**Mean SBCAPE**	**Mean 0-1km Shear**	**Mean 0-3km Shear**	**Mean 0-1km SRH**	**Mean 0-3km SRH**	**Mean SBCAPE**
April Crossers	15	18.5	24.9	108.4	162.2	2189.2	19.9	27.7	129.1	188.8	726.6	19.4	28.1	119.0	176.7	817.8
May Crossers	5	9.4	15.6	49.0	81.2	1408.6	11.2	14.8	44.4	60.2	1051.8	12.4	18.0	57.6	89.6	1421.0
July Crossers	4	9.7	22.0	49.2	101.7	2738.3	10.25	19.5	53.0	98.0	1667.5	7.25	17.3	36.3	86.0	2022.0
April Non-crossers	17	13.8	20.9	72.3	123.3	1054.2	13.5	22.1	70.5	117.5	683.8	13.3	22.2	72.5	119.5	523.6
May Non-crossers	12	7.6	16.2	41.6	75.3	1855.3	8.4	14.1	41.6	70.9	1527.3	9.8	15.0	50.5	75.4	1003.3
June Non-crossers	3	3.0	15.7	13.3	62.0	1825.3	5.7	14.7	26.7	74.3	1783.7	7.7	13.0	31.0	70.0	1246.7
July Non-crossers	4	10.8	21.8	59.3	106.0	1566.0	11.3	21.3	64.3	122.0	1839.0	12.0	21.0	70.3	124.8	1853.0

Table 11: Weather Forecast Offices ranked based on the strength of bulk shear and SRH, separated by crossing and non-crossing supercells (blue line), for the upstream, peak, and downstream points.

Upstream							Peak					Downstream				
WFO	n	Mean 0-1km Shear	Mean 0-3km Shear	Mean 0-6km Shear	Mean 0-1km SRH	Mean 0-3km SRH	Mean 0-1km Shear	Mean 0-3km Shear	Mean 0-6km Shear	Mean 0-1km SRH	Mean 0-3km SRH	Mean 0-1km Shear	Mean 0-3km Shear	Mean 0-6km Shear	Mean 0-1km SRH	Mean 0-3km SRH
FFC Crosser	6	21.8	27.5	33.1	137.5	202.3	22.5	29.0	33.0	144.3	203.2	22.3	30.2	32.8	146.6	202.5
FCX Crosser	12	16.9	24.6	32.5	104.0	163.7	19.7	25.5	30.0	127.3	187.4	18.4	26.6	29.0	115.4	176.6
MRX Crosser	14	14.5	23.7	29.2	78.3	135.1	16.8	23.2	26.1	102.1	150.7	15.4	23.4	26.0	92.2	143.2
GSP Crosser	7	14.5	21.8	25.7	82.4	132.4	13.8	21.5	24.5	77.6	115.7	12.7	18.4	22.3	74.6	107.8
RLX Crosser	6	12.6	18.2	25.0	59.0	92.8	15.5	24.2	27.2	93.7	137.5	14.3	25.0	26.8	70.0	119.5
JKL Crosser	6	9.2	17.3	25.2	43.8	77.5	10.8	18.5	21.8	46.8	82.7	11.2	20.7	23.2	48	96.7
MRX Non-Crosser	2	25.5	31.5	37.0	178.5	291.0	20.0	27.5	35.5	117.5	169.0	22.0	30.5	36.5	138.0	202.5
GSP Non-Crosser	2	12.0	24.0	24.0	60.0	122.0	11.0	17.5	20.0	49.5	82.5	16.0	17.5	25.0	92.0	110.5
FFC Non-Crosser	2	12.5	16.5	18.0	59.5	89.5	18.0	23.0	29.0	20.6	62.0	17.0	22.0	28.0	96.5	132.0
JKL Non-Crosser	18	9.9	20.0	27.6	51.4	99.6	10.7	18.3	26.5	53.0	95.1	10.6	18.8	26.6	53.9	94.5
RLX Non-Crosser	16	8.2	15.7	23.8	40.1	70.8	9.2	16.4	24.7	43.2	81.1	9.8	17.2	25.0	47.9	85.4
FCX Non-Crosser	3	5.0	13.6	21.0	21.3	58.0	4.3	14.3	21.6	20.6	62.0	4.6	10.6	21.3	19.6	48.0

Table 12: As in Table 9, but for CAPE parameters.

Upstream					Peak			Downstream		
WFO	**n**	**SBCAPE**	**MLCAPE**	**MUCAPE**	**SBCAPE**	**MLCAPE**	**MUCAPE**	**SBCAPE**	**MLCAPE**	**MUCAPE**
FFC Crosser	6	3074.2	2637.0	3130.8	551.2	130.3	861.5	624.2	335.8	624.2
GSP Crosser	7	2871.3	2515.4	2895.3	964.3	700.4	1094.9	994.7	688.8	1015
MRX Crosser	14	2170	1941.1	2221.4	1174.6	787.4	1224.5	1337.7	980.8	1448.7
FCX Crosser	12	1902.4	1644.7	1966.7	851.0	351.3	851.9	1056.1	510.6	1089.3
JKL Crosser	6	1776.0	1571.3	1848.0	989.7	739.5	1082.5	1526.5	1144.0	1785.3
RLX Crosser	6	1361.2	1184.0	1471.3	217.3	88.0	433.8	248.5	105.5	450.7
FCX Non-Crosser	3	2152.3	1799.0	2155.3	2265.7	1980.3	2283.7	1913.3	2182.3	2484.7
JKL Non-Crosser	18	1405.2	1249.3	1627.1	1120.9	1008.9	1313.1	991.4	939.1	1238.8
RLX Non-Crosser	16	1449.2	1206.3	1551.3	1364.4	1184.7	1498.6	827.9	734.4	940.8
GSP Non-Crosser	2	1417.5	1073.5	1417.5	896.5	667.5	964.5	708	578	754.5
MRX Non-Crosser	2	1277.5	1100.0	1338.5	605.0	394.0	605.0	334.5	242.0	335.5
FFC Non-Crosser	2	1561.5	696.5	1561.5	448.5	30.5	448.5	550.0	108.0	550.0

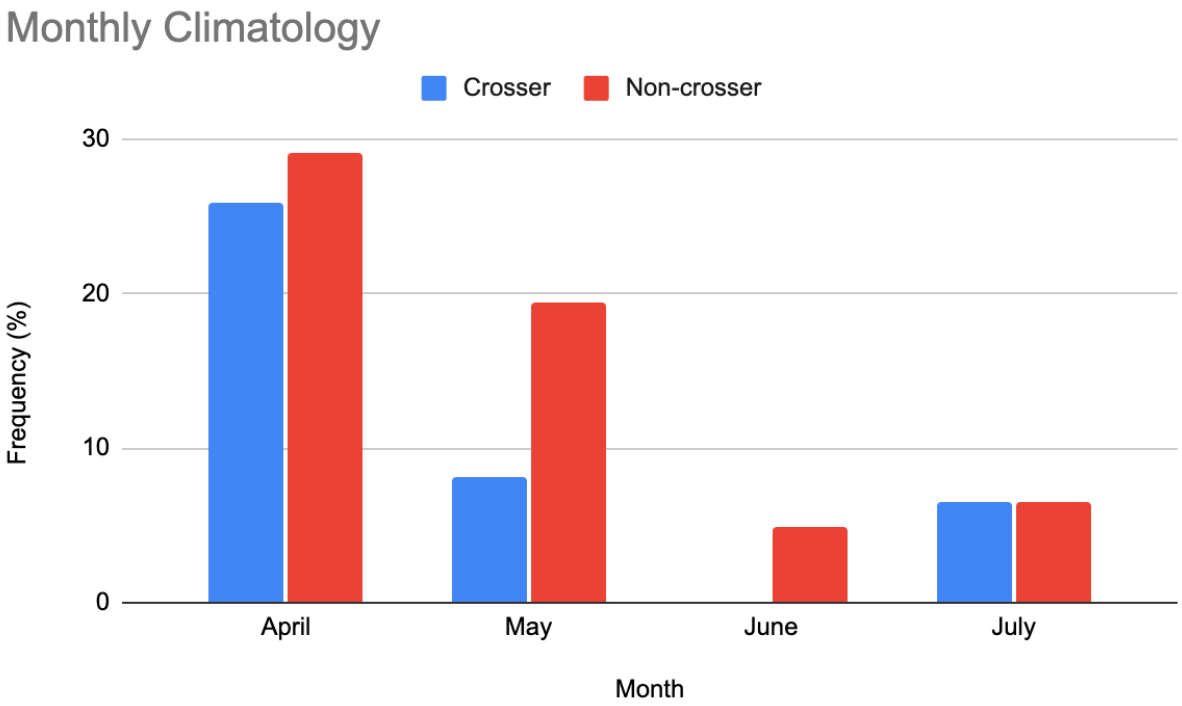

Figure 4.1: The monthly percentage of isolated supercells. The frequency of crossing and non-crossing supercells were calculated by dividing the number of crossing supercells of the given month by the total number of crossing supercells. The same calculation was done for the non-crossing supercells.

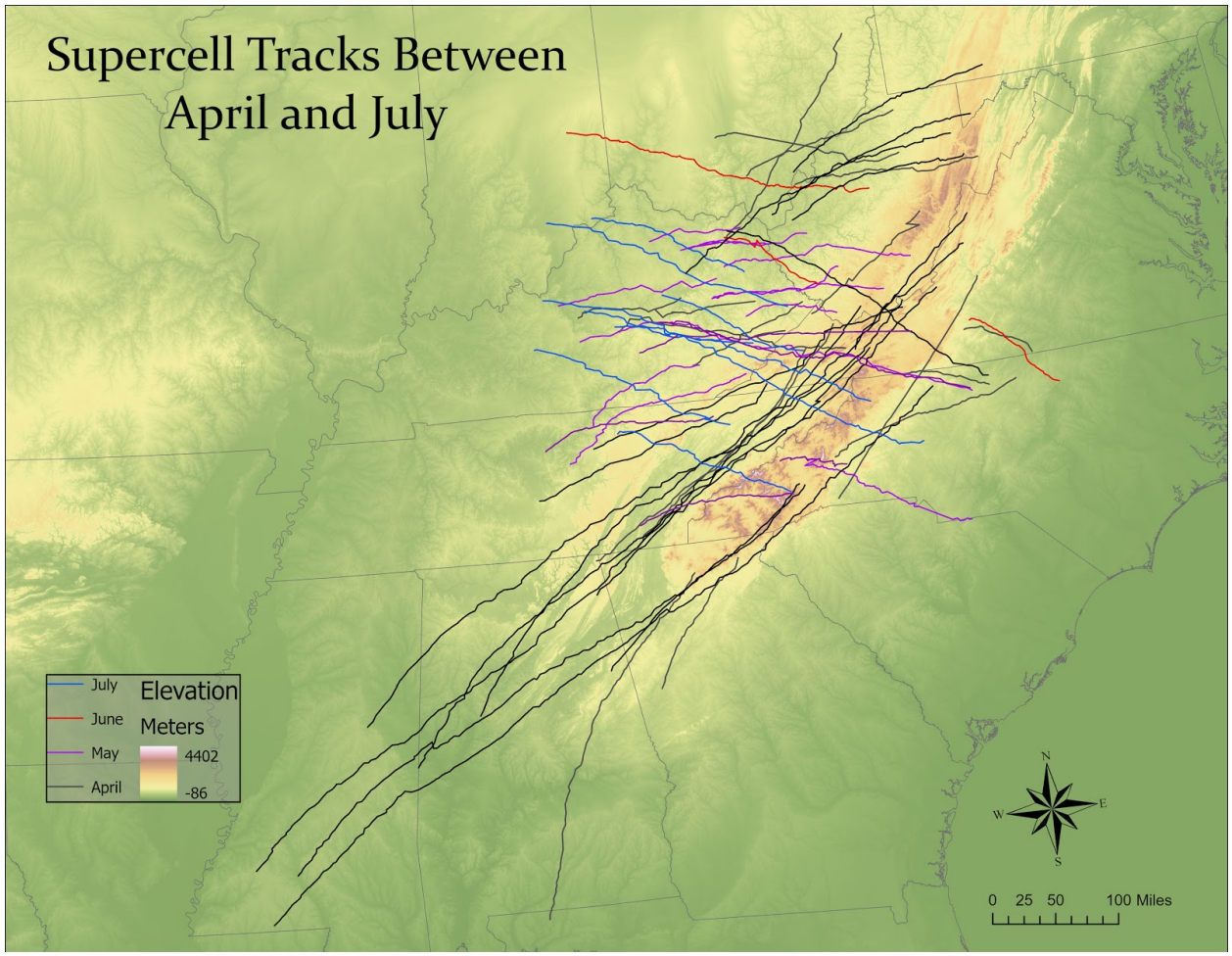

Figure 4.2: The tracks of the supercells separated by the month in which they occurred.

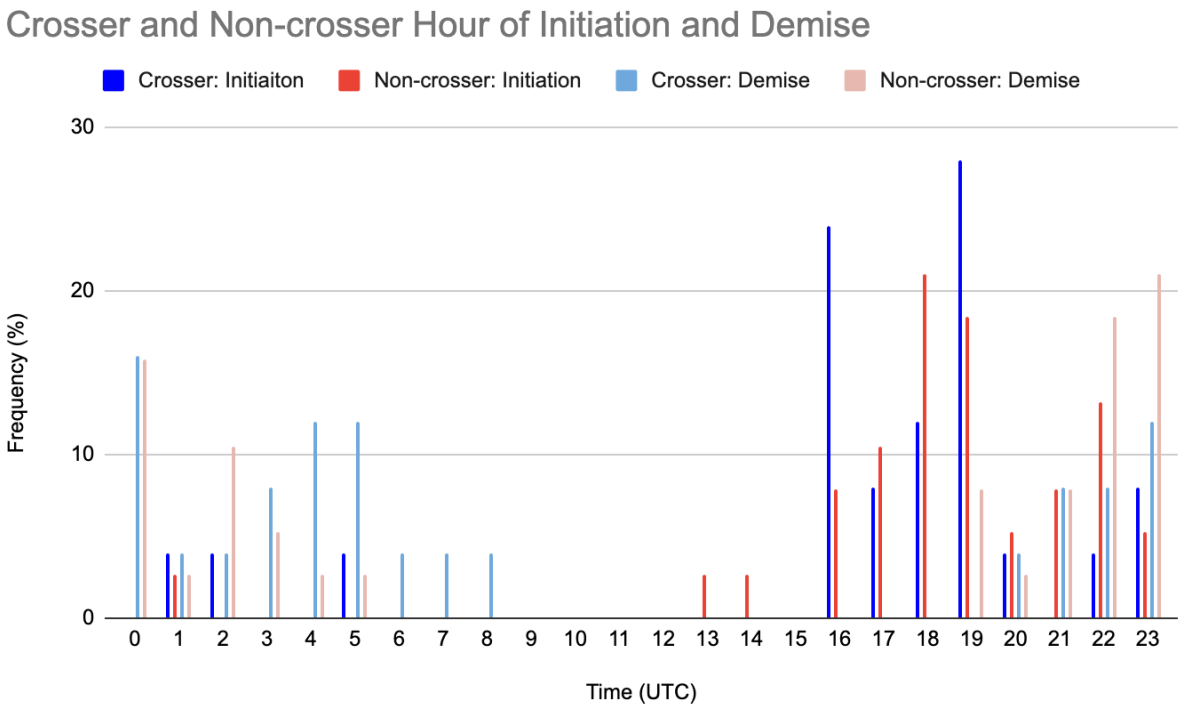

Figure 4.3: The percentage of the hour of initiation and demise of the supercells. The frequency of the hour of initiation and demise were calculated by dividing the number of crossing supercells which initiated at a given hour, by the total number of crossing supercells. The same calculation was done for the non-crossing supercells.

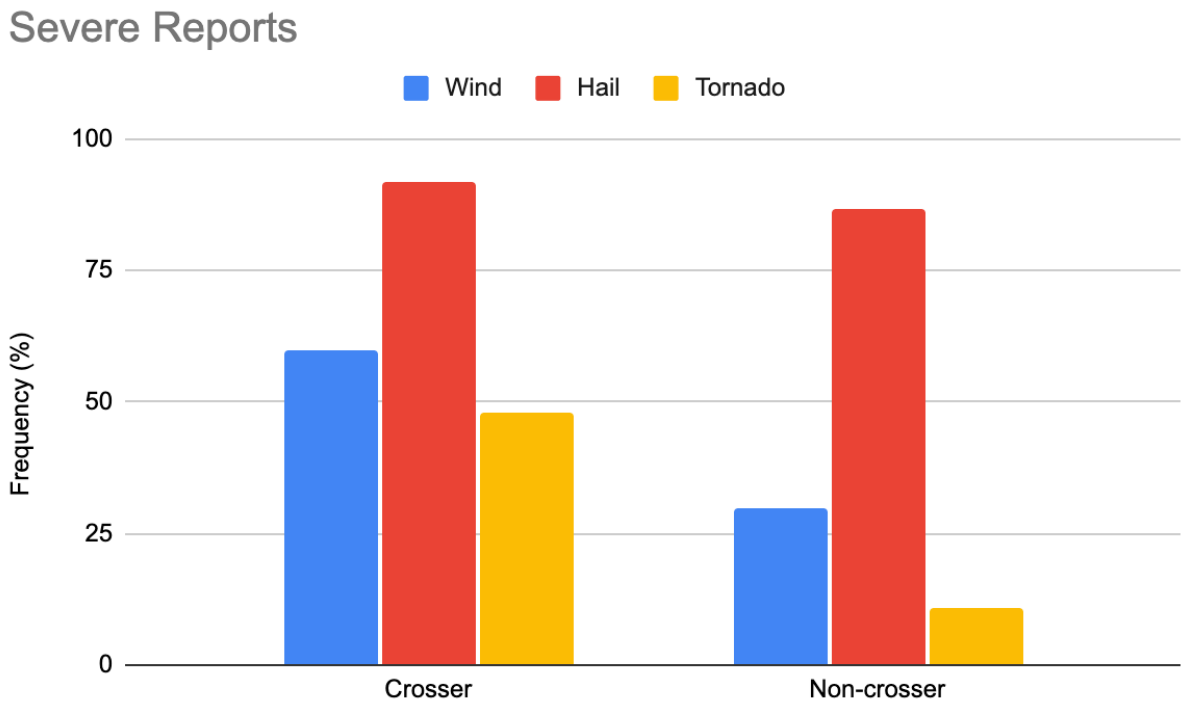

Figure 4.4: The percentage of severe weather reports from the supercells for the crossers and non-crossers. The frequency of severe reports were calculated by dividing the number of crossing supercells which produced a given severe weather threat, by the total number of crossing supercells. The same calculation was done for the non-crossing supercells.

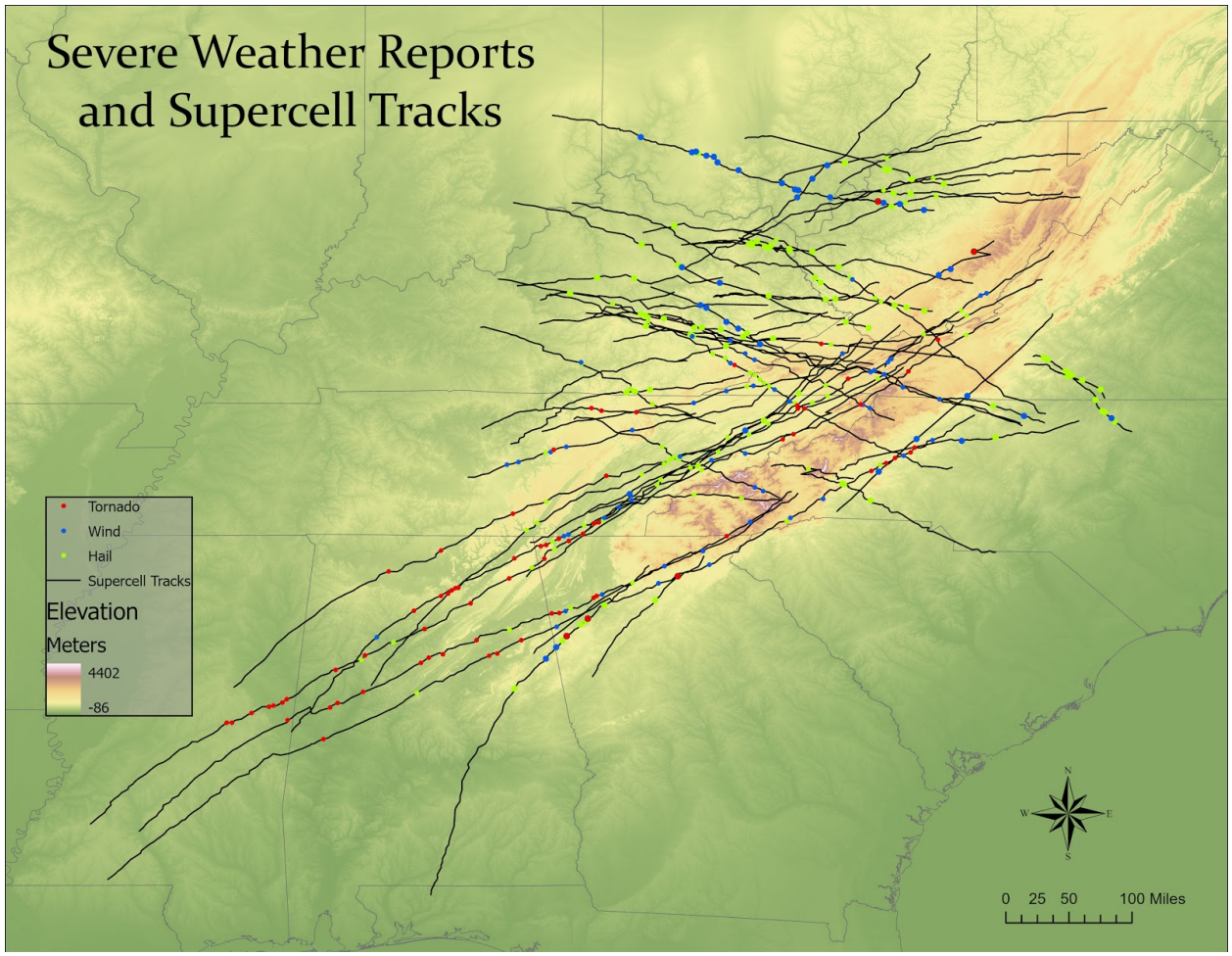

Figure 4.5: A map of the supercell tracks and points where severe weather was reported.

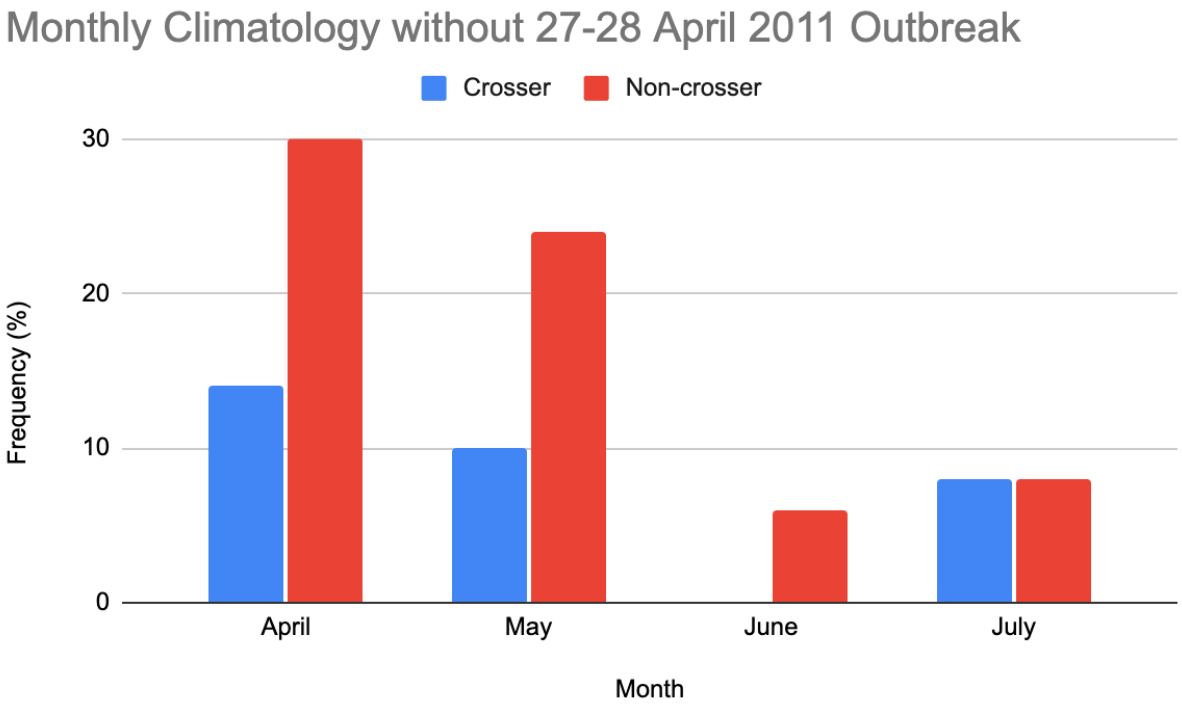

Figure 4.6: Same as Fig. 4.1, but with the 27-28 April 2011 Outbreak removed.

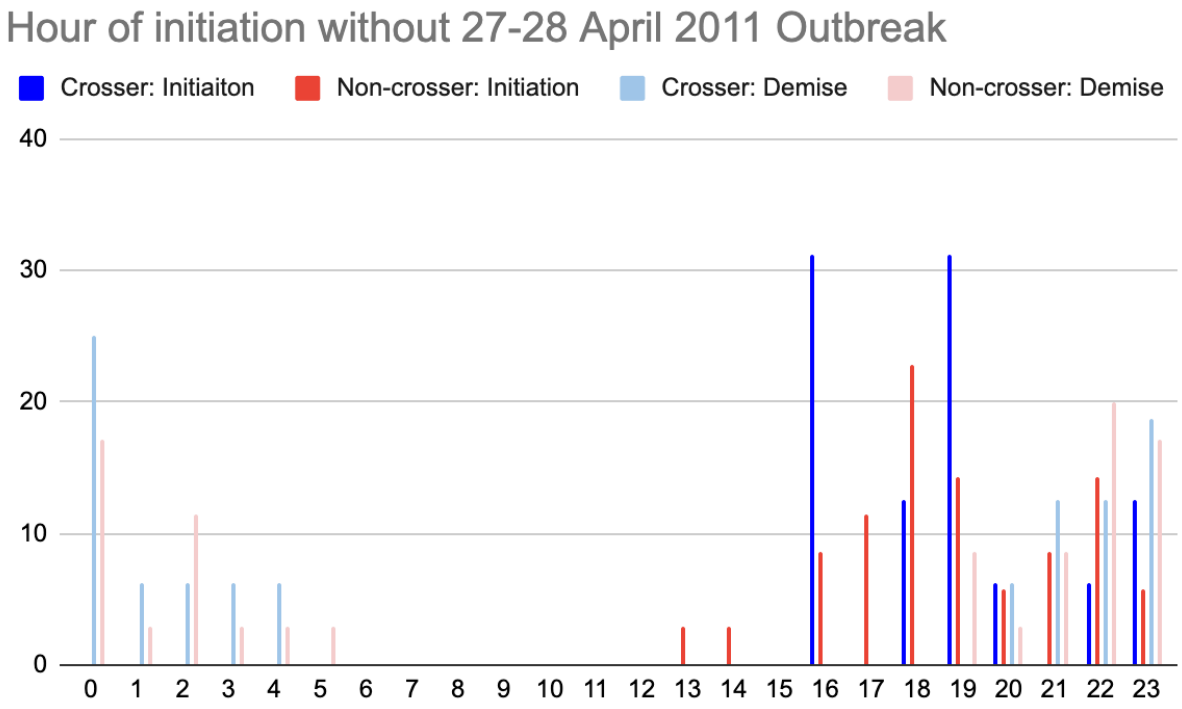

Figure 4.7: The same as Fig. 4.3, but with the 27-28 April 2011 Outbreak removed.

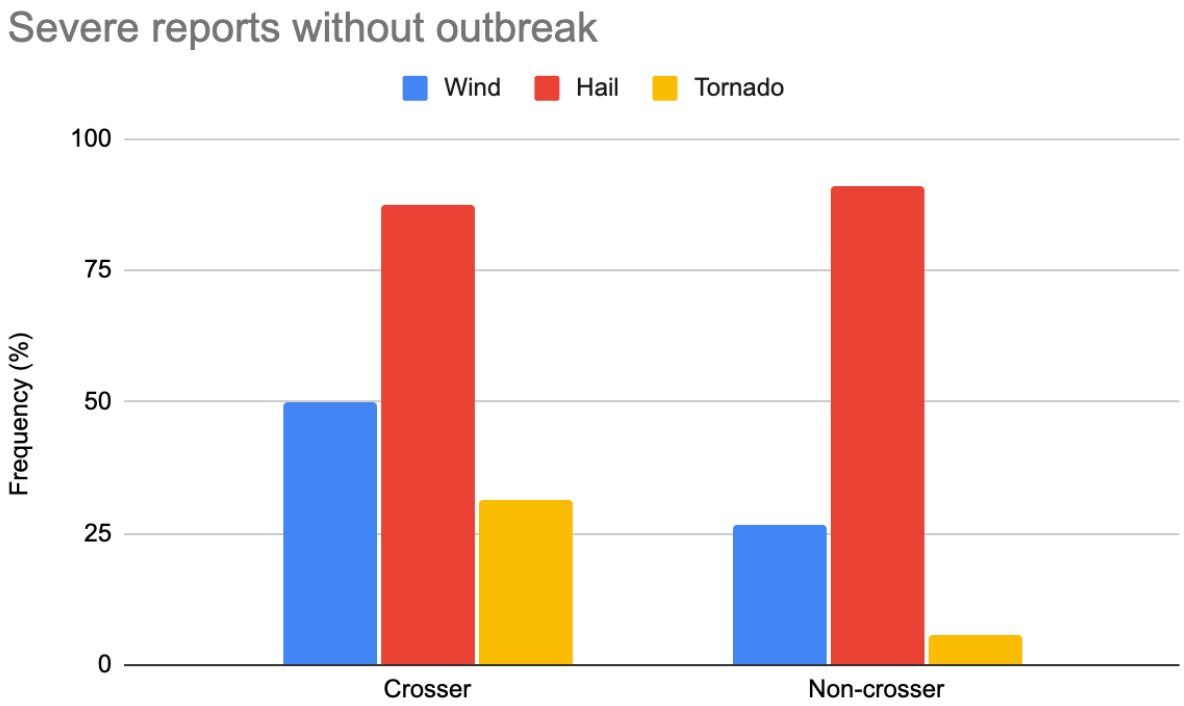

Figure 4.8: The same as Fig. 4.4, but with the 27-28 April 2011 Outbreak removed.

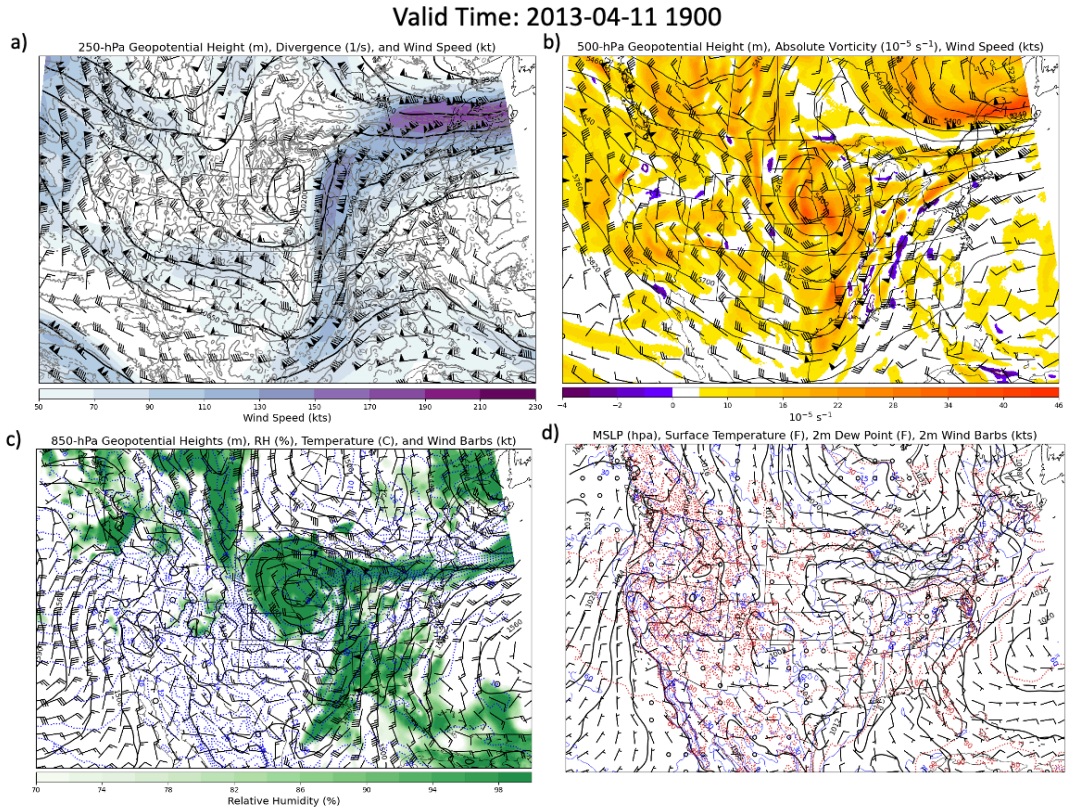

Figure 4.9: Synoptic maps representing the typical a) 250 hPa height, divergence, and wind speed, b) 500 hPa height, absolute vorticity, wind speed, c) 850 hPa height, relative humidity, temperature (blue dotted lines), and wind speed, and d) surface mean sea level pressure, temperature (red dotted lines), dew point temperature (blue dotted lines), and wind speed patterns associated with crossing supercells.

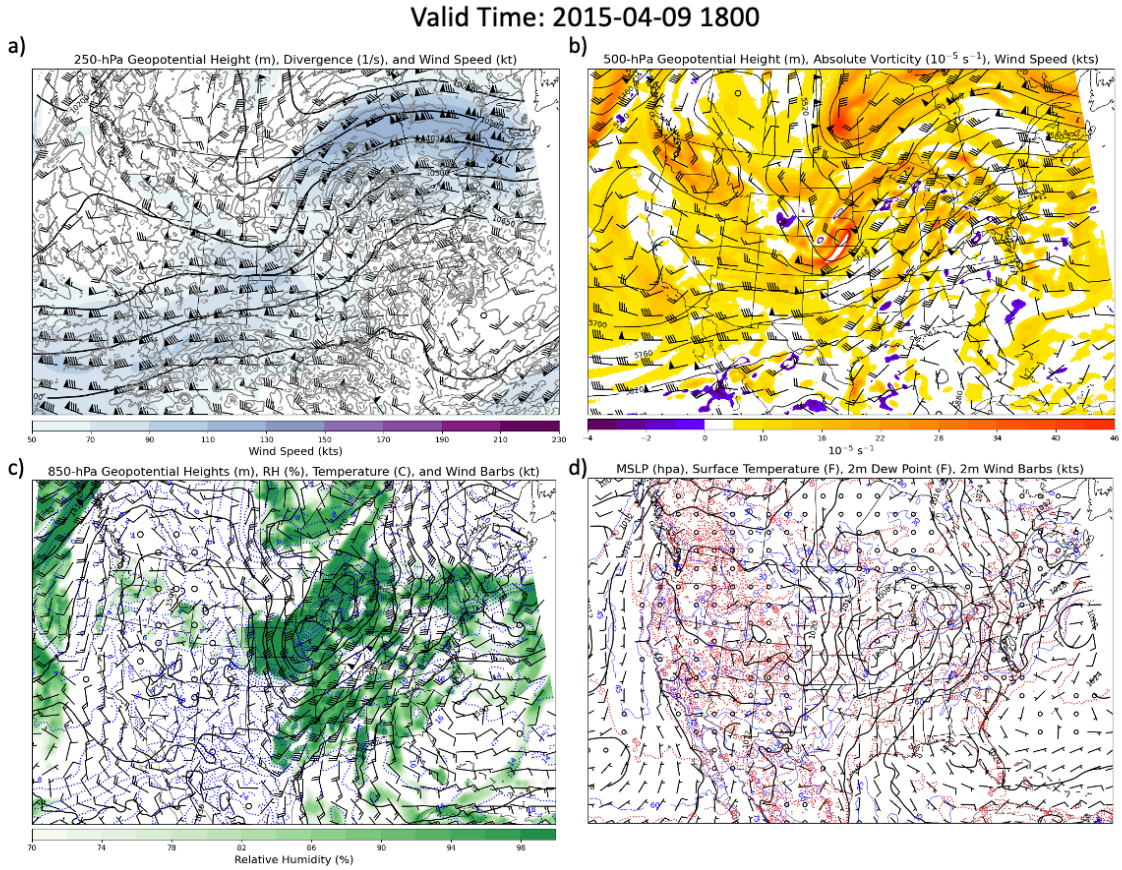

Figure 4.10: As in as figure 4.9, but representing non-crossing supercells.

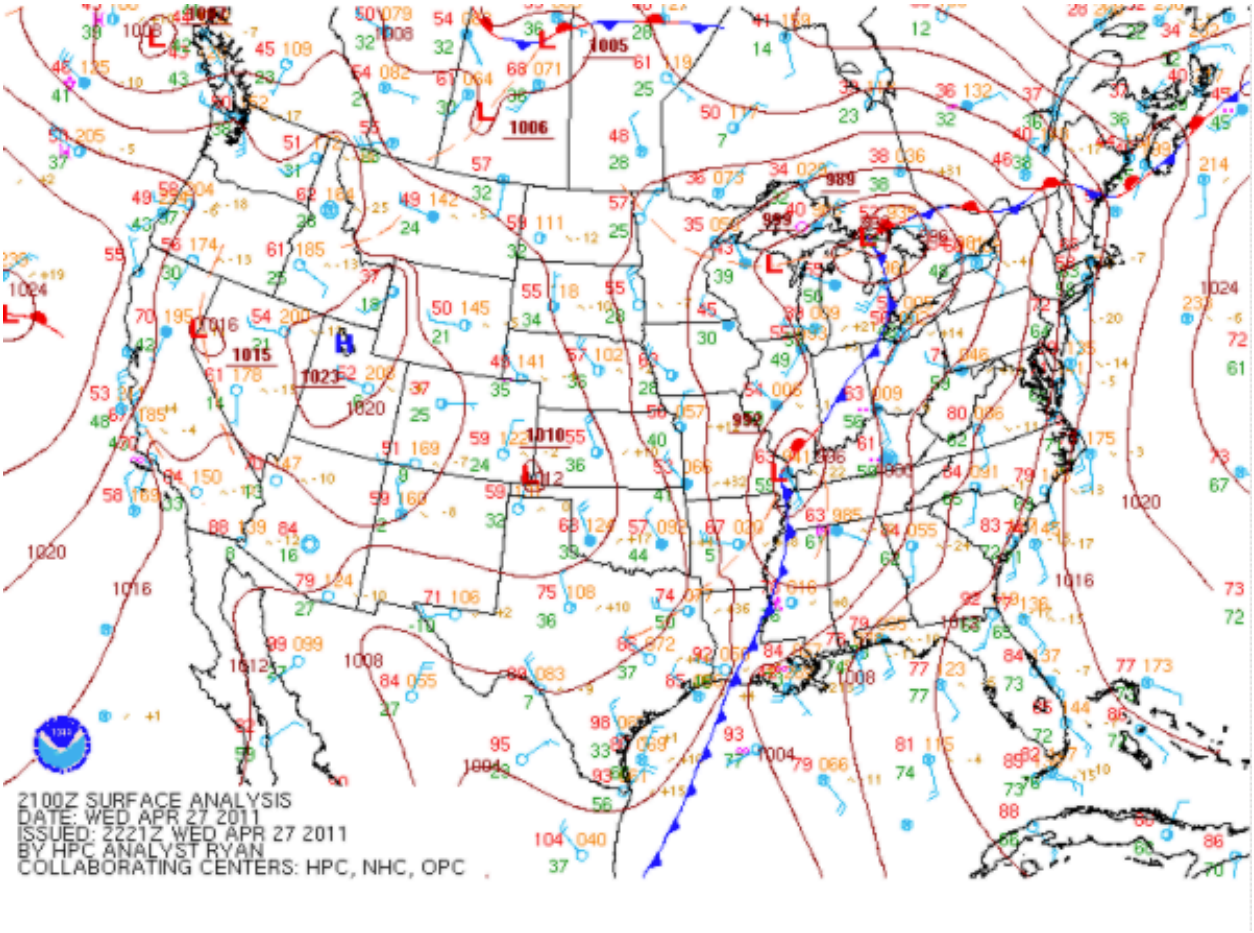

Figure 4.11: From the Weather Prediction Center, a surface analysis representing cases associated with a cold front.

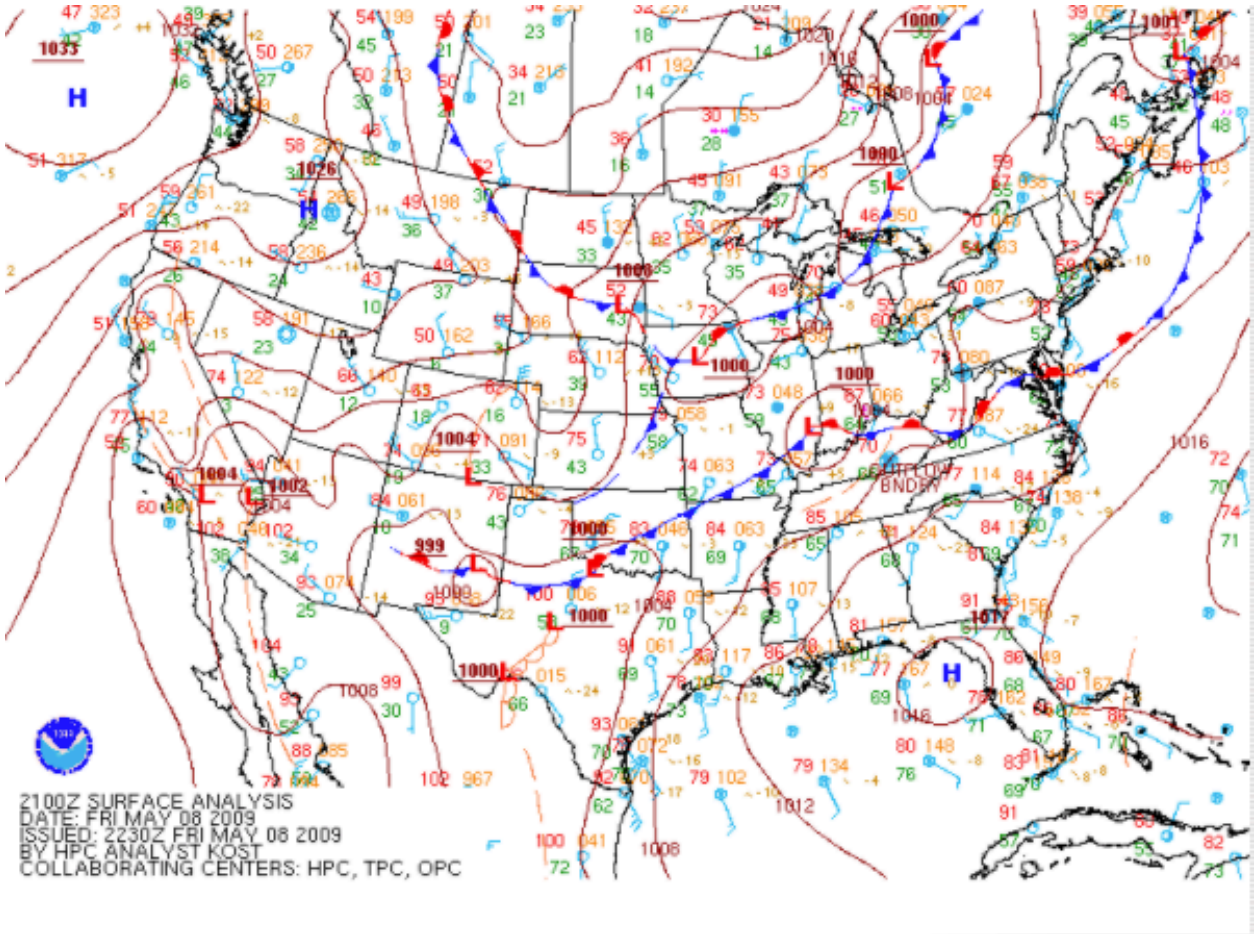

Figure 4.12: As in Fig. 4.11, but for cases associated with a stationary front and an outflow boundary.

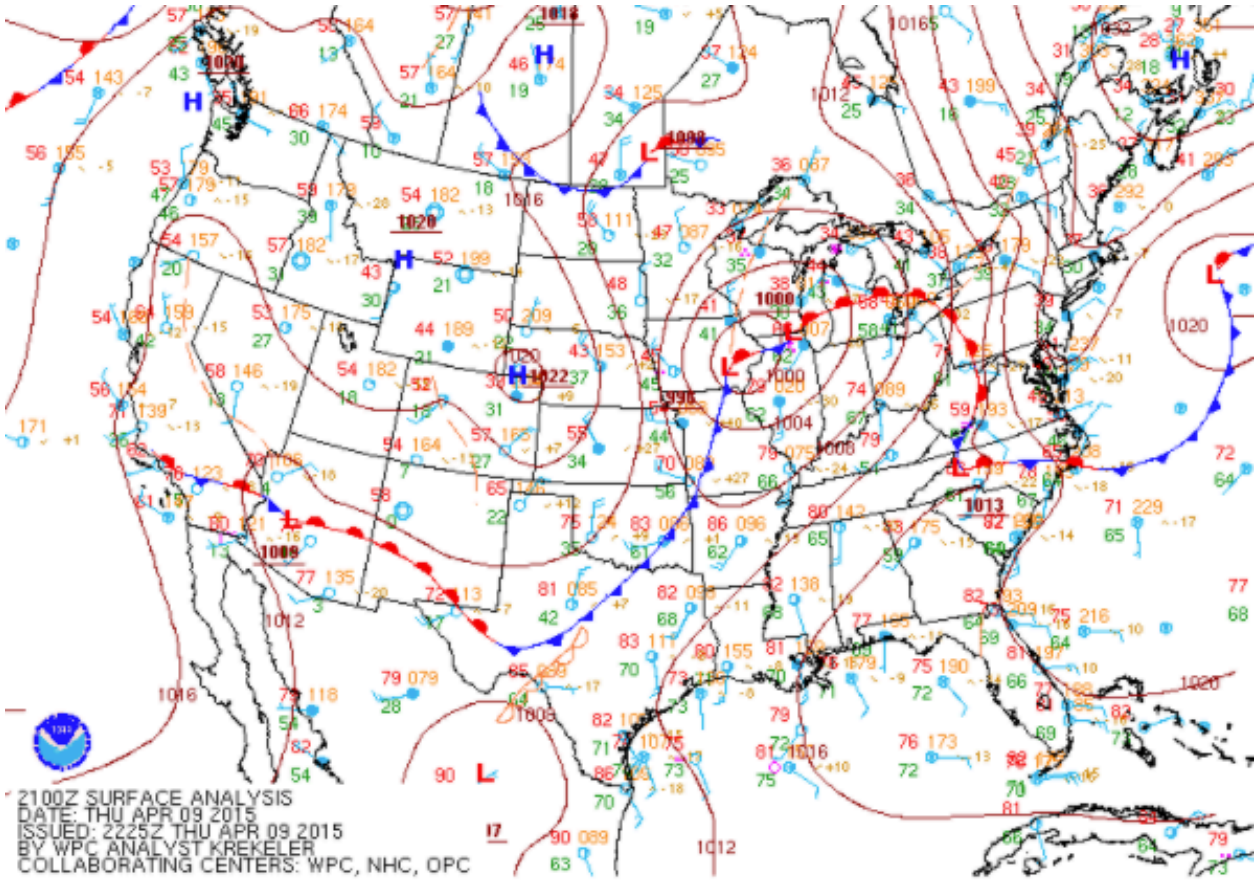

Figure 4.13: Figure 4.12: As in Fig. 4.11, but for cases associated with a stationary front.

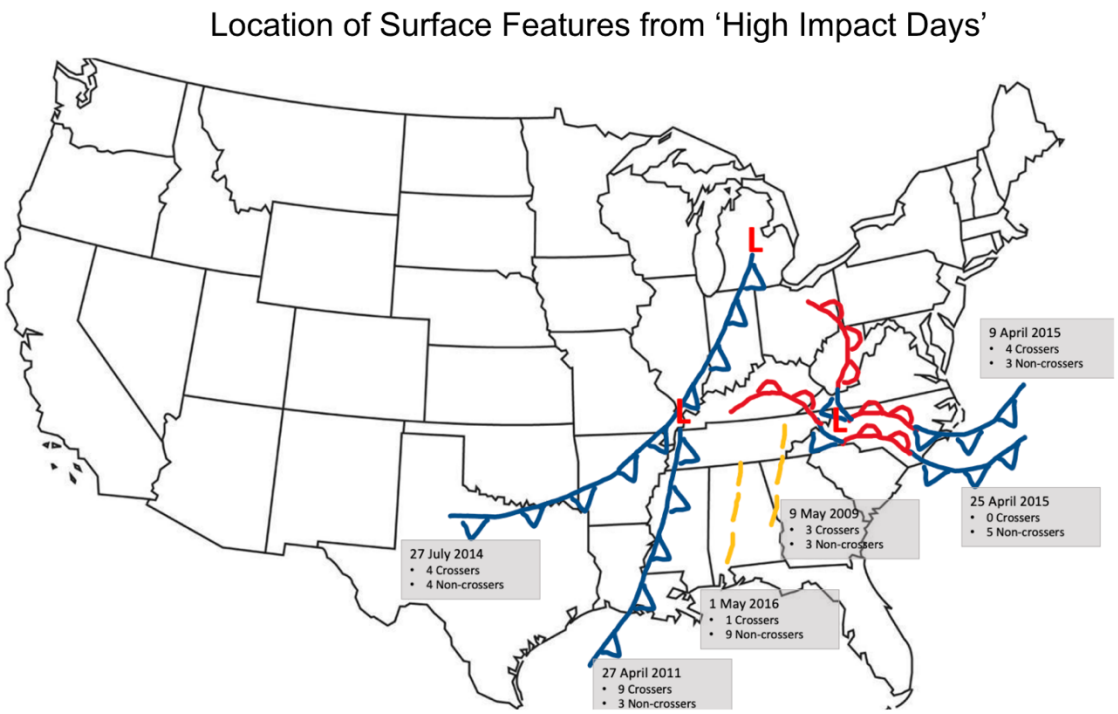

Figure 4.14: The locations of the surface features (i.e., cold fronts (blue lines), stationary fronts (red and blue lines), low pressures (red 'L'), and outflow boundaries (yellow dashed lines) from the 'high impact days" (5+ supercells occurring on one day).

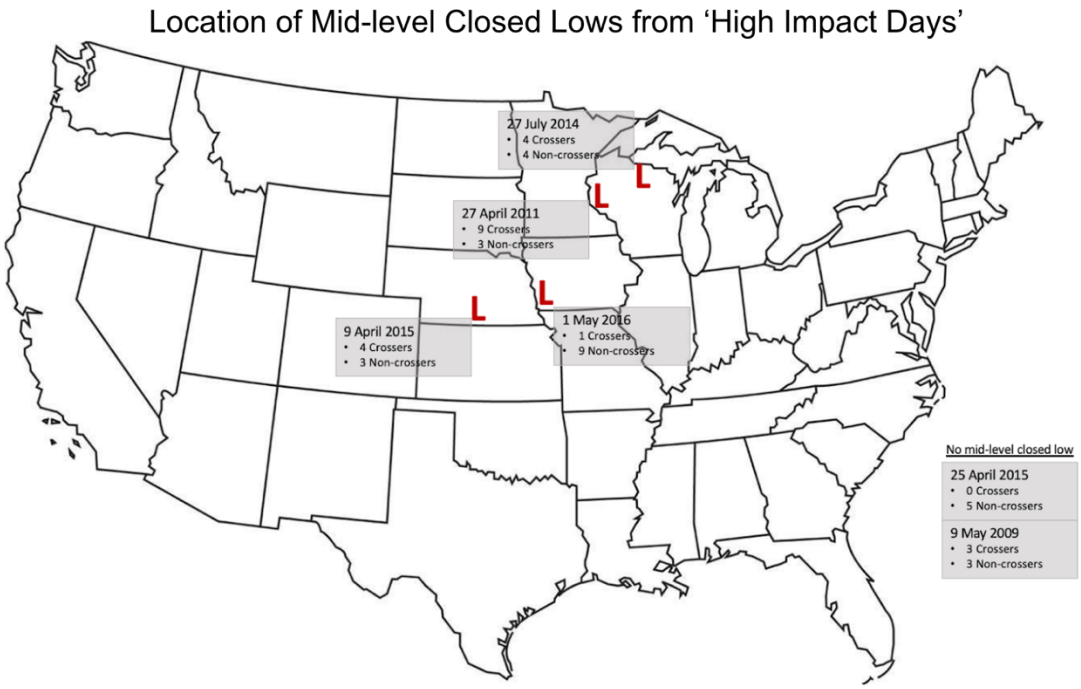

Figure 4.15: The location of mid-level closed lows (red 'L') from 'high impact days' (5+ supercells occurring on one day).

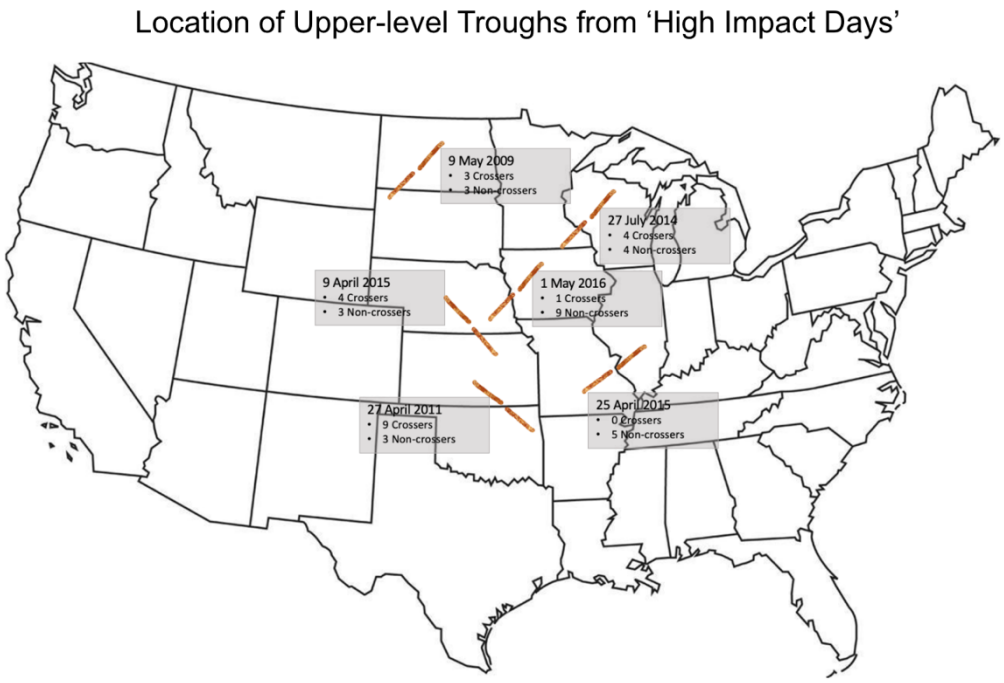

Figure 4.16: The location and tilt of upper-level trough axes (brown dashed lines) from the 'high impact days' (5+ supercells occurring on one day).

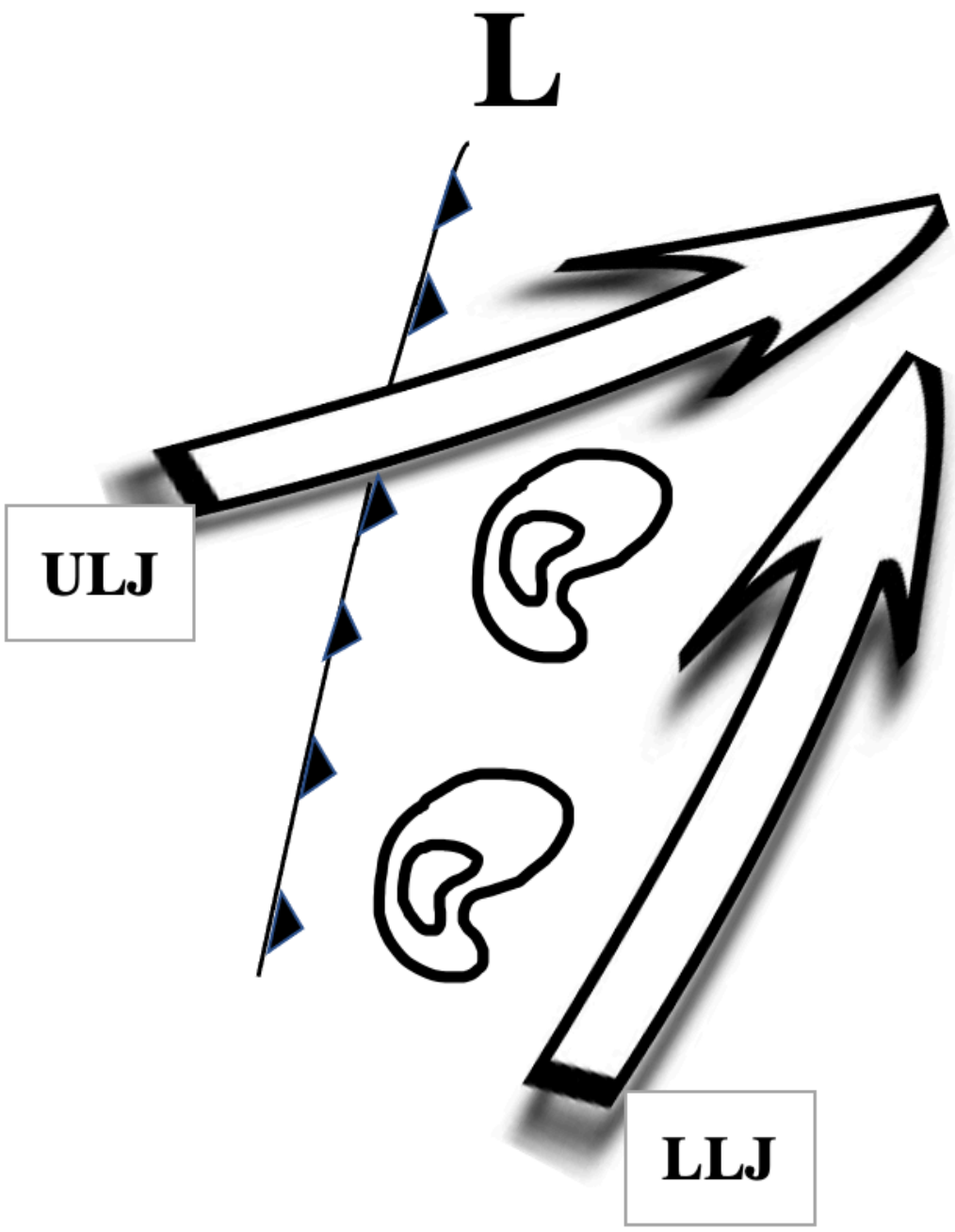

Figure 4.17: Depiction of a typical synoptic setup for crossing supercells, with cells initiating ahead of a cold front, a low-level jet present, and to the right of an upper-level jet.

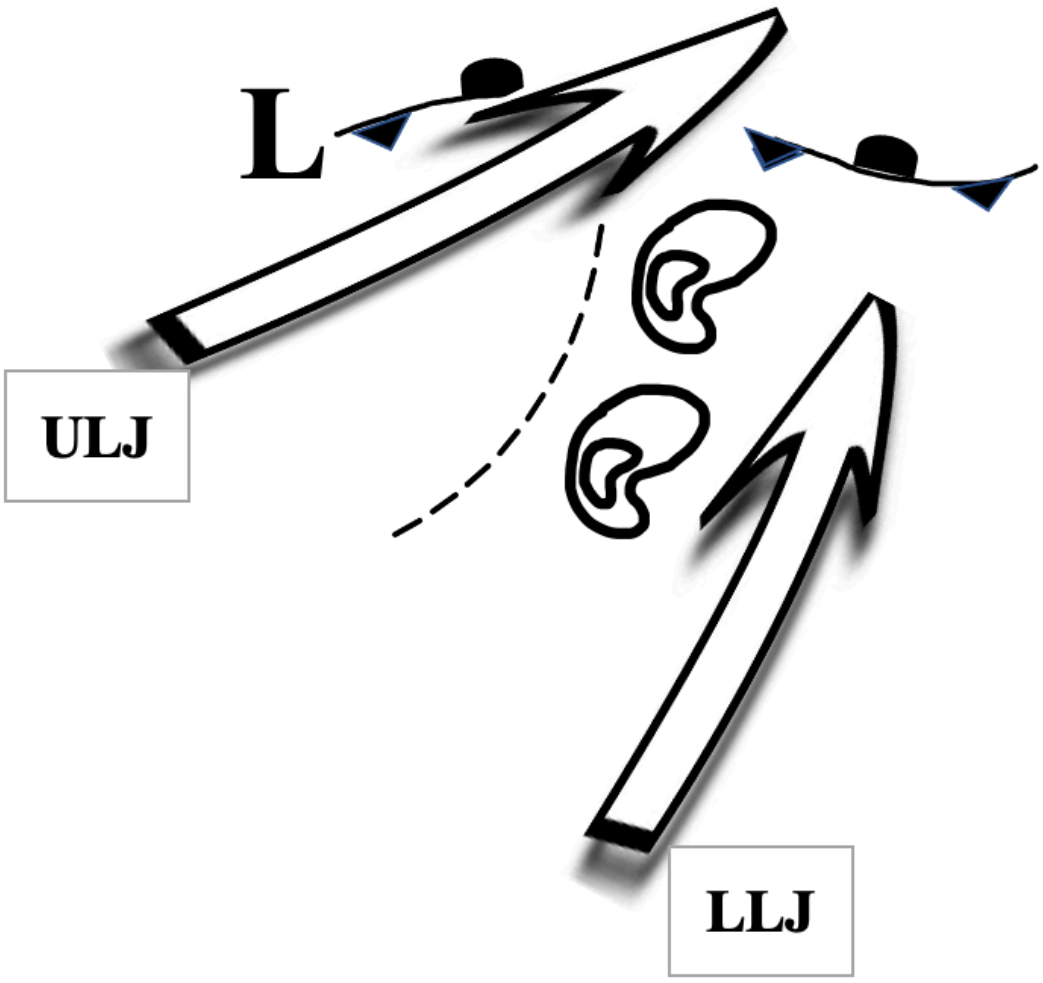

Figure 4.18: Depiction of a typical synoptic setup for non-crossing supercells, with cells initiating ahead of an outflow boundary, a stationary front present, a low-level jet present, and to the right of an upper-level jet.

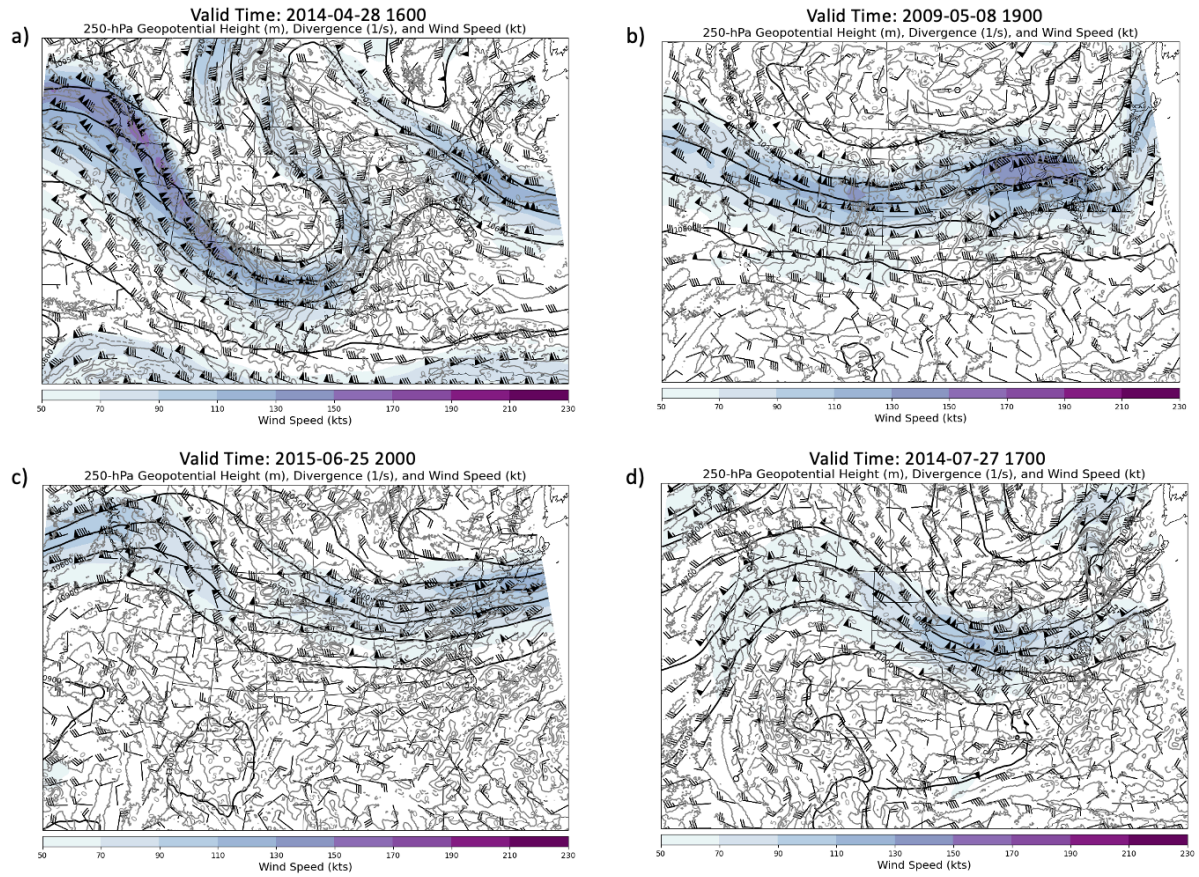

Figure 4.19: Typical 250 hPa pattern associated with a) April, b) May, c) June, and d) July supercells.

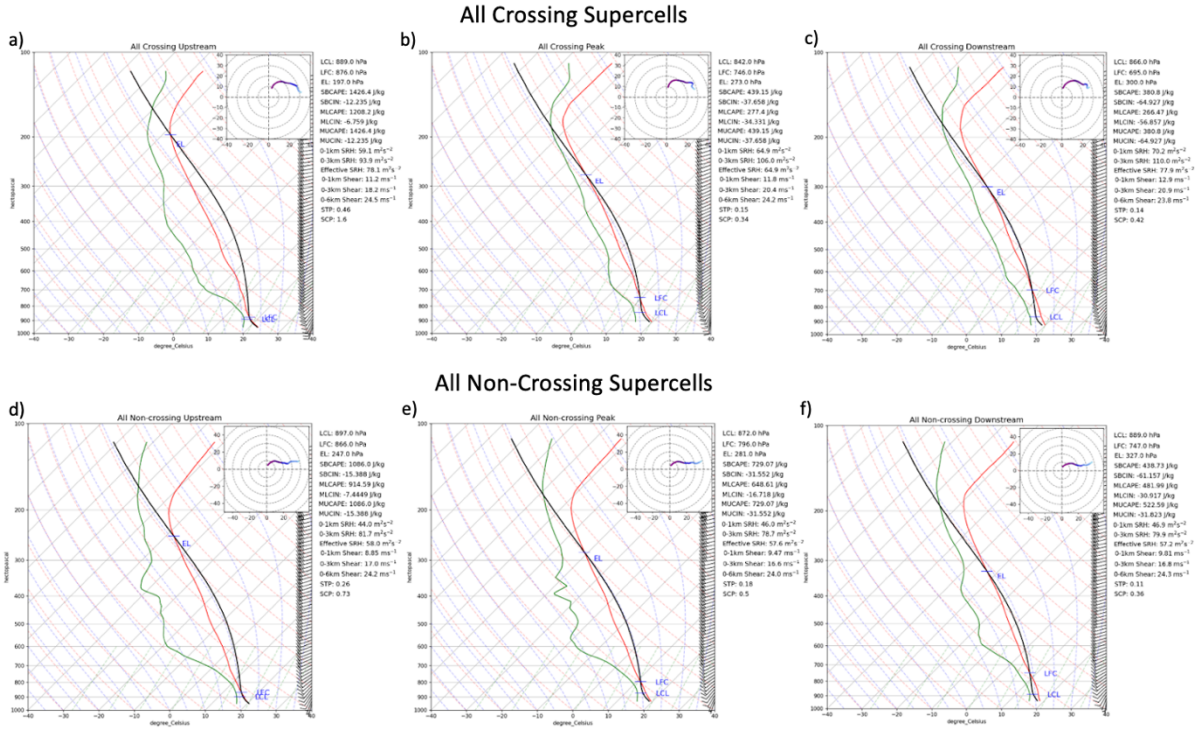

Figure 4.20: Composite soundings and hodographs of the (a) and (d) upstream points, (b) and (e) peak elevation points, and (c) and (f) downstream points for the crossers and non-crossers respectively.

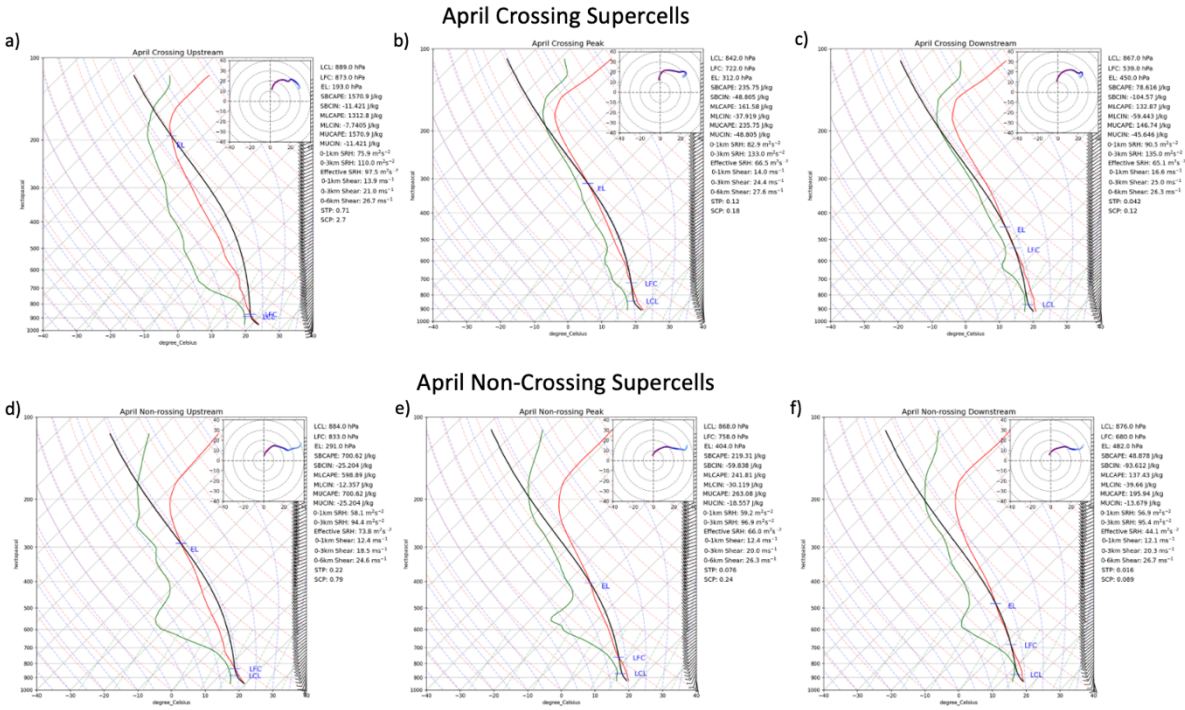

Figure 4.21: As in Fig. 4.17, except for the supercells that occurred in April.

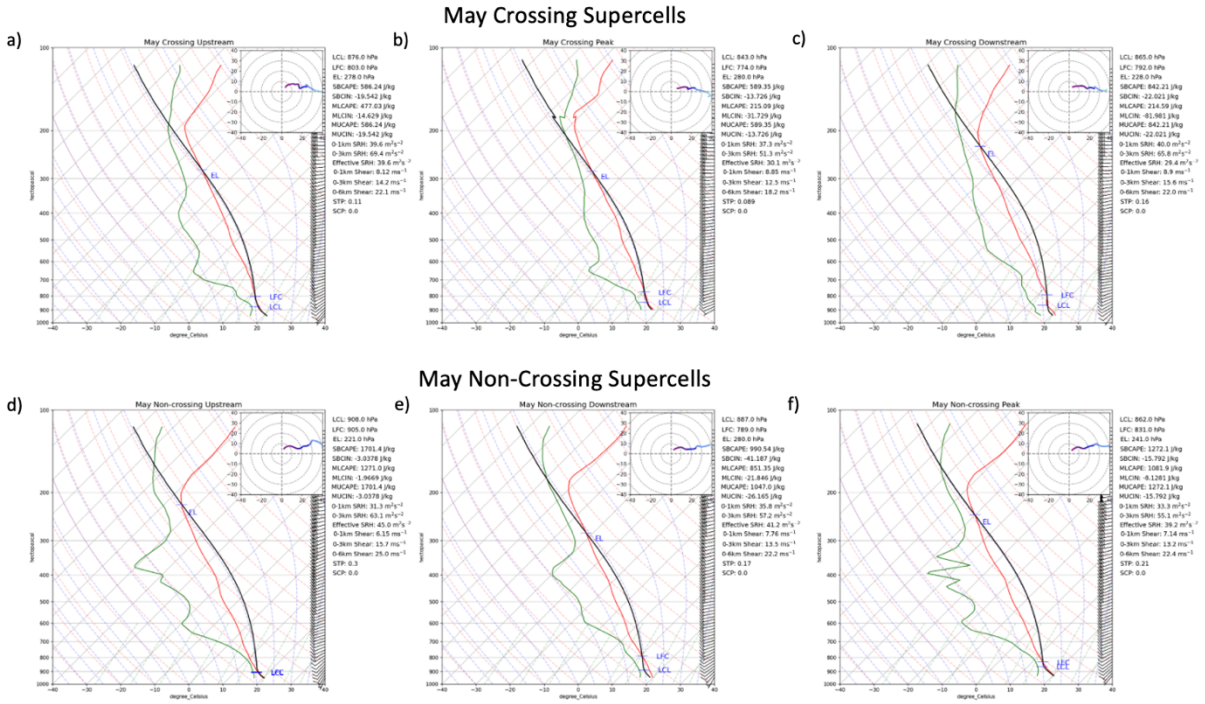

Figure 4.22: As in Fig. 4.17, except for the supercells that occurred in May.

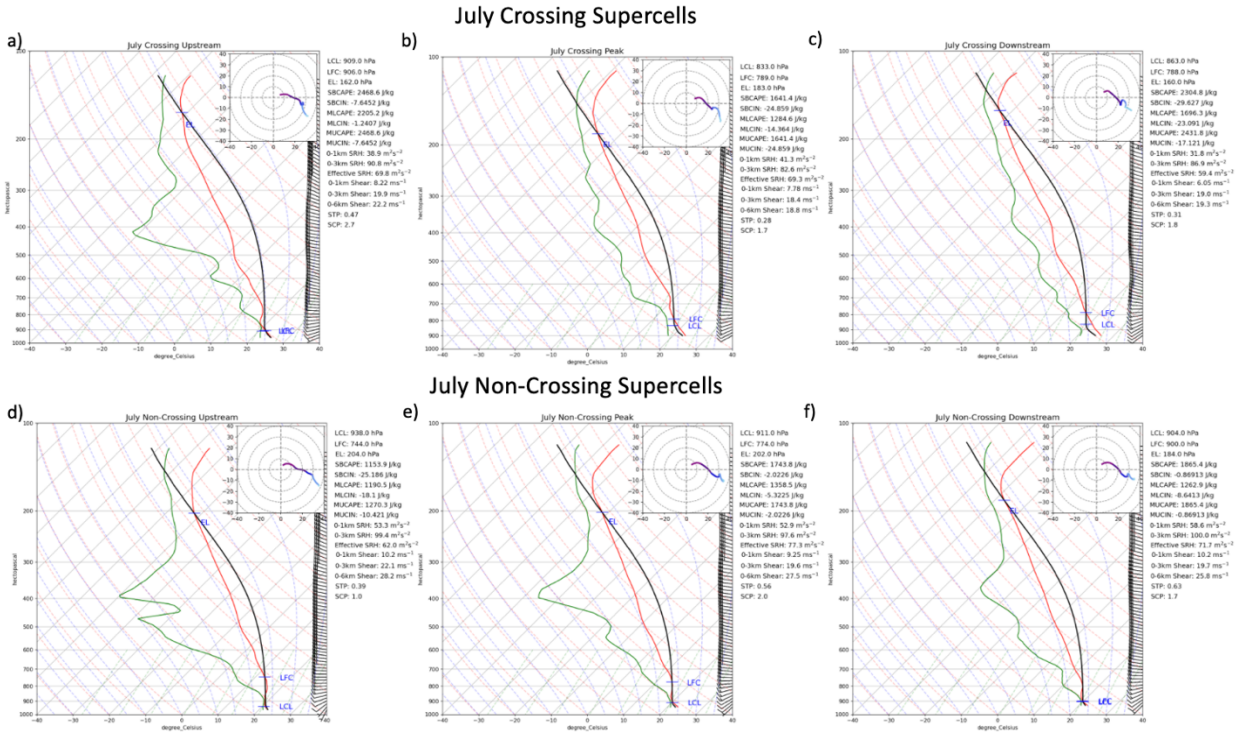

Figure 4.23: As in Fig. 4.17, except for the supercells that occurred in July.

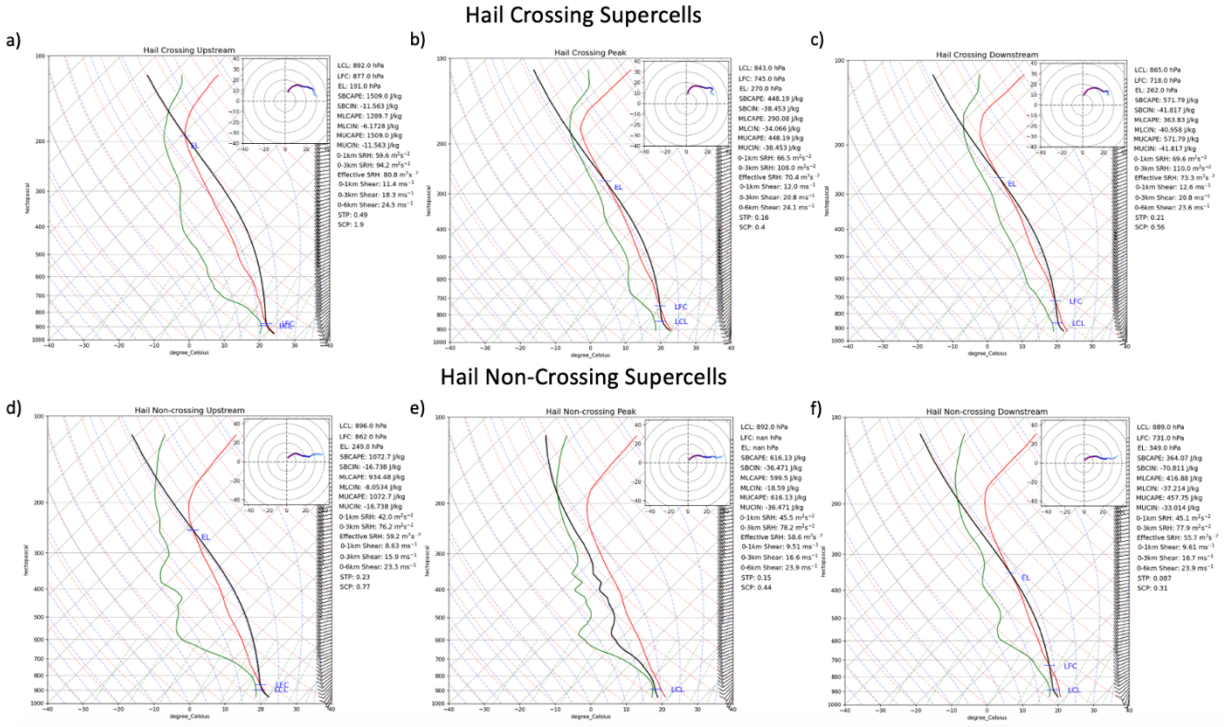

Figure 4.24: As in Fig. 4.17, except for the supercells that produced severe hail.

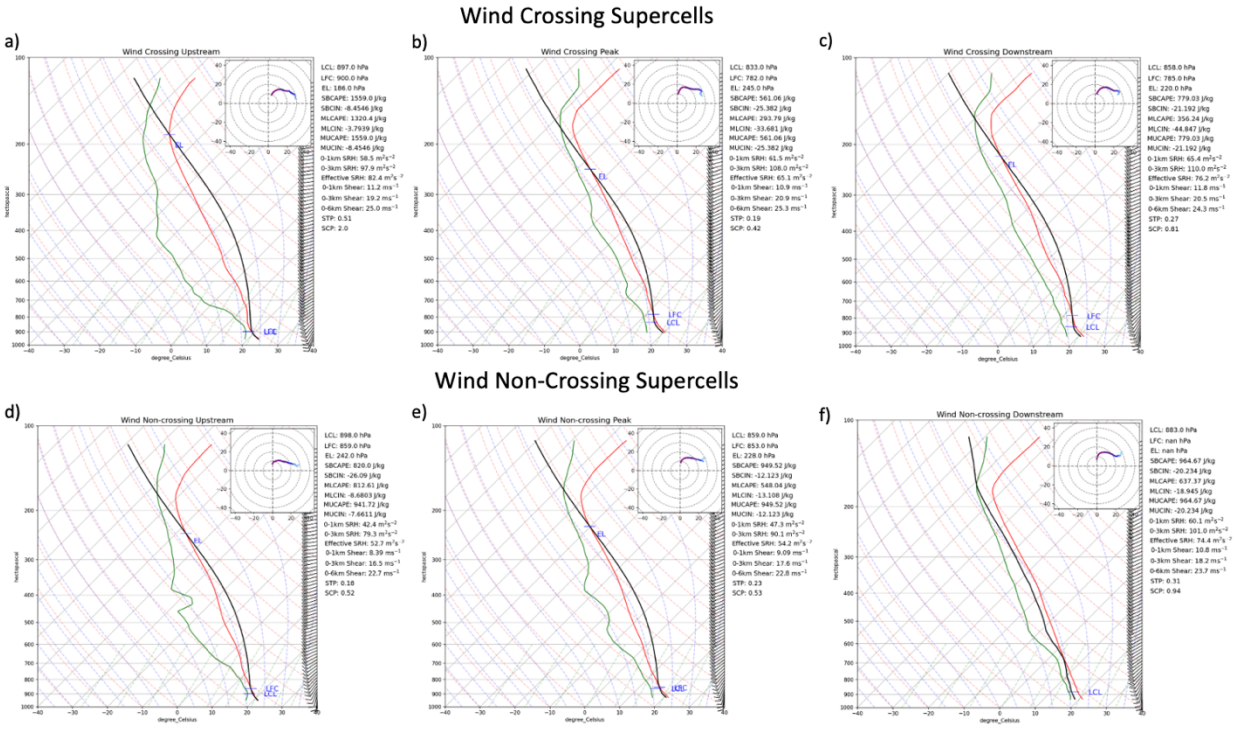

Figure 4.25: As in Fig. 4.17, except for the supercells that produced severe wind.

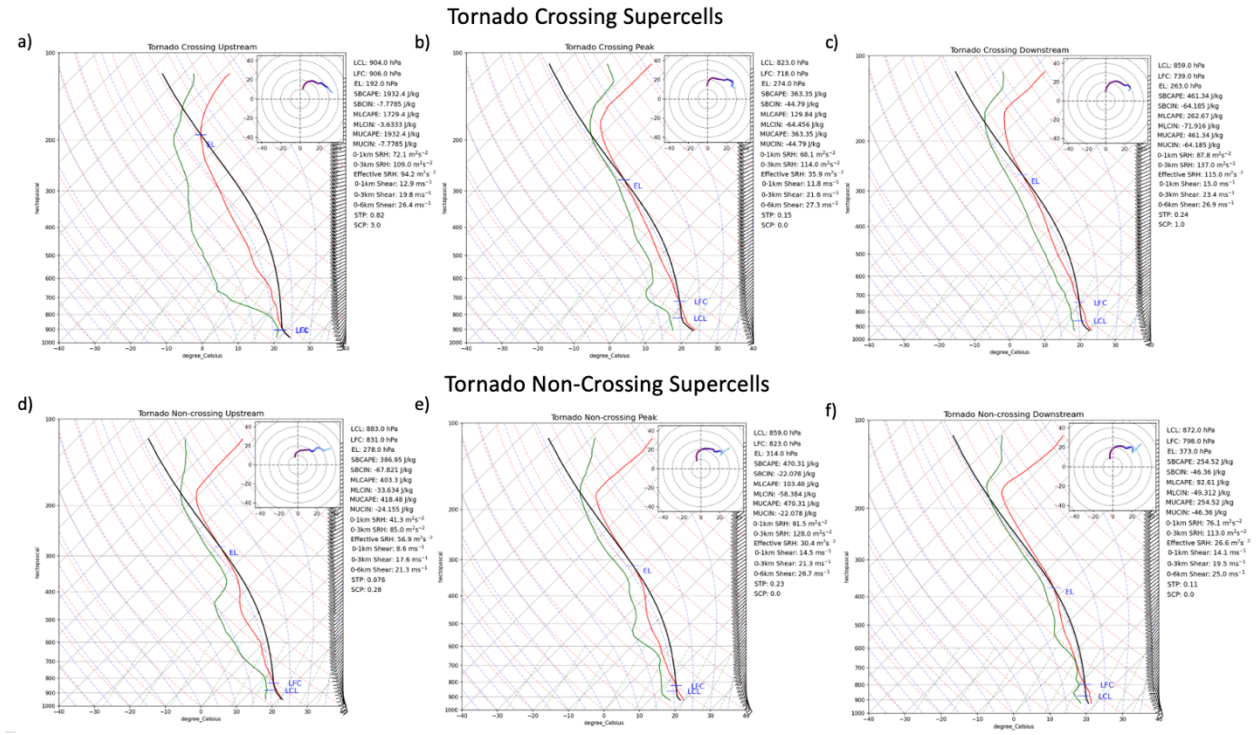

Figure 4.26: As in Fig. 4.17, except for the supercells that produced tornadoes.

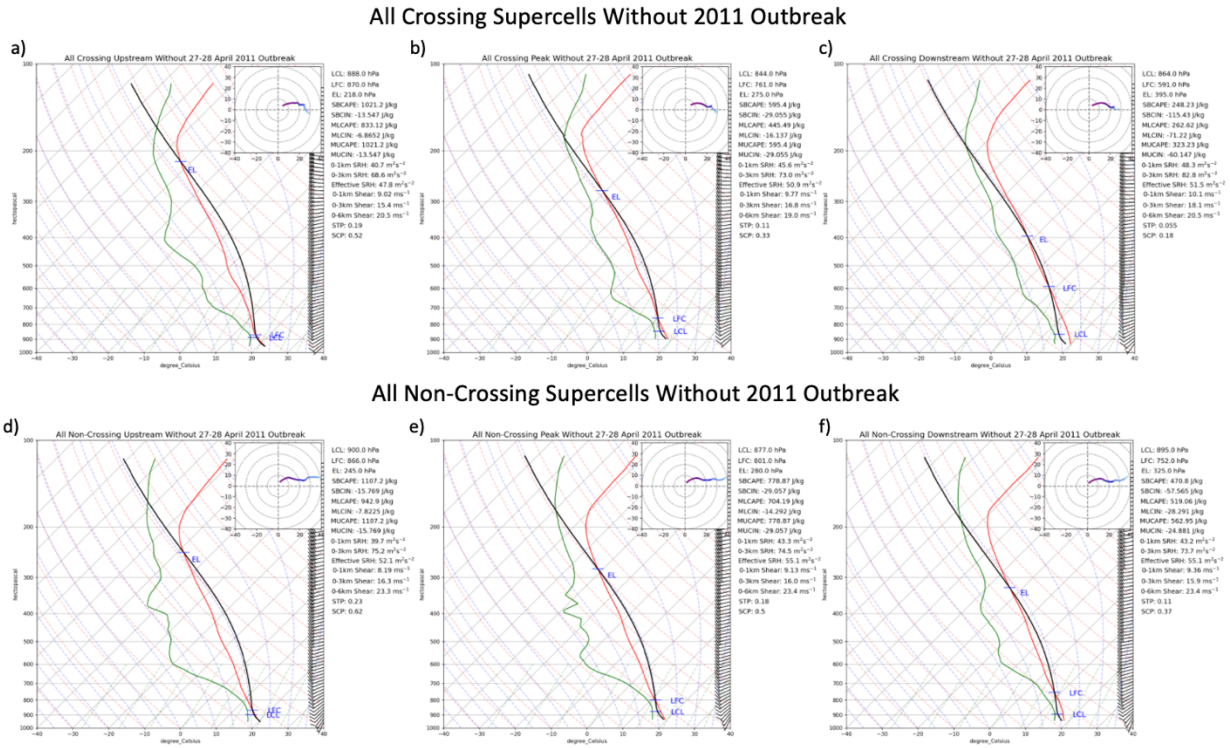

Figure 4.27: As in Fig. 4.17, except with the 27-28 April 2011 supercells removed.

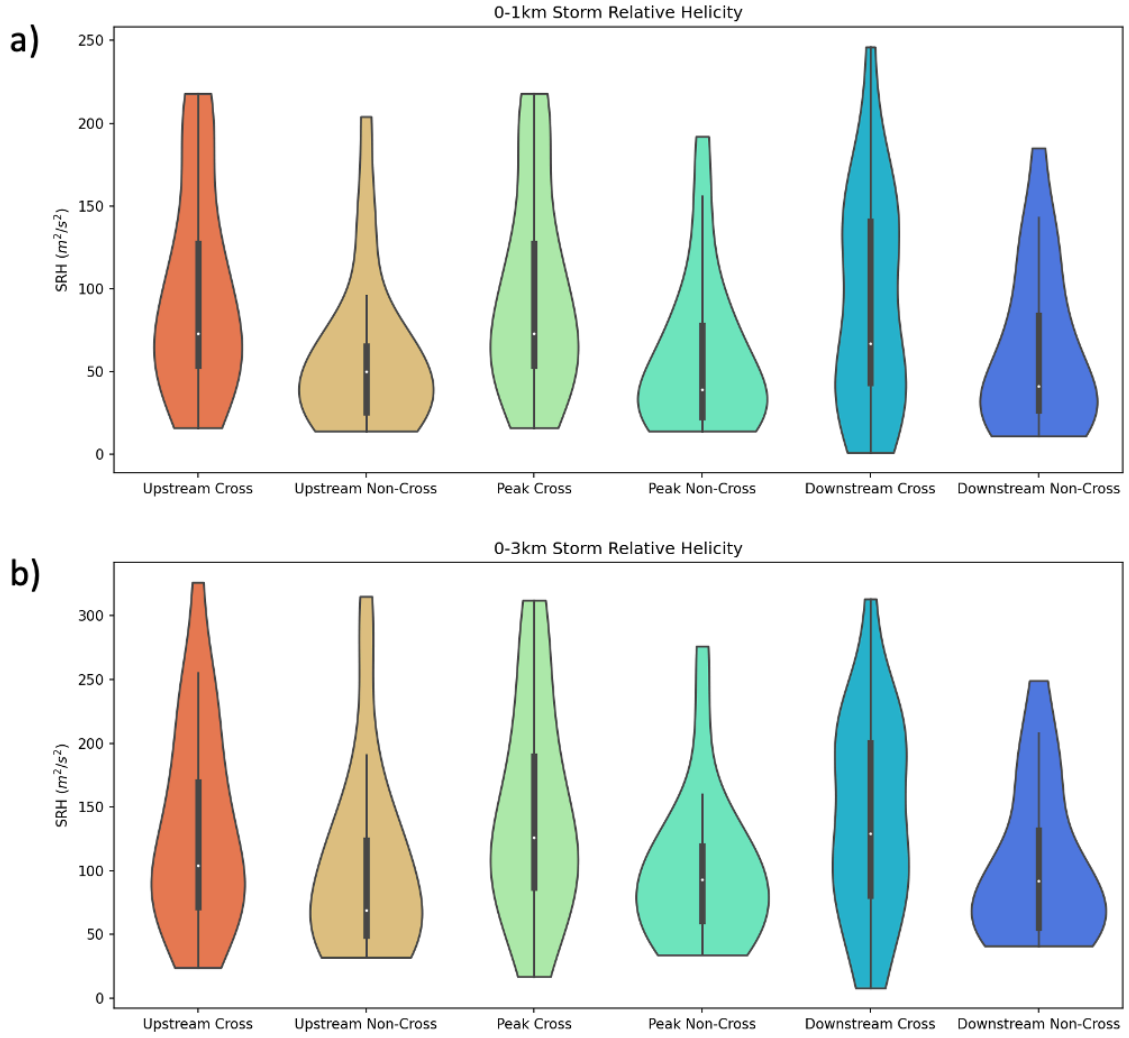

Figure 4.28: Violin plots representing the median (white dot), first quartile (lower thick black line), third quartile (upper thick black line), lower adjacent value (lower thin black line), upper adjacent value (upper thin black line), and distribution of the values of a) 0-1km SRH and b) 0-3km SRH with respect to the upstream, peak, and downstream points for all of the crossers and non-crossers.

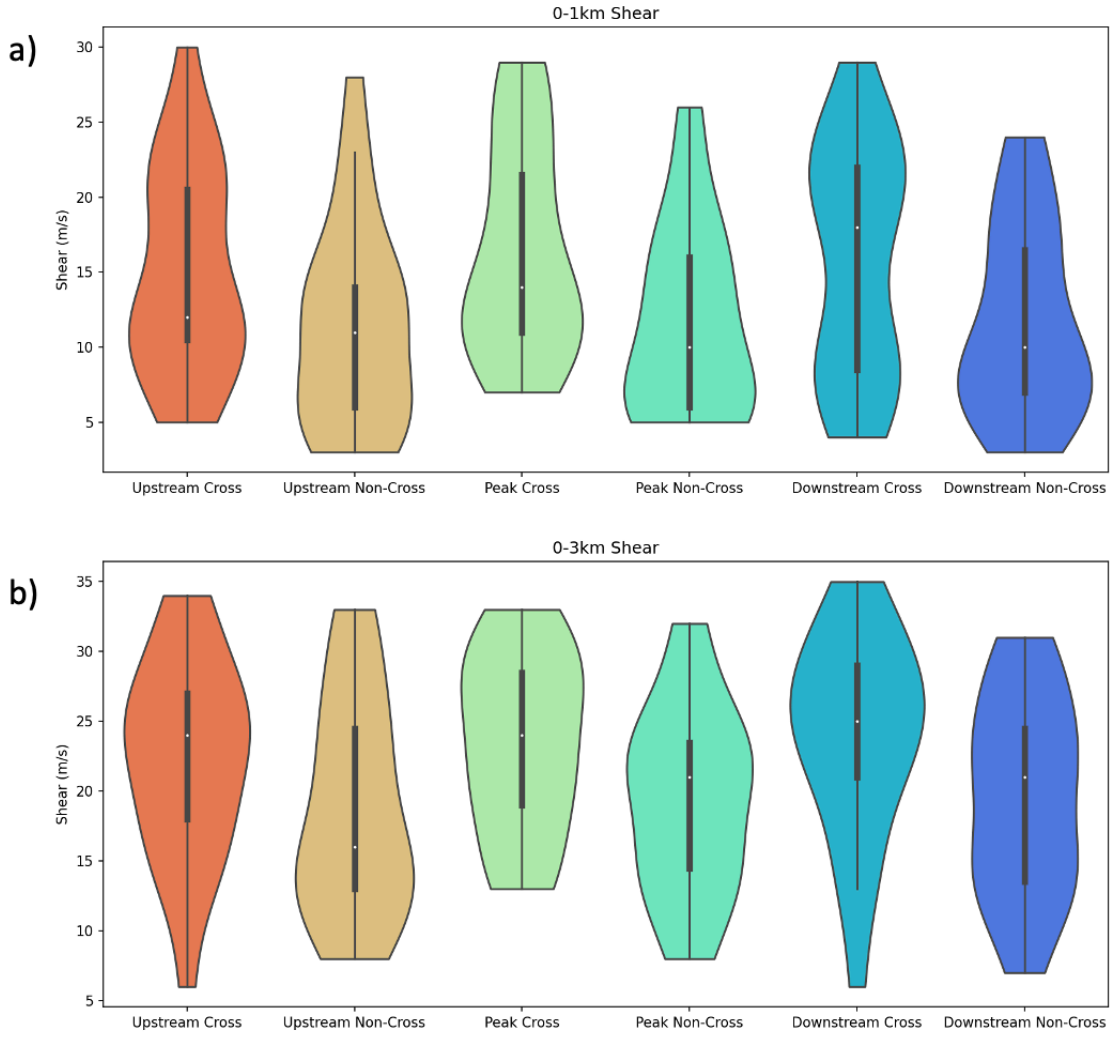

Figure 4.29: As in Fig. 4.25, but for the a) 0-1 km and b) 0-3 km bulk shear across the upstream, peak, and downstream points.

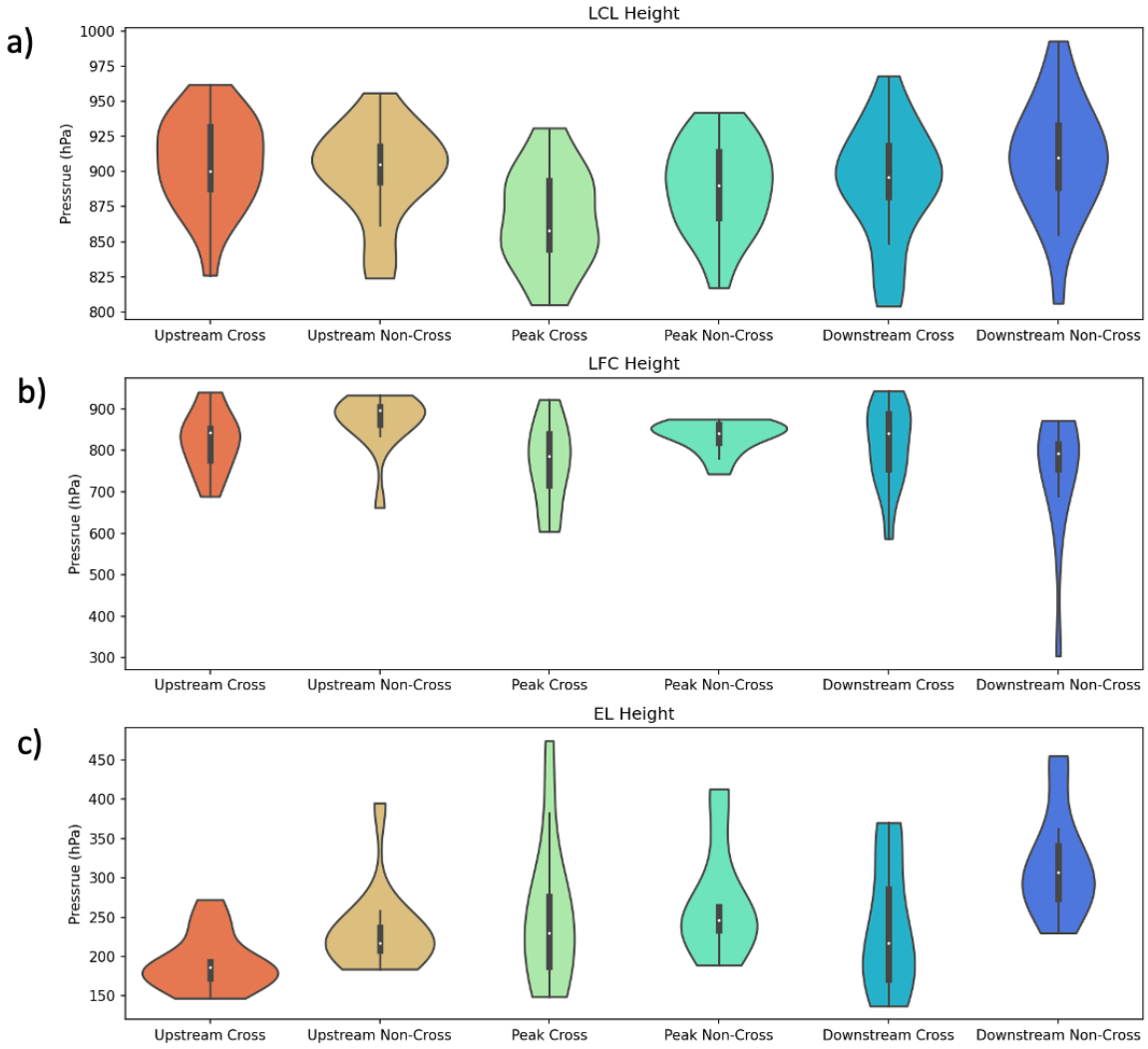

Figure 4.30: As in Fig. 4.25, but for the a) LCL, b) LFC, and c) EL across the upstream, peak, and downstream points.

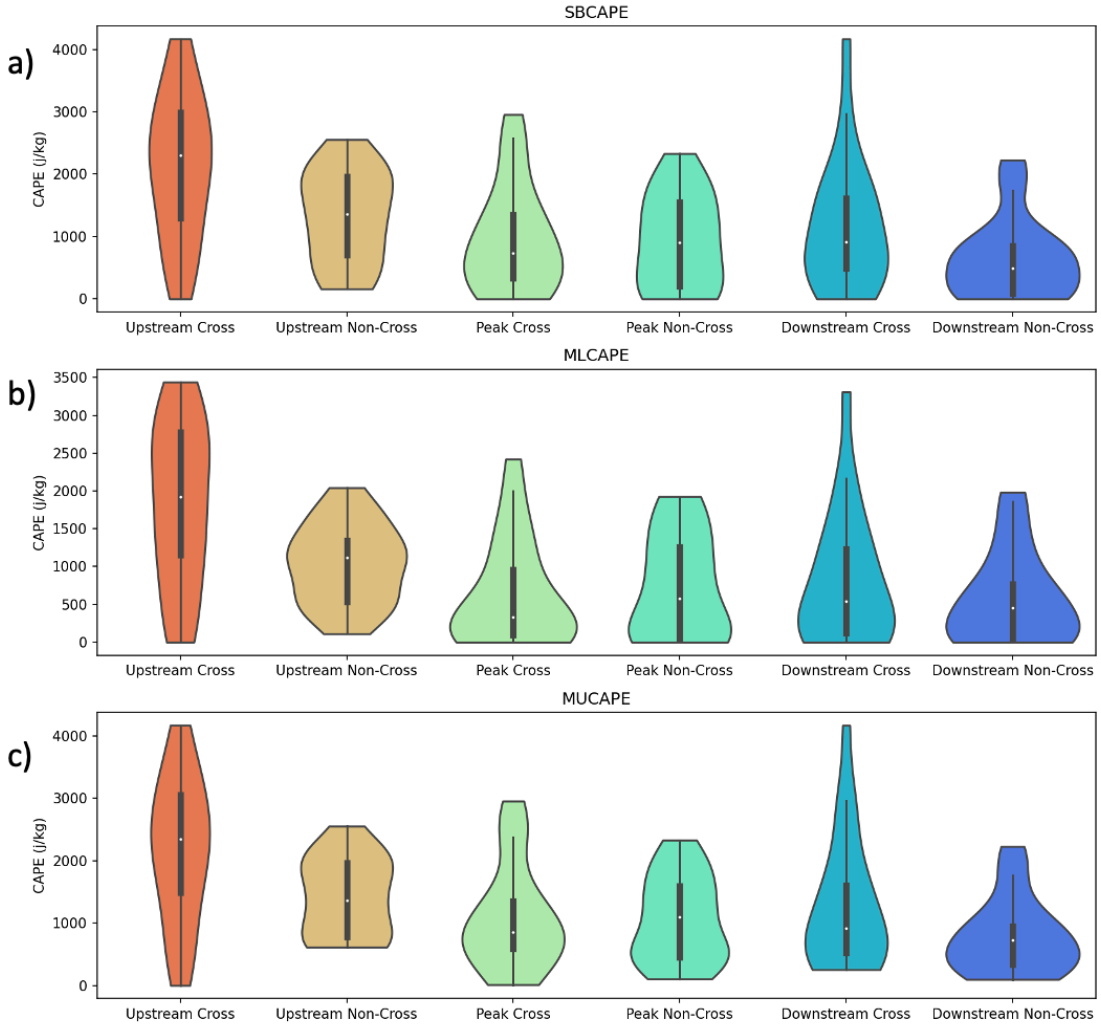

Figure 4.31: As in Fig. 4.25, but for the a) SBCAPE, b) MLCAPE and c) MUCAPE across the upstream, peak, and downstream points.

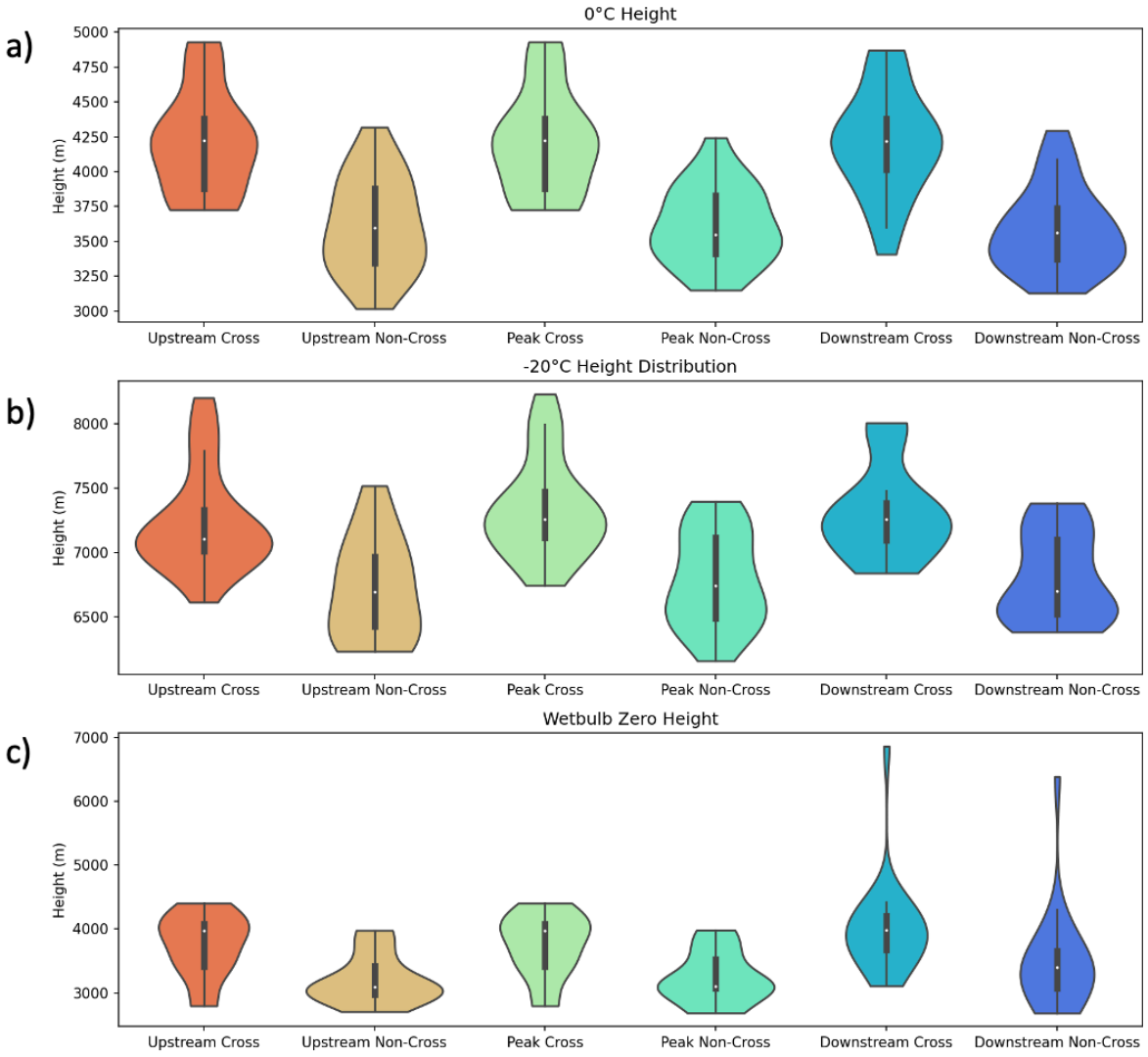

Figure 4.32: As in Fig. 4.25, but for the a) 0°C height, b) -20°C height, and c) wet bulb-zero height across the upstream, peak, and downstream points.

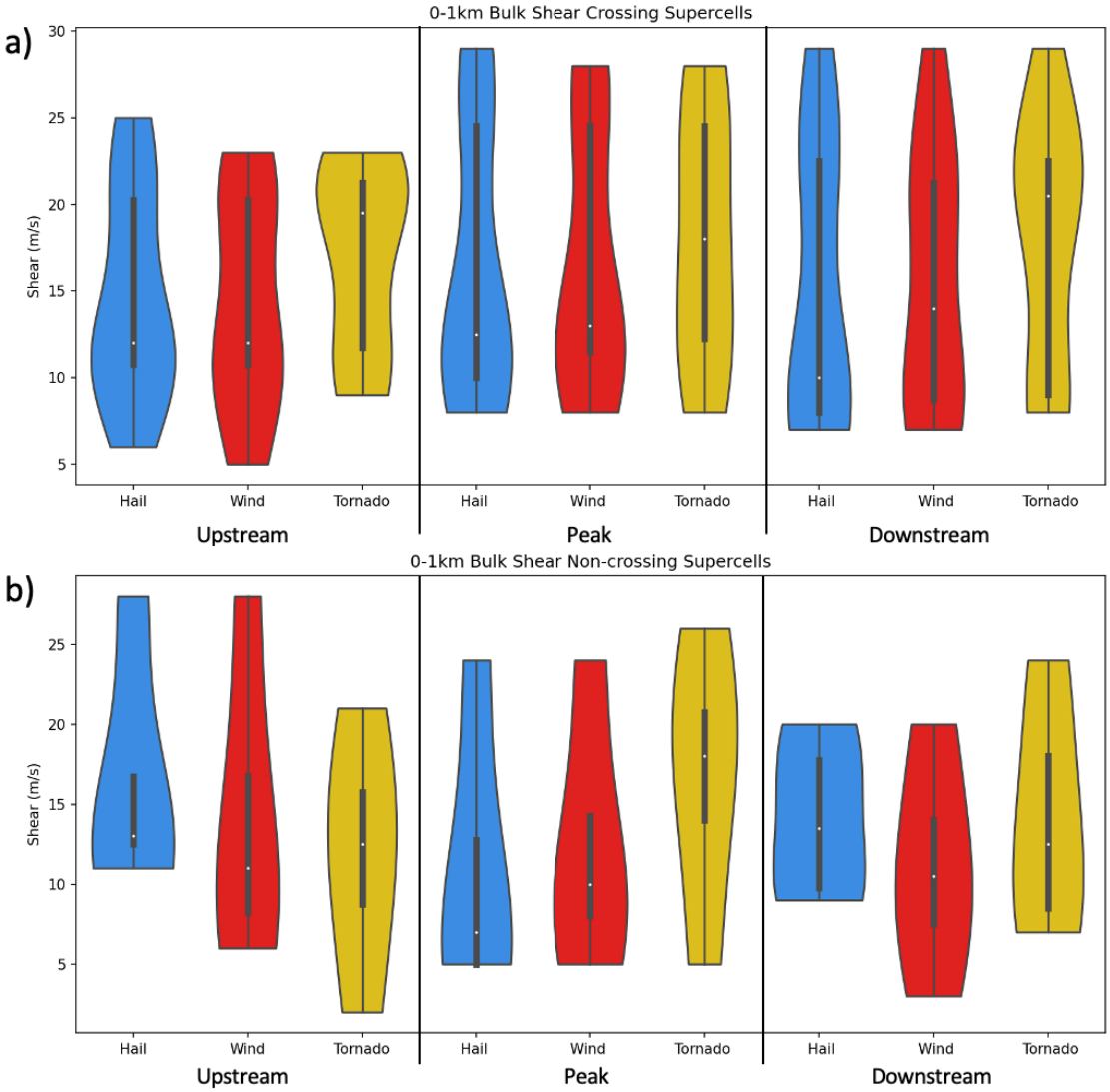

Figure 4.33: As in Fig. 4.25, but for a) crossing and b) non-crossing supercells that produced severe hail (blue), severe wind (red), and tornadoes (yellow) at the upstream, peak, and downstream points.

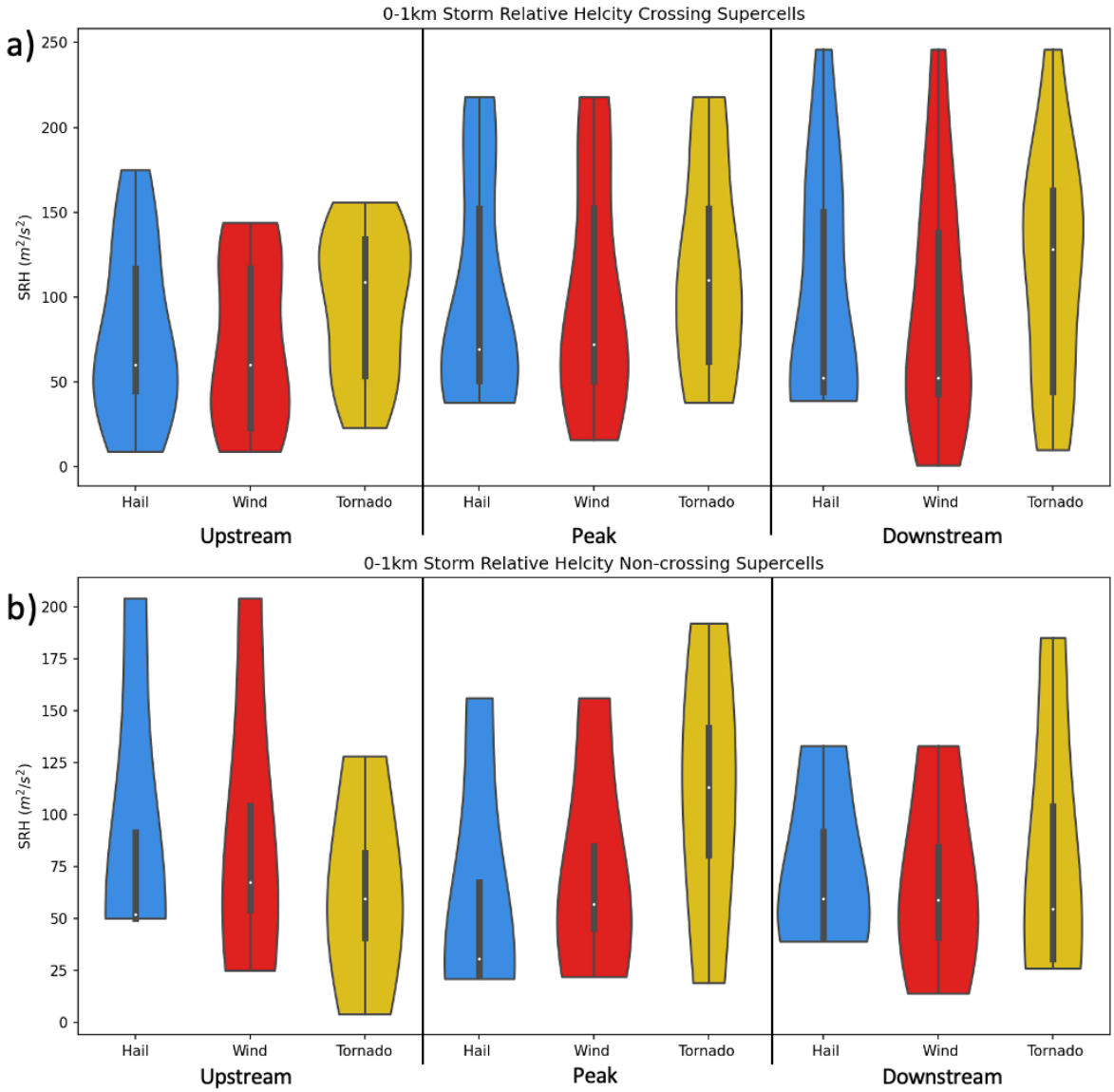

Figure 4.34: As in Fig. 4.30, but for 0-1km storm relative helicity.

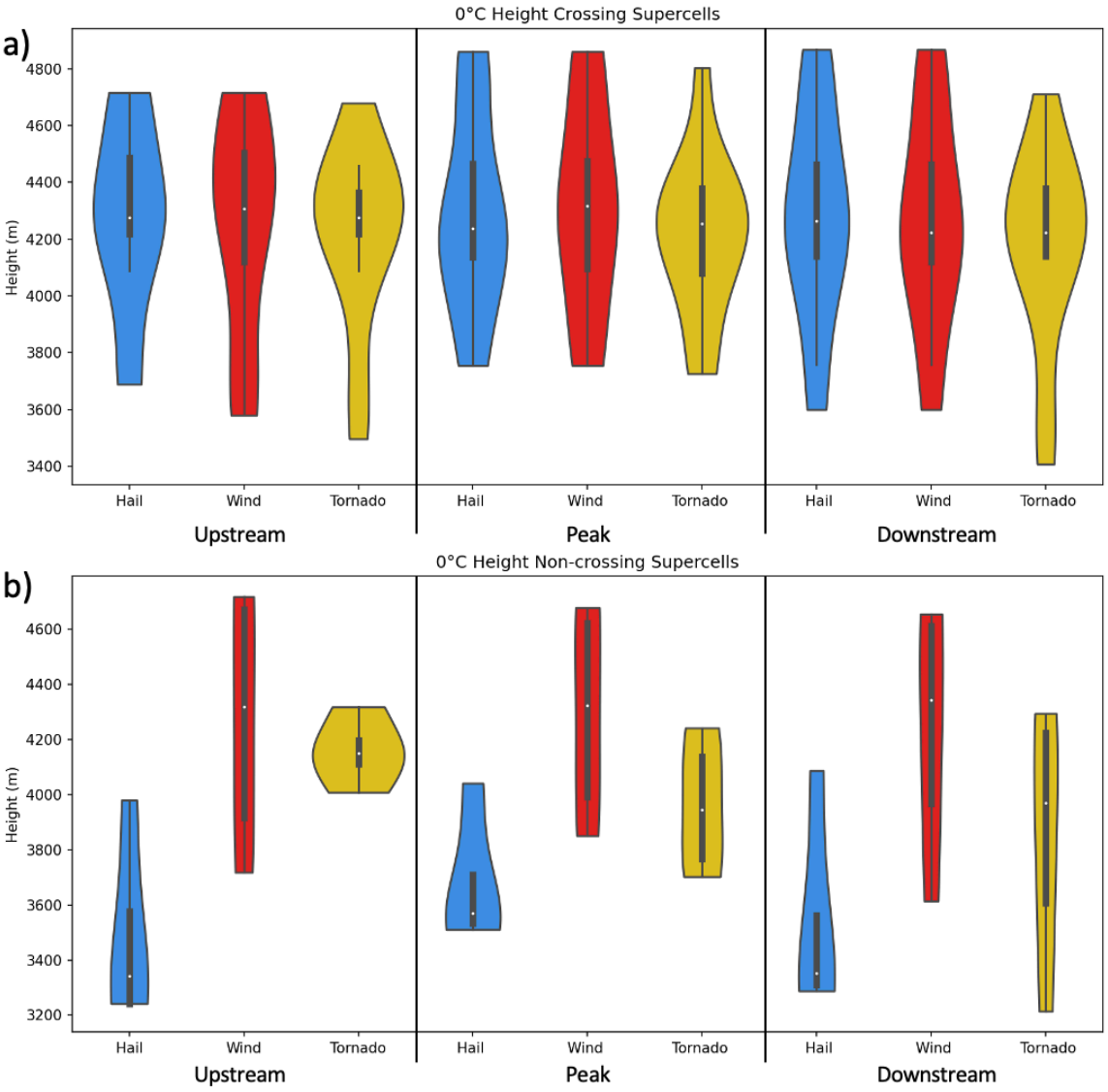

Figure 4.35: As in Fig. 4.30, but for 0°C height.

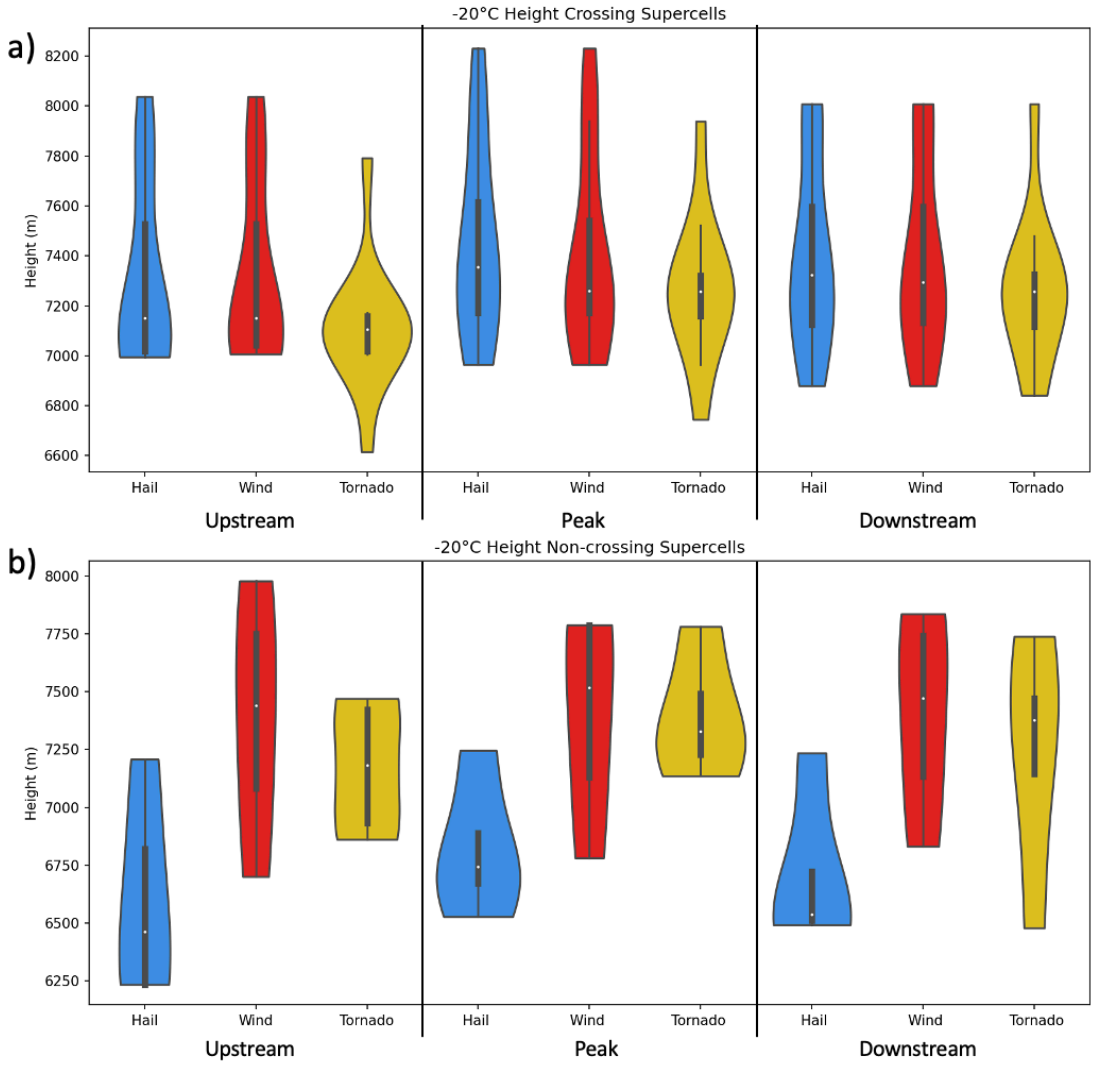

Figure 4.36: As in Fig. 4.30, but for -20°C height.

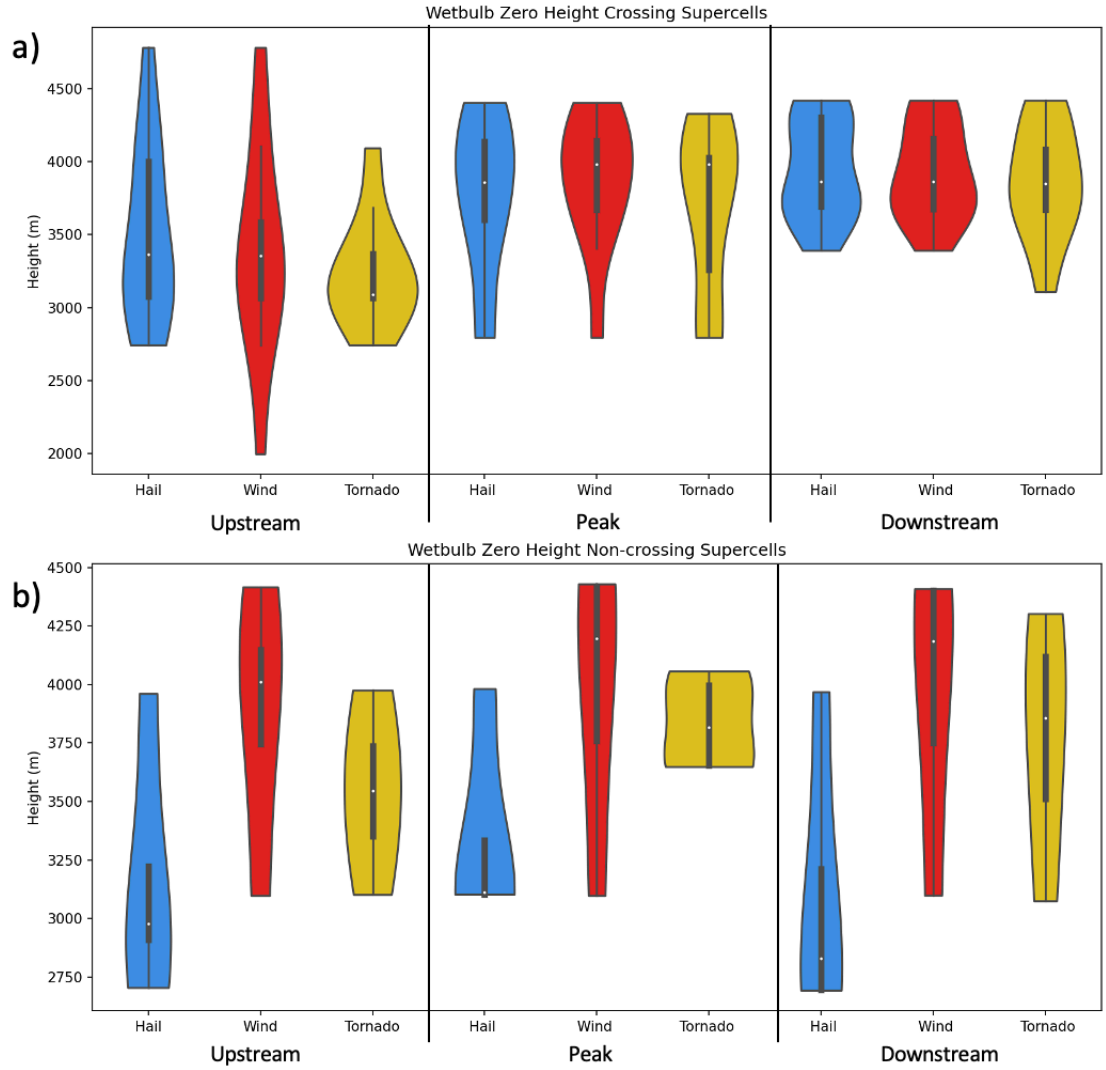

Figure 4.37: As in Fig. 4.30, but for wet bulb-zero height.

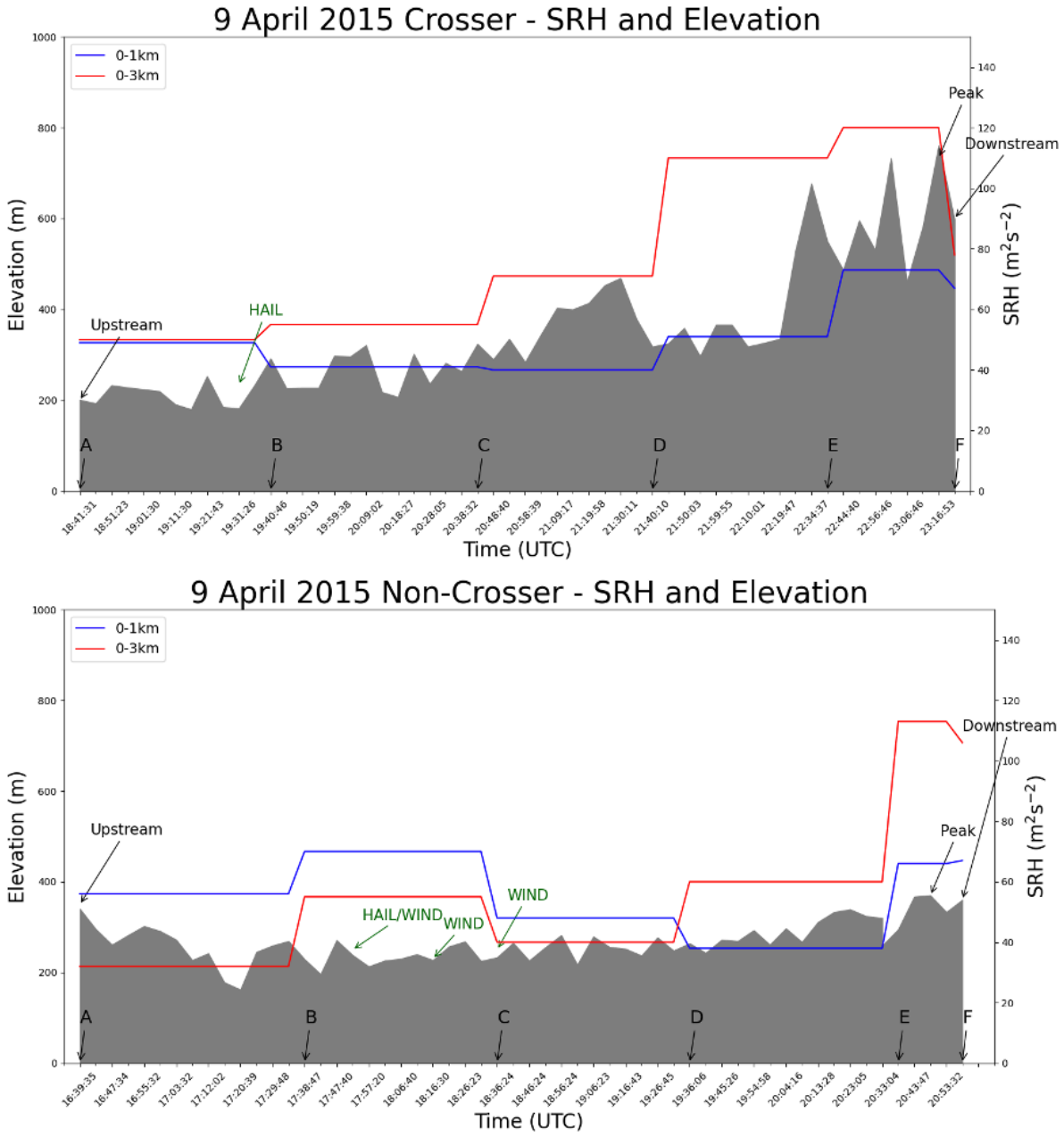

Figure 4.38: Example of 0-1 km (blue) and 0-3km (red) SRH with respect to terrain (grey), severe weather (green), and the upstream, peak, and downstream points. A-F indicates when the soundings were pulled.

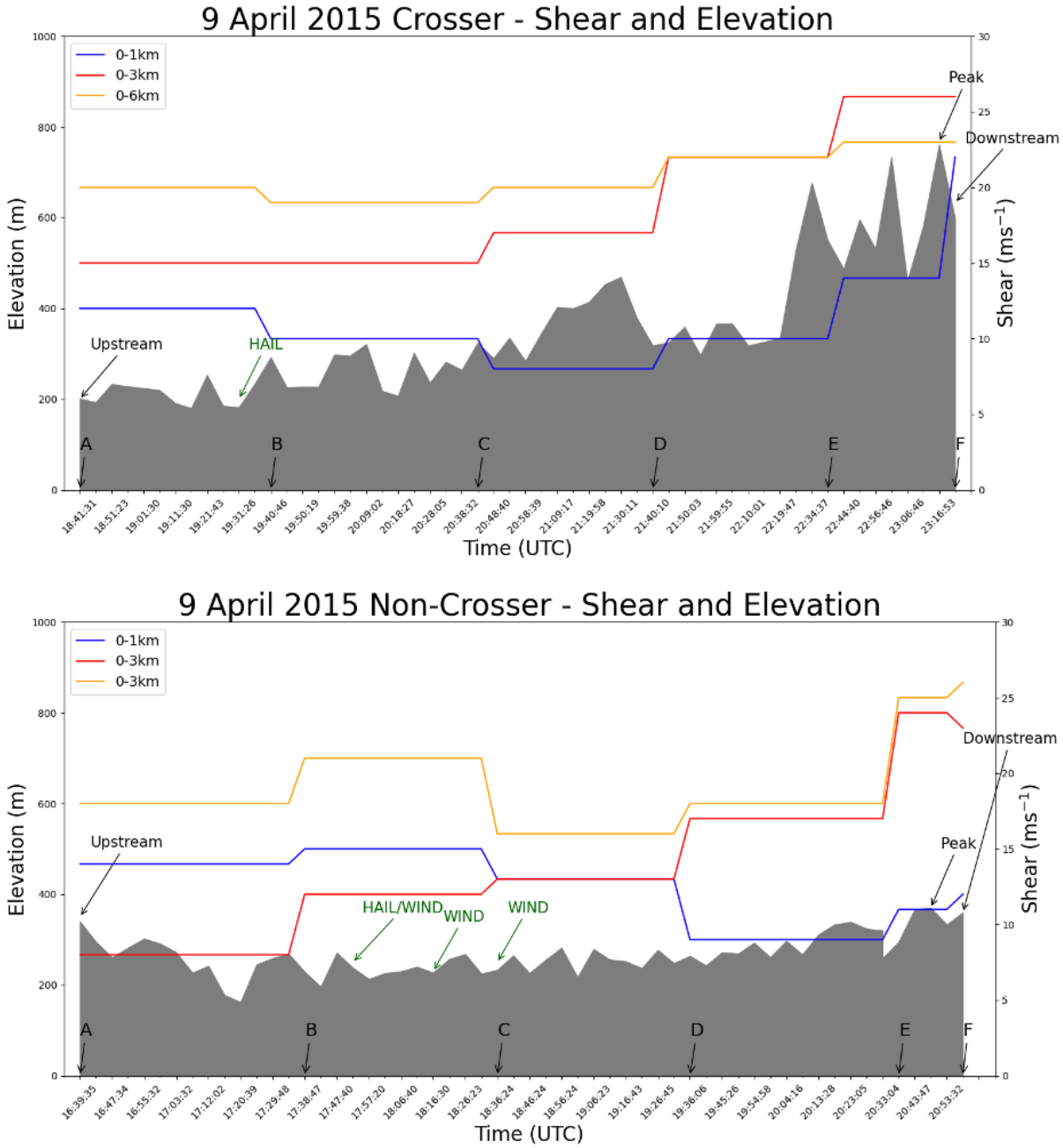

Figure 4.39: As in Fig 4.35, but for 0-1 km (blue), 0-3 km (red), and 0-6 km bulk shear.

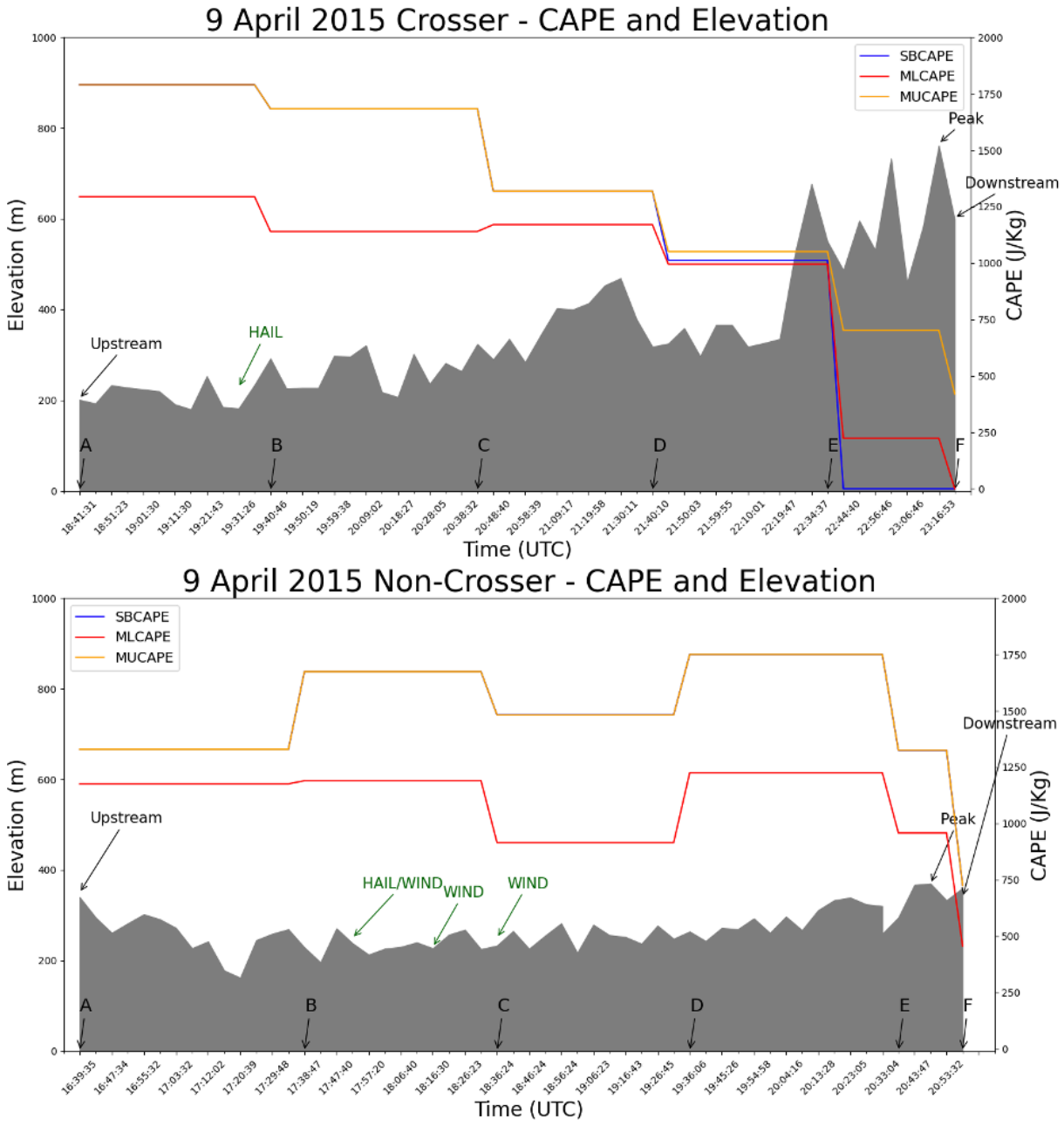

Figure 4.40: As in Fig. 4.35, but for SBCAPE (blue), MLCAPE (red), and MUCAPE (yellow).

CHAPTER 5: SUMMARY AND FUTURE WORK

5.1 Summary

This study analyzed 62 isolated supercells that occurred within the Appalachian Mountains to better understand how supercells interact with complex terrain. The goal of this project was to examine the environments of these supercells to determine if there were differences between crossing and non-crossing supercells to aid in short-term forecasting.

Most of the analyzed supercells occurred in April and May (Figs. 4.1-4.2; Table 2), which is consistent with the frequency of supercells across the United States as well as in the Appalachian region (e.g., Gaffin and Parker 2006; Stonefield and Hudgins 2006; Lane 2008). The time of supercell initiation across the Appalachian region also followed a similar trend of initiation of supercells across the United States with initiation occurring around the afternoon and evening time due to daytime heating and the demise of the supercell occurring during the evening and overnight hours (Fig. 4.3). Severe hail was the most likely severe threat reported (Fig. 4.4). Overall, the crossing supercells tended to produce tornadoes and severe wind reports more frequently than the non-crossing supercells.

However, it is important to note that many of these supercells were produced from only a handful of dates, such as the 27-28 April 2011 outbreak, which may limit the representativeness of environments from all supercells that occur in the Appalachian region (Table 2; Figs. 4.6-4.8). Due to the nature of these supercells clustering on a handful of dates, forecasters will have to be situationally-aware of the environments and associated variability. Their attention is more likely to be split among a few supercells in typical scenarios when supercells interact with terrain, which is more of an operational challenge.

When analyzing the storm scale environments of these supercells, the lowest 3 km of SRH and shear seemed to be the most important parameters in determining if supercells would cross the entirety of either the Cumberland Plateau, Allegheny Mountains, or the Blue Ridge Mountains (e.g., Gaffin and Parker 2006; Lane 2008; Table 9; Figs. 4.25-4.26). This supports previous research of supercells in the Appalachian Mountains, in which the increase in low-level SRH and shear may be due to terrain effects (e.g., Bosart et al. 2006; Gaffin 2012; Prociv 2012). Instability was not a reliable predictor in whether a supercell will traverse the Appalachian Mountains and is consistent with previous studies (e.g., Gaffin and Parker 2006; Lane 2008; Figs. 4.28)

Furthermore, the lowest 3 km of SRH and shear helped to distinguish between severe hail and severe wind-producing supercells from tornado-producing supercells, whereas there were no statistically or physically significant differences between severe producing supercells with regards to CAPE (Figs. 4.30-4.31). Tornado producing supercells tended to have larger values of SRH and shear than severe wind or severe hail-producing supercells. Additionally, supercells that produced severe hail tended to have lower 0°C, -20°C, and wet bulb-zero heights than the other severe-producing supercells (Figs. 4.32-4.34).

The values of SRH and bulk shear also tended to decrease from April through July (Table 10). This may be due to the synoptic pattern becoming more zonal over time, which would decrease the amount of shear in the atmosphere (Figs. 4.9-4.10). The opposite was true with regards to CAPE; CAPE tended to increase from April to July and is likely due to the increase in radiational heating during the summer months. Supercells also tended to become drier over time, with the relative humidity, surface and mixed-layer θ_e values decreasing, and this may explain why less supercells occurred in June and July (Fig. 4.1).

When the supercells were separated based on which WFO they occurred in, patterns emerged with regards to SRH and shear. The non-crossing supercells that occurred in the WFOs located partially in the Cumberland Plateau (MRX and JKL), had larger values of SRH and shear than the crossing supercells. This might indicate that supercells that cross the Blue Ridge require stronger dynamical forcing than supercells that cross the Cumberland Plateau (Table 11). Additionally, the RLX WFO had the least amount of CAPE out of the 6 offices. This may be because RLX is the farthest north office and the low-level jet, which brings warm moist air that helps to increase CAPE, might not reach the region.

5.2 Operational Applications

When identifying whether isolated supercells will or will not cross the entirety of the Appalachian Mountains, there are a few important patterns and thresholds that forecasters can use. Additionally, there are thresholds for the key parameters that forecasters can hone in on to identify if supercells might produce either severe hail, wind, or tornadoes.

5.2.1 Synoptic-scale Features

The following synoptic setup may aid forecasters in pattern recognition for these isolated supercells in the Appalachian Mountains. Forecasters may be able to recognize patterns that might indicate if supercells will cross the Appalachian Mountains.

1. Crossing supercells tended to be associated with a negatively tilted upper-level trough (64%) and non-crossing supercells were associated with a positively tilted trough (72%; Table 5).
2. About 70% of crossing supercells were accompanied by a surface low pressure located in the Midwest (52%) or the Northeast (20%; Table 7).

3. Surface boundaries are important to the development of supercells within this region, as all of the supercells analyzed in this project occurred within 100 kilometers of a boundary (Figs. 4.11-4.15; Table 8). Crossing supercells tended to initiate ahead of a cold front (56%), while non-crossers were accompanied by a stationary front and initiated near an outflow boundary (54%).

5.2.2 *Near-Storm Environments*

Using the 75th percentiles, as this was a natural separation between crossing and non-crossing supercells, thresholds for key storm-scale parameters were calculated to identify if supercells would cross the entirety of the Appalachian Mountains. The upstream environments were used to calculate these thresholds as these environments can help forecasters to identify if supercells will occur and if they will be strong enough to cross complex terrain. The lowest 3 km of SRH and shear, as well as the surface and mixed-layer $_{e}$ were the most important parameters when distinguishing between crossing and non-crossing supercells (Table 9; Figs. 4.25-4.26). The 27-28 April 2011 crossing supercells were removed to create the SRH and shear thresholds, as the wind dynamic parameters of the outbreak were statistically significantly different than those of the rest of the dataset, and would have skewed the thresholds.

1. Supercells that had over 58 m^2s^{-2} and 104 m^2s^{-2} of 0-1 km and 0-3 km of SRH respectively, indicated that supercells may cross. About 52% and 60% (respectively) of crossers met this threshold, while 41% of non-crossers met this criteria.
2. If the supercells had over 12 ms^{-1} and 22 ms^{-1} of 0-1 km and 0-3 km of bulk shear respectively, these supercells tended to cross the entirety of the Appalachians. About 60% and 56% (respectively) of crossers met this criteria, while 41% and 30% (respectively) of non-crossers met this threshold.

3. The moisture tended to be higher for the crossing supercells and these supercells were favored when the surface and mix-layer θ_e were over 340 (60% of crossers and 30% of non-crossers) and 339 (65% of crossers and 25% of non-crossers) Kelvin respectively.

5.2.3 Severe Weather Production

A similar approach was used to calculate thresholds for supercells that produced severe weather, using the 75th percentiles. These thresholds can help the NWS forecasters determine if supercells might produce severe weather in the Appalachian Mountains. It is important to note that the crossing supercells that produced severe weather during the 27-28 April 2011 outbreak were not removed from the dataset when comparing SRH and shear as the distributions of the parameters were not statistically significantly different, and when the subset was removed, the sample size dramatically decreased. However, this may have led to an overestimation of these parameters.

1. Crossing supercells that produced severe weather tended to have over 122 m^2s^{-2} (30% of all crossers) and 169 m^2s^{-2} (35% of all crossers) of 0-1 km and 0-3 km SRH and over 20 ms^{-1} (40% of all crossers) and 27 ms^{-1} (30% of all crossers) of 0-1 km and 0-3 km of bulk shear.
2. Non-crossing supercells that produced severe weather had lower thresholds for SRH and bulk shear than crossing supercells with the environments having 0-1 km and 0-3 km of SRH over 65 m^2s^{-2} (33% of all non-crossing supercells) and 114 m^2s^{-2} (33% of all non-crossing supercells) respectively, and over 13 ms^{-1} (39% of all non-crossing supercells) and 21 ms^{-1} (33% of all non-crossing supercells) of 0-1 km and 0-3 km of bulk shear respectively.

3. Supercells that produced tornadoes tended to have a 0-1 km of SRH over 134 m^2s^{-2} (25% of all crossers) and 0-3 km of SRH over 183 m^2s^{-2} (35% of all crossers). This may help forecasters distinguish between supercells that might produce tornadoes and supercells that might produce other severe weather types.
4. Supercells that produced severe hail can be identified using thresholds for 0°C, -20°C, and wet bulb-zero heights. Crossing supercells tended to have a 0°C height of less than 4440 m (80% of all crossers), a -20°C height less than 7333 m (85% of all crossers), and a wet bulb-zero height of less than 3747 m (85% of all crossers).
5. Non-crossing supercells tended to have a 0°C height of less than 4173 m (70% of all non-crossers), a -20°C height less than 7097 m (63% of all non-crossers), and a wet bulb-zero height of less than 3491 m (58% of all non-crossers).

5.3 Future Work

Future research on this topic could include an analysis of additional isolated supercells that occurred in the Appalachian Mountains. While this study included 62 isolated supercells, a larger dataset could help solidify the findings within this project, especially with regards to analyzing the data in the different subcategories (i.e., severe production, monthly production, and WFO). Since several of these subcategories had small sample sizes, there was a higher likelihood of sample bias.

Another avenue of research could include storm-scale numerical simulations to identify how these supercells progress over shorter periods of time. These simulations could include the storm-scale environments found in this study and test them against varying terrain features (no terrain, idealized bell-shaped terrain, and realistic terrain). The simulations could help to identify when wind dynamics (SRH and shear) strengthen as supercells approach the varying terrain.

Finally, these simulations could determine the importance of boundaries with regards to the supercells in the Appalachian Mountains.

References

Benjamin, S. G., D. Dévényi, S. S. Weygandt, K. J. Brundage, J. M. Brown, G. A. Grell, D., Kim, B. E. Schwartz, T. G. Smirnova, T. L. Smith, and G. S. Manikin, 2004: An Hourly Assimilation–Forecast Cycle: The RUC, *Monthly Weather Review*, *132*(2), 495-518. Retrieved Dec 5, 2020.

Benjamin, S. G., G. A. Grell, J. M. Brown, T. G. Smirnova, and R. Bleck, 2004: Mesoscale Weather Prediction with the RUC Hybrid Isentropic–Terrain-Following Coordinate Model. *Mon. Wea. Rev.*, 132, 473–494.

Benjamin, S. G., and Coauthors, 2016: A North American Hourly Assimilation and Model Forecast Cycle: The Rapid Refresh, *Monthly Weather Review*, *144*(4), 1669-1694. Retrieved Dec 5, 2020.

Blumberg, W. G., K. T. Halbert, T. A. Supinie, P. T. Marsh, R. L. Thompson, and J. A. Hart, 2017: SHARPpy: An Open-Source Sounding Analysis Toolkit for the Atmospheric Sciences. *Bull. Amer. Meteor. Soc.*, 98, 1625–1636.

Bosart, L., A. Seimon, K. D. LaPenta, and M. J. Dickinson, 2006: Supercell Tornadogenesis over Complex Terrain. The Great Barrington, Massachusetts, Tornado on 29 May 1995. *Wea. Forecasting*, 21, pp. 897-922.

Brooks, H. E., and R. B. Wilhelmson, 1993: Hodograph Curvature and Updraft Intensity in Numerically Modeled Supercells, *Journal of Atmospheric Sciences*, *50*(12), 1824-1833.

Bryan, G. H., and J. M. Fritsch, 2002: A benchmark simulation for moist nonhydrostatic numerical models. *Mon. Wea. Rev.*, 130, 2917-2928.

Bunkers, M.J., 2006: An Observational Examination of Long-Lived Supercells. Part I: Characteristics, Evolution, and Demise. *Wea. Forecasting*, 21, 673-688.

Clark, A. J., Schaffer, C. J., Gallus , W. A., Jr., and Johnson-O'Mara, K. (2009). Climatology of Storm Reports Relative to Upper-Level Jet Streaks, *Weather and Forecasting*, *24*(4), 1032-1051.

Concannon, P. R., H. E. Brooks, and C. A. Doswell III, 2000: Climatological risk of strong to violent tornadoes in the United States. Preprints, *Second Symp. on Environmental Applications*, Long Beach, CA, Amer. Meteor. Soc., 212–219.

Coniglio, M. C., 2012: Verification of RUC 0–1-h Forecasts and SPC Mesoscale Analyses Using VORTEX2 Soundings. *Wea. Forecasting*, 27, 667–683.

Craven, J. P., and H. E. Brooks, 2004: Baseline climatology of sounding-derived parameters associated with deep moist convection. Nat. Wea. Dig., 28, 13-24.

Davenport, C. E., and Parker, M. D., 2015: Impact of Environmental Heterogeneity on the Dynamics of a Dissipating Supercell Thunderstorm, *Monthly Weather Review*, *143*(10), 4244-4277.

Davies-Jones, R.,1984: Streamwise Vorticity: The Origin of Updraft Rotation in Supercell Storms, *Journal of Atmospheric Sciences*, *41*(20), 2991-3006. Retrieved Dec 4, 2020.

Evans, C., S. J. Weiss, I. L. Jirak, A. R. Dean, and D. S. Nevius, 2018: An Evaluation of Paired Regional/Convection-Allowing Forecast Vertical Thermodynamic Profiles in Warm-Season, Thunderstorm-Supporting Environments. *Wea. Forecasting*, 33, 1547–1566.

Gaffin, D. M., S. S. Parker, 2006: A Climatology of Synoptic Conditions Associated with Significant Tornadoes across the Southern Appalachian Region. *Wea. Forecasting*, 21, 735-751.

Gaffin, D.,M., 2012: The Influence of Terrain During the 27 April 2011 Super Tornado Outbreak and 5 July 2012 Derecho around the Great Smoky Mountains National Park. *26th Conf. on Severe Local Storms,* Nashville TN, Amer. Meteor. Soc.

Geerts, B., T. Andretta, S. Luberda, J. Vogt, Y. Wang, and L. D. Oolman, 2009: A case study of a long-lived tornadic mesocyclone in a low-CAPE complex-terrain environment. *Electronic J. Severe Storms Meteor*., 4 (3), 1-29.

Gilmore, M. S., and Wicker, L. J., 1998: The Influence of Midtropospheric Dryness on Supercell Morphology and Evolution, *Monthly Weather Review*, *126*(4), 943-958.

Gropp, M. E., and C. E. Davenport, 2018: The Impact of the Nocturnal Transition on the Lifetime and Evolution of Supercell Thunderstorms in the Great Plains. *Wea. Forecasting*, 33, 1045–1061.

Honda, T., and Kawano, T., 2015: How does mid-tropospheric dry air affect the evolution of supercellular convection? *Atmospheric Research,* 157, 1-16.

James, R. P., and Markowski, P. M., 2010: A Numerical Investigation of the Effects of Dry Air Aloft on Deep Convection, *Monthly Weather Review*, *138*(1), 140-161.

Katona, B., P. Markowski, C. Alexander, S. Benjamin, 2016: The Influence of Topography on Convective Storm Environments in the Eastern United States as Deduced from the HRRR. *Wea. Forecasting,* 31, 1481-1490.

Keighton, S., K. Kostura, C. Liscinsky., 2004: Examination of Tornadic and Non-tornadic Supercells in Southwest Virginia on 28 April 2002. *22nd Conf. on Severe Local Storms, Amer. Meteor. Soc,* Hyannis, MA.

Kuchera, E. L., and M. D. Parker, 2006: Severe Convective Wind Environments. *Wea. Forecasting*, 21, 595–612.

Lane, J., 2008: A Comprehensive Climatology of Significant Tornadoes in the Greenville-Spartanburg, South Carolina County Warning Area (1880-2006). Eastern Region Technical Attachment, no. 2008-01.

Lemon, L. R., and C. A. Doswell, 1979: Severe Thunderstorm Evolution and Mesocyclone Structure as Related to Tornadogenesis. *Mon. Wea. Rev.*, 107, 1184–1197.

Lenning, E., H. E. Fuelberg, and A. I. Watson, 1998: An Evaluation of WSR-88D Severe Hail Algorithms along the Northeastern Gulf Coast. *Wea. Forecasting*, 13, 1029–1045.

Lyza, A. W., and K. Knupp, 2014: An Observational Analysis of Potential Terrain Influences on Tornado Behavior. *27th Conf. on Severe Local Storms,* Madison, WI, Amer. Meteor. Soc.

Magee, K. S., and C. E. Davenport, 2020: An Observational Analysis Quantifying the Distance of Supercell-Boundary Interactions in the Great Plains*.17th Conf. on Mesoscale Processes,* San Diego, CA.

Markowski, P. M., J. M. Straka, E. N. Rasmussen, and D. O. Blanchard, 1998: Variability of Storm-Relative Helicity during VORTEX. *Mon. Wea. Rev.*, 126, 2959–2971.

Markowski, P.M., N. Dotzek, 2011: A Numerical Study of the Effects of Orography on Supercells. Atmospheric Research 100, 457-478.

May, R., 2016: Metpy: An open-source toolkit for Meteorology. *96th Conference, Annual American Meteorological Society, Sixth Symposium on Advances in Modeling and Analysis Using Python,* New Orleans, LA.

Miglietta, M., 2017: Numerical Simulations of a Tornadic Supercell over the Mediterranean. *Wea. Forecasting*, 32, p. 1209-1226.

Moller, A. R., C. A. Doswell, M. P. Foster, and G. R. Woodall, 1994: The Operational Recognition of Supercell Thunderstorm Environments and Storm Structures. *Wea. Forecasting*, 9, 327–347.

Prociv, K.A., 2012: Terrain and Landcover Effects of the Southern Appalachian Mountains on the Rotational Low Level Wind Fields of Supercell Thunderstorms.

Rasmussen, E. N., S. Richardson, J. M. Straka, P. M. Markowski, and D. O. Blanchard, 2000: The Association of Significant Tornadoes with a Baroclinic Boundary on 2 June 1995. *Mon. Wea. Rev.*, 128, 174–191.

Reames, L. J., 2017: Diurnal Variations in Severe Weather Forecast Parameters of Rapid Update Cycle-2 Tornado Proximity Environments. *Wea. Forecasting*, 32, 743–761.

Rotunno, R., and J. Klemp, 1985: On the Rotation and Propagation of Simulated Supercell Thunderstorms, *Journal of Atmospheric Sciences*, *42*(3), 271-292. Retrieved Dec 4, 2020

Scheffknecht, P., S. Serafin, and V. Grubišić., 2017: A long-lived supercell over mountainous terrain. Q.J.R. Meteorol. Soc., 143: 2973-2986.

Schneider, D., G., 2009: The Impact of Terrain on Three Cases of Tornadogenesis in the Great Tennessee Valley. National Weather Association, Electronic Journal of Operational Meteorology, 2009-EJ11.

Sherburn, K. D., and M. D. Parker, 2014: Climatology and Ingredients of Significant Severe Convection in High-Shear, Low-CAPE Environments. *Wea. Forecasting*, 29, 854–877.

Smith, G.M., Y. Lin, R. Yevgenii., 2016: Orographic Effects on Supercell: Development and Structure, Intensity and Tracking. Environment and Natural Resources Research, 6, no. 2.

Stonefield, R. C., J. E.Hudgins, 2006: A Severe Weather Climatology for the WFO Blacksburg, Virginia, County Warning Area. NOAA Technical Memorandum, NWS ER-99.

Sumrall, P., P. Market, and S. Rochette, 2020: Using DCIN and DCAPE to Evaluate Severe Surface Winds in a Case of Elevated Convection. *100th Conference, Annual American Meteorological Society, Severe Local Storms Symposium,* Boston, MA.

Tang, B., M. Vaughan, R. Lazear, Corbosiero, K., Bosart, L., 2016: Topographic and Boundary Influences on the 22 May 2014 Duanesburg New York, Tornadic Supercell. *Wea. Forecasting*, 31, pp. 107-127.

Thompson, R. L., and R. Edwards, 2000: An Overview of Environmental Conditions and Forecast Implications of the 3 May 1999 Tornado Outbreak. *Wea. Forecasting*, **15**, 682–699.

Thompson, R.L., R. Edwards, J.A. Hart, K.L. Elmore, and P. Markowski, 2003: Close Proximity Soundings within Supercell Environments Obtained from the Rapid Update Cycle. *Wea. Forecasting,* 18, 1243–1261.

Thompson, R., L., C. M. Mead, R. Edwards, 2007: Effective Storm-Relative Helicity and Bulk Shear in Supercell Thunderstorm Environments. *Wea. Forecasting,* 22, 102-115.

USGS, 2019: 3D Elevation Program. Accessed 22 March 2019. https://www.usgs.gov/core-science-systems/ngp/3dep/about-3dep-products-services?qt-science_support_page_related_con=0#qt-science_support_page_related_con

Weisman, M. L., and J. B. Klemp, 1982: The Dependence of Numerically Simulated Convective Storms on Vertical Wind Shear and Buoyancy. *Mon. Wea. Rev.*, 110, 504–520.

Weisman, M. L., and J. B. Klemp, 1984: The Structure and Classification of Numerically Simulated Convective Storms in Directionally Varying Wind Shears. *Mon. Wea. Rev.*, 112, 2479–2498.

Weisman, M. L., and R. Rotunno, 2000: The Use of Vertical Wind Shear versus Helicity in Interpreting Supercell Dynamics, *Journal of the Atmospheric Sciences*, *57*(9), 1452-1472.

Witt, A., M. D. Eilts, G. J. Stumpf, J. T. Johnson, E. D. W. Mitchell, and K. W. Thomas, 1998: An Enhanced Hail Detection Algorithm for the WSR-88D. *Wea. Forecasting*, 13, 286–303.